



Skolkovo Institute of Science and Technology

MATERIAL DESIGN AND OPTIMIZATION OF THERMAL MANAGEMENT MATERIALS
BASED ON BORON NITRIDE, GRAPHENE, AND CARBON NANOTUBES POLYMER
NANOCOMPOSITES

Doctoral Thesis

by

MOHAMMAD OWAIS

DOCTORAL PROGRAM IN MATERIALS SCIENCE AND ENGINEERING

Supervisor
Dr. Sergey Abaimov

Moscow - 2023

© Mohammad Owais 2023

I hereby declare that the work presented in this thesis was carried out by myself at Skolkovo Institute of Science and Technology, Moscow, except where due acknowledgement is made, and has not been submitted for any other degree.

Candidate (Mohammad Owais)

Supervisor (Dr. Sergey Abaimov)

Abstract

Heat dissipation in microelectronic devices, such as computers and mobile phones, has long been a bottleneck. The miniaturization of integrated circuits on motherboards has created an urgent need for ultra-advanced thermally conductive thermal management materials (TMMs) that can rapidly dissipate heat. To this polymeric TMMs emerge as a promising solution. These composites combine lightweight polymer matrices with thermally conductive fillers like graphene and carbon nanotubes (CNTs), surpassing the thermal conductivity of traditional metals such as Al and Cu. This elevated thermal conductivity results from the formation of a conductive network within the polymer matrix, offering significant advantages in weight reduction and improved heat dissipation. In this dissertation, we aim to explore various manufacturing techniques to develop TMMs that can be produced in large quantities and are economically viable, making them accessible for widespread industrial usage and with the aim of surpassing the thermal conductivity of traditional TMMs typically employed in the industry, which typically ranges around 4.0 W/mK. Furthermore, the goal of this research work is to study the use of low to optimum thermally conductive filler loadings such as, boron nitride (BN), graphene oxide (GO), CNTs within the polymers such as Epoxy resin, Poly vinyl alcohol (PVA) to achieve the maximum enhancement in the thermal conductivity by utilizing different ways, such as reduction of fillers inside polymers, self-assembly of filler materials to be used within polymeric matrices, and using different fabrication techniques. The fabrication of polymer composites is divided into three chapters illustrating the transition of our research work from thermally conductive filler/polymer structures such as: BN / PVA 3D frameworks to reduced GO / PVA films as thermal interface material and CNTs/ epoxy composites

as under-filled materials. These composites exhibited commendable thermal conductivities (ranging from 0.48 W/mK to 5.1 W/mK), contrasting with the ~0.15-0.19 W/mK of neat polymers while the electrical properties of all these above-mentioned polymer composites had a great variation with 13 orders of magnitude with low to high electrical resistivities depending on the application in which they will be best suited for industry. For instance, CNTs/ epoxy had low value of electrical resistivity around 2.23 Ω cm, making them suitable for applications that require making of conductive films such as touch screens and LCDs. The low electrical resistivity of CNTs ensures efficient charge transfer, while the high thermal conductivity ensures that the film does not overheat. Similarly, reduced GO/ PVA films had a mid-range low electrical resistivity of value around $8 \times 10^3 \Omega$ cm but on the other hand BN / PVA 3D framework 3D frameworks had a quite high value of around $1 \times 10^{15} \Omega$ cm. These 3D structures maintain the electrical insulation with high electrical resistivity, which reduces the risk of electrical damage, short circuit and failure due to high temperatures. Hence, this property helps to increase the lifespan of the material, making it a more durable choice for TMMs. Simultaneously, the increased thermal conductivity enables in the efficient heat transfer, leading to improved heat dissipation and thermal management characteristics. To conclude, we fabricated a set of polymer composites that exhibited high thermal conductivities with tunable electrical resistivity to be employed in applications associated with electronics industry.

Publications

1. **Owais, M.**; Javed, M.H.; Akram, M.Z.; Paxton, W.F.; Akhatov, I.S.; Abaimov, S.G. Review—Recent Advances in Thermally Conductive Paper-Like Films. *ECS Journal of Solid-State Science and Technology*. 2021, 10, 033001
2. **Owais, M.**; Shiverskii, A.; Sulimov, A.; Ostrizhiniy, D.; Popov, Y.; Mahato, B.; Abaimov, S.G. Scalable Fabrication of Thermally Conductive Layered Nacre-like Self-Assembled 3D BN-Based PVA Aerogel Framework Nanocomposites. *Polymers* 2022, 14, 3316.
3. **Owais, M.**; Shiverskii, A.; Pal, A.K.; Mahato, B.; Abaimov, S.G. Recent Studies on Thermally Conductive 3D 3D framework/Foams with the Segregated Nanofiller Framework. *Polymers* 2022, 14, 4796
4. Butt, H.A[†]; **Owais, M.** [†]; Sulimov, A.; Ostrizhiniy, D.; Lomov, S.V.; Akhatov, I.S.; Abaimov, S.G.; Popov, Y.A. CNT/Epoxy-Masterbatch Based Nanocomposites: Thermal and Electrical Properties. *In Proceedings of the 2021 IEEE 21st International Conference on Nanotechnology (NANO), Montreal, QC, Canada, 28–30 July 2021*; pp. 417–420.

[†] = Authors contributed equally

5. **Owais, M.** et.al. “Low-Temperature Reduction of Graphene Oxide: A Novel Pathway for Thermally Conductive Polymer Films”. (*Submitted*)

Conference presentations

1. CNT/Epoxy-Masterbatch Based Nanocomposites: Thermal and Electrical Properties. *In Proceedings of the 2021 IEEE 21st International Conference on Nanotechnology (NANO), Montreal, QC, Canada, 28–30 July 2021*; pp. 417–420.

2. Scalable fabrication of thermally conductive flexible diethyl glycol reduced graphene oxide polymer films". International Conference of Students, Postgraduates and Young Scientists, International Youth Scientific Forum "Lomonosov-2023".

Book chapter

1. **Owais, M.** et.al. BN-Based PCM Composites for Thermal Management: Synthesis and Performance Assessment. Springer nature. Part of the Composites Science and Technology book series (CST). https://doi.org/10.1007/978-981-99-2866-8_1

Personal contribution to each publication

In regards to the review papers, my contributions primarily revolve around assuming the role of the first author. As the first author, I undertook a substantial portion of the workload, encompassing various aspects such as conceptualization, formal analysis, investigation, and the composition of the original draft. Additionally, I played an integral role in the subsequent stages of the writing process, including reviewing, analyzing, and editing the content.

1. Owais, M.; Javed, M.H.; Akram, M.Z.; Paxton, W.F.; Akhatov, I.S.; Abaimov, S.G. Review—Recent Advances in Thermally Conductive Paper-Like Films. ECS J. Solid State Sci. Technol. 2021, 10, 033001
2. Owais, M.; Shiverskii, A.; Pal, A.K.; Mahato, B.; Abaimov, S.G. Recent Studies on Thermally Conductive 3D 3D framework/Foams with the Segregated Nanofiller Framework. Polymers 2022, 14, 4796

In contrast, my involvement in other published papers primarily revolves around conducting concrete experimental work as an individual contributor. In these instances, I actively engaged in tasks such as conceptualization, formal analysis, investigation, and the composition of the original draft. Furthermore, I assumed responsibility for the subsequent stages of the writing process, including reviewing, analyzing, and editing the content.

1. Owais, M.; Shiverskii, A.; Sulimov, A.; Ostrizhiny, D.; Popov, Y.; Mahato, B.; Abaimov, S.G. Scalable Fabrication of Thermally Conductive Layered Nacre-like Self-Assembled 3D BN-Based PVA Aerogel Framework Nanocomposites. Polymers 2022, 14, 3316

2. Butt, H.A†.; Owais, M. †; Sulimov, A.; Ostrizhiniy, D.; Lomov, S.V.; Akhatov, I.S.; Abaimov, S.G.; Popov, Y.A. CNT/Epoxy-Masterbatch Based Nanocomposites: Thermal and Electrical Properties. In Proceedings of the 2021 IEEE 21st International Conference on Nanotechnology (NANO), Montreal, QC, Canada, 28–30 July 2021; pp. 417–420.

† = Authors contributed equally.

Within the scope of this thesis, my contributions encompass a comprehensive study of the thermal properties and electrical resistivity of CNTs epoxy composites. Specifically, I undertook tasks related to the overall study, the writing process, facilitating discussions, and the meticulous editing of the content. Conversely, my colleague focused on the piezoelectric behavior of CNTs epoxy composites, which, though pertinent to the overall research topic, is not discussed within the context of this particular thesis due to its irrelevance. It is important to note that the research work I have independently contributed to is extensively discussed in chapter 5 of this dissertation.

3. Owais, M. et.al. “Fabrication of High-Performance Flexible, Thermally Conductive reduced Graphene Oxide Polymer Films”. (Submitted).

I take sole responsibility for all aspects of the experimental work, including the meticulous execution, thorough analysis, and subsequent interpretation of the results. Furthermore, the entire manuscript, from its conception to its completion, has been crafted exclusively by me.

Acknowledgements

I would like to express my deep gratitude and appreciation to the following individuals and organizations who have played a significant role in the completion of my PhD thesis:

First and foremost, I am immensely grateful to my supervisor, Sergey Abaimov, for his guidance, unwavering support, and valuable insights throughout the entire duration of my research. Apart from his academic suggestions, he's been with me and gave me moral support in my extremely worse times when my parents were very sick and I had to travel back to Pakistan in an emergency. He trusted me with my research skills and I completed my thesis on time albeit being stuck in my country for 8 months after the Covid times.

I extend my heartfelt thanks to the members of my doctoral thesis committee, Professor Stepan Lomov, Professor Aslan Kasimov and Professor Sergey Abaimov, for their valuable time, thoughtful feedback, and constructive criticism during the evaluation of my thesis. Their expertise and constructive suggestions have immensely contributed to enhancing the quality and rigor of my research. Moreover, special thanks to Professor Alexander Korsunsky, Professor Alexei Buchachenko and Professor Artem Abakomov for their help regarding the improvement of my thesis.

I would like to acknowledge the support and encouragement provided by the faculty members and staff of Skoltech. Their dedication to academic excellence and commitment to fostering a conducive research environment have been invaluable in shaping my academic journey.

I am grateful to my colleagues and fellow researchers like Aleksei Shiverskii, Milad Jafarypouria for their stimulating discussions, valuable insights, and camaraderie. Their support and collaboration have enriched my research experience and provided me with valuable perspectives from different disciplines.

I am deeply grateful to my friends specially Hassan Butt, Amit Pal, Zain Akram and Zainab Waris and family specially my mother for their unwavering support, understanding, and encouragement throughout my PhD journey. Their love, patience, and belief in my abilities have been a constant source of motivation and strength.

Finally, I would like to express my profound appreciation to Skoltech again for their financial support. The funding provided by Skoltech has been instrumental in facilitating my research, including conducting experimental research, data collection, access to library resources, and dissemination of findings.

To everyone who has contributed in one way or another, whether mentioned explicitly or not, I offer my heartfelt gratitude. Your support and encouragement have been invaluable, and I am truly grateful for your contributions to the successful completion of this thesis.

Table of Contents

Abstract.....	3
Publications.....	5
Conference presentations	5
Book chapter	6
Personal contribution to each publication	7
Acknowledgements.....	9
List of Symbols, Abbreviations	14
Chapter 1. Introduction	15
1.1 Background and motivation	15
1.2 Objectives.....	17
Chapter 2. Review of the Literature	18
2.1 Thermal Management Materials (TMMs).....	18
2.1.1 Types of TIMs	19
2.1.2 Applications of TIMs.....	21
2.2 Polymers as heat dissipator	22
2.2.1 Thermal conductivity	24
2.2.2 Mechanism of thermal conductivity in polymers.....	27
2.2.3 Mechanism of thermal conductivity in polymer composites	29
2.2.4 Role of Interface.....	30
2.3 Thermally conductive three-dimensional (3D) framework materials	31
2.3.1 Thermally conductive aerogel 3D scaffold structure	33
2.3.2 Epoxy Infiltrated 3D framework.....	40
2.4 Thermally conductive polymer films/papers.....	43
2.5 Conclusion.....	49
Chapter 3. Thermally Conductive Self-Assembled 3D BN-Based PVA Framework Nanocomposites	51
3.1 Introduction	51
3.2 Research objectives	52
3.3 Experimental	53
3.3.1 Materials.....	53
3.3.2 Methodology	53

3.3.3 Characterizations	55
3.4 Results and discussion.....	56
3.4.1 Fourier-transform infrared (FTIR).....	56
3.4.2 Energy dispersive spectrometer (EDS).....	58
3.4.3 Optical contact angle analyzer.....	59
3.4.4 Morphology of 3D framework by scanning electron microscopy (SEM).....	61
3.4.5 Thermal conductivity.....	63
3.4.6 X-ray Diffraction (XRD).....	65
3.4.7 Electrical resistivity	66
3.4.8 Thermogravimetric Analyzer (TGA).....	68
3.5 Conclusion.....	69
Chapter 4. Thermally conductive reduced graphene oxide polymer films	72
4.1 Introduction	72
4.2 Research objectives	72
4.3 Experimental	73
4.3.1 Materials	73
4.3.2 Methodology.....	73
4.3.2.1 Reduction of graphene oxide (GO)	73
4.3.2.2 Preparation of polymer composite films	73
4.4 Results and Discussion.....	75
4.4.1 Reduction of graphene oxide (GO)	75
4.4.1.1 Fourier-transform infrared (FTIR).....	75
4.4.1.2 UV-Visible spectroscopy.....	76
4.4.1.3 Raman spectroscopy	77
4.4.1.4 Transmission electron microscopy (TEM) and Energy dispersive spectrometer (EDS)	78
4.4.1.5 Scanning electron microscope (SEM)	83
4.4.2 PVA based polymer nanocomposite films	84
4.4.2.1 Optical contact angle analyzer.....	84
4.4.2.2 Atomic force microscopy (AFM)	87
4.4.2.3 Electrical resistivity	88
4.4.2.4 Thermal conductivity.....	90
4.5 Conclusion.....	92

Chapter 5. CNT masterbatch based epoxy nanocomposites	94
5.1 Introduction	94
5.2 Research objectives	95
5.3 Experimental	96
5.3.1 Materials	96
5.3.2 Methodology	96
5.3.3 Characterization	98
5.4 Results and discussion	99
5.4.1 Microstructural Analysis	99
5.4.2 Electrical resistivity	101
5.4.3 Thermal conductivity	102
5.4.4 Thermal stability	104
5.4.5 Differential scanning calorimetry (DSC) analysis	106
5.5 Conclusion	109
Chapter 6. Conclusion	111
Bibliography	113
Appendix	122

List of Symbols, Abbreviations

Boron Nitride- BN

Carbon nanotubes- CNTs

Diethylene glycol- DEG

Electrical resistivity- ER

Epoxy resin- ER

Graphene oxide- GO

Multi walled carbon nanotubes - MWCNTs

Poly-vinyl alcohol- PVA

Single walled carbon nanotubes – SWCNTs

Thermal conductivity – TC

Thermal interface materials – TIMs

Thermal management materials- TMMs

Water contact angle – WCA

Vacuum assisted filtration - VAF

Chapter 1. Introduction

1.1 Background and motivation

Advancements in science and technology have led to the evolution of microelectronic devices that require miniaturization, high levels of integration, and high-power consumption. These developments pose new challenges for the conventional and traditional heat conductors. Electronic gadgets release a substantial amount of heat energy during operation as a result of tightly packed and powerful semiconductor chips and integrated circuits. If this heat cannot be effectively dissipated, it will be concentrated in small areas, creating local hotspots with extremely high temperatures. This can negatively impact the performance and lifespan of microelectronic devices. Thus, efficient heat management systems are crucial to lower the temperature of local hotspots in high-power electronics system [1-5]. On this matter, thermal interface materials (TIMs) are critical components of heat management systems which play an essential role in dissipating heat energy in electronic devices. As overheated environments limit the development of microelectronics and integrated circuits with higher powers and levels of integration, efficient thermal management systems are becoming increasingly important. TIMs, which have become integral to the electronics and aerospace industries, exhibit a direct impact on the quality of the entire polymer composite system, as they are one of the forms of thermal management systems, and the thermal conductivity (k) of such composite material directly determines the quality of the entire system.

While organic polymers possess excellent properties, such as electrical insulation, high stiffness, low weight, low cost, outstanding mechanical properties, and machinability, they exhibit poor thermal conduction due to multiple factors, including the amorphous arrangement and vibrations of their molecular chains [6]. For most polymers, phonon thermal conduction is the dominant

pathway, and their amorphous structure and molecular vibrations cause massive phonon scattering. This results in most neat polymers being thermal insulators or relatively poor heat conductors with thermal conductivity values ranging from 0.1-0.2 W m⁻¹ K⁻¹ [7]. As a result, pure polymers are inadequate for facilitating heat dissipation conundrums, which is critical for accelerating the minimization and integration of components in the modern electronics industry.

Thermal management materials (TMM) or thermal interface materials (TIMs) play a crucial role in dissipating heat generated in electronic devices [8]. The electrical resistivity of these materials is an important property that affects their performance in thermal management applications. Low electrical resistivity in TMM or TIMs is beneficial because it allows for better electrical conductivity, which helps to dissipate the heat generated by electronic devices more efficiently. When heat is generated, it can cause an increase in temperature, which can negatively affect the performance of electronic devices. Hence, by having low electrical resistivity, TMM or TIMs can help to reduce the amount of heat generated by the electronic device, preventing overheating and improving the overall performance and lifespan of the device [9]. On the other hand, high electrical resistivity in TMM or TIMs can also be beneficial in certain applications. For instance, in situations where there is a need to isolate electrical components or prevent electrical interference, high electrical resistivity can be advantageous. TMM or TIMs can prevent electrical current from passing through them by having high electrical resistance, preventing electrical interference or short circuits. Overall, the electrical resistivity of TMM or TIMs plays an important role in determining their effectiveness in thermal management-based applications. Whether low or high, the electrical resistivity of these composite materials can provide important benefits depending on the specific application and the requirements of the electronic device.

1.2 Objectives

The primary aim of my thesis research is delineated as follows:

1. Investigation of different thermally conductive filler nanomaterials like graphene, carbon nanotubes and boron nitride in various thermoset and thermoplastic polymers like epoxy resin and polyvinyl alcohol to study the thermal and electrical properties of the polymer composite system based on their morphological structure and mechanisms involved.
2. To achieve maximum improvement in the thermal conductivity of TMMs or TIMs compared to the traditional TMMs currently employed in industry with TC of $\sim 4\text{W/mK}$ by investigating the effect of low (≤ 10 wt.%) to optimum filler loading concentration by weight within a polymer matrix. The study aims to identify the optimum filler concentration and investigate the relationship between filler loading concentration and thermal conductivity to maximize the thermal management performance with simultaneous investigation of electrical resistivity. As the filler nanomaterials are extremely expensive, so our objective is to develop a scalable economically viable fabrication method for TMMs.
3. Augmentation of the thermal conductivity of polymer composites, which can be achieved by using a complex of various techniques, including orientation of the fillers via self-assembly within the polymers, reducing the filler materials like graphene oxide, and utilizing the most suitable mixing methods.

Chapter 2. Review of the Literature

The 21st-century microelectronics industry relies heavily on the production of miniaturized and highly thermally conductive components that can efficiently dissipate heat energy, making them essential for aerospace, automotive, military, computer, and cell phone applications. Overheating in electronic devices is a major cause of equipment failure, leading to PCB failure, malfunction, or short circuit [10,11]. To address this issue, there is a critical need to develop thermal interface materials (TIMs) or thermal management materials (TMMs) that can dissipate heat energy at a rapid pace. With the continued growth of the electronic industry, especially in the development of cellular devices, tablets, and computers, substrates with high thermal conductivity and reduced thickness are essential for ensuring enhanced thermal performance, longevity, and reliability. Consequently, the development of new TMMs or TIMs that can effectively dissipate heat energy is crucial for improving the overall performance and reliability of electronic devices.

2.1 Thermal Management Materials (TMMs)

Thermal management materials refer to materials used in electronic devices to manage heat generated during their operation. The efficiency and reliability of electronic devices can be affected by excessive heat, which can cause degradation in performance or even device failure. These materials are designed to dissipate heat efficiently with ensuring the proper functioning of electronic devices. Hence, one of the TMMs used nowadays and in recent years is TIMs.

Thermal interface materials (TIMs) are materials that are used to fill the air gaps between two surfaces that are in contact with each other, such as an electronic device and a heat sink. These materials are designed to improve the thermal transfer between the two surfaces by reducing the thermal resistance at the interface. TIMs are typically available in a wide variety of forms, including pastes, greases, tapes, films, and phase change materials.

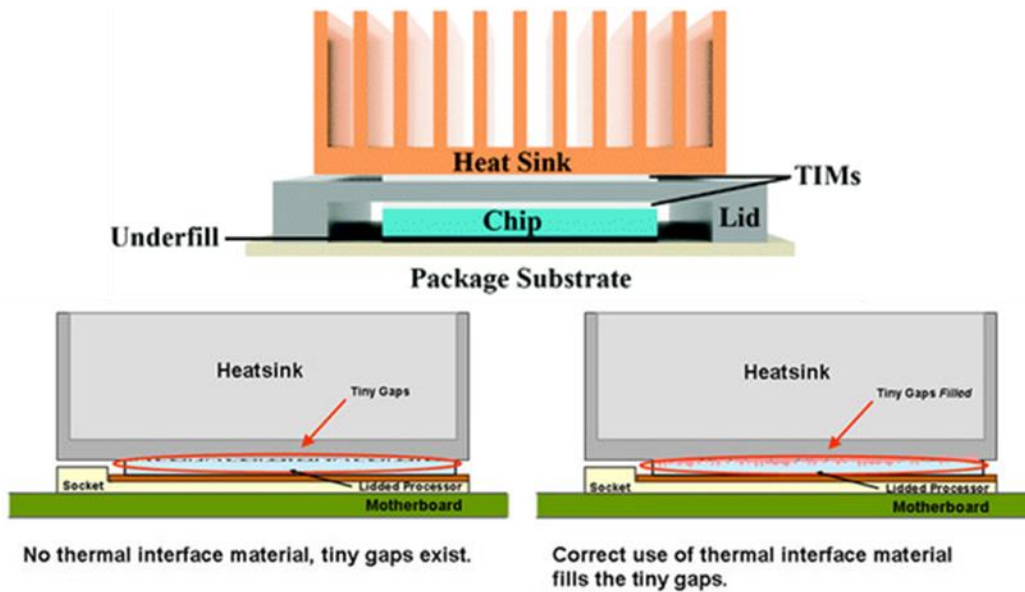


Figure 1. Typical representation of thermal interface materials (TIMs) [12]. Reprinted with permission from Royal Society of Chemistry, Copyright 2021.

2.1.1 Types of TIMs

Thermal interface materials can be categorized into various types based on their intended applications. These categories include:

1. **Thermal Paste:** Thermal paste is a semi-liquid viscous material that is used to fill the air gaps between two surfaces. It is made up of a combination of thermal conductive particles, such as ceramic, graphitic, or metal, and a carrier, such as silicone or oil. The paste is applied to the surface of the device or heat sink, and then the two surfaces are pressed together. The paste fills the air gaps and improves the thermal transfer between the two surfaces.

2. **Thermal Grease:** Thermal grease is similar to thermal interface paste, but it has a higher viscosity. It is used in applications where a thicker layer of material is needed to fill larger gaps between the two surfaces.
3. **Thermal Interface Tape:** Thermal interface tape is a material that is used to attach a heat sink to an electronic device. It is a double-sided tape that has a thermal conductive layer on one side and an adhesive layer on the other side. The tape is applied to the heat sink, and then the heat sink is pressed onto the device.
4. **Phase Change Materials:** Phase change materials are materials that can absorb or release heat as they change from a solid to a liquid or vice versa. They are used as thermal interface materials because they can conform to the shape of the two surfaces and fill the air gaps between them. When the device heats up, the phase change material absorbs the heat and melts, filling the gaps between the surfaces. When the device cools down, the phase change material solidifies, maintaining the contact between the two surfaces.
5. **Thermal pads:** Thermal pads are a type of TIMs mostly made up of elastomers that are used in electronic devices to enhance heat transfer between the heat-generating device and the heat sink. These pads are made of a soft, pliable material that is filled with a thermally conductive compound, which helps to improve the thermal conductivity between the two surfaces. One of the key advantages of thermal pads is their ability to conform to irregular surfaces, which helps to fill gaps and voids between the heat-generating device and the heat sink. This enhances the surface area of contact and reduces the thermal resistance, resulting in improved heat dissipation and better performance of the electronic device.
6. **Thermal papers/films:** Thermal papers or films are a type of TIMs that can be used to improve heat transfer in electronic devices. These materials are made of a thin film or paper

that is filled with a thermally conductive filler materials, such as graphene, carbon nanotubes, ceramic particles, graphite, or metal powders with polymer. They are designed to fill the gaps between the heat-generating device and the heat sink, reducing the thermal resistance and improving the overall thermal performance of the system. Thermally conductive films and papers offer several advantages over other types of TIMs. They are typically thin and flexible, allowing them to conform to irregular surfaces and provide good contact between the two surfaces. They also have a high thermal conductivity, which enables them to transfer heat more efficiently than other types of TIMs. In addition, they are often easy to apply and can be cut to size, making them a versatile choice for many different applications. Thermally conductive films and papers are commonly used in applications where a precise fit is necessary, such as in LED lighting, automotive electronics, and computer components. They can also be used in high-performance applications, such as in aerospace and defense, where thermal management is critical for reliable operation.

2.1.2 Applications of TIMs

Thermal interface materials are used in a wide range of applications, including:

1. Electronic devices: TIMs are used in electronic devices, such as laptops, desktops, servers, and mobile phones, to improve the thermal transfer between the device and its heat sink.
2. Automotive: TIMs are used in automotive applications to improve the thermal transfer between the engine and the heat exchanger.
3. Aerospace: TIMs are used in aerospace applications to improve the thermal transfer between the spacecraft and its heat exchanger.

2.2 Polymers as heat dissipator

Polymers are essential in the production of TMMs or TIMs for thermal management applications. They are used to provide the necessary properties for specific applications. These polymers can be further classified into two categories: thermoset and thermoplastic polymers. In this dissertation, we will focus on their usage in the electronic industry in detail.

Thermoset polymers, are a type of synthetic polymer that, once molded and cured, cannot be melted or reshaped through heating. They exhibit high resistance to heat and chemical changes, making them suitable for applications requiring durability and stability, such as in automotive parts, electrical insulators, and composites. Common examples such as epoxy resins, phenolic resins, and polyimides. They can be used in thermal management systems due to their excellent thermal stability and mechanical strength at high temperatures. One common application of thermoset polymers in thermal management is as encapsulating materials for electronic components [13-15]. When electronic components generate heat during operation, encapsulating them in thermoset polymers can help dissipate the heat, preventing damage to the components and increasing their lifespan. Thermoset polymers can also be used as adhesives in bonding heat sinks or other thermal management components to electronic devices. The high thermal conductivity of some thermoset polymers, such as epoxy resins filled with thermally conductive fillers like the family of graphite or ceramic, can help transfer heat away from the electronic components to the heat sink. Furthermore, thermoset polymers can be used as insulation materials in high-temperature environments. Their high glass transition temperature and low thermal expansion coefficient make them ideal for use in applications such as electrical insulation in motors or transformers [16]. In summary, thermoset polymers are useful materials for thermal management systems due to their excellent thermal stability, mechanical strength, and thermal conductivity.

On the other hand, thermoplastic polymers offer advantages in thermal management applications due to their high thermal conductivity, stability at high temperatures, ease of processing, and recyclability. Thermoplastic polymers are a type of synthetic polymer that can be melted and reshaped multiple times when heated. They soften upon heating and solidify when cooled, making them highly versatile for various manufacturing processes. Common examples include polyethylene, polypropylene, and PVC. They can be used as TIMs, housing materials for electronic components, packaging materials, and matrix materials in composite structures [10,17-20]. These TIMs are commonly used in electronic packaging systems to improve thermal conduction over the interface between two solid surfaces, such as a heat source and a heat sink. The fundamental goal of TIMs is to close any residual small gaps/voids or spaces between the two surfaces in order to increase the surface area in contact, which improves the thermal conduction phenomenon. The commercially available TIMs can be categorized into different types, including thermal grease, thermal pads, phase change materials, gels, thermally conductive adhesives, and solders but these traditional TIMs have some limitations. For example, thermal grease can be messy during processing and lead to a dried-out interface; Thermal pads are not as effective as thermal pastes in dissipating heat energy and are not reusable. They also present a compromise among contradictory objectives such as filling voids, to hold high filler loading concentration for high thermal conductivity, and possessing high stiffness. Recently, thermally conductive films have become increasingly popular as an alternative to traditional TIMs. These highly thermally conductive films/papers can offer a clean alternative solution to traditional TIMs, providing high thermal conductivity, enhanced mechanical properties, electrical insulation characteristics, good flame retardancy, simplicity, and durability [10,21-23]. Hence, the flexibility of these films with high thermal conductivity makes them ideal candidates for use in the electronics industry as thermal

interface materials, replacing current TIMs. These films thus, have gained speedy popularity in applications such as LED lighting, integrated circuit packaging, circuit and power transformer bonding, power transistors, connecting heat sinks, thermal management of batteries, and plasma displays[24-26]. Overall, the use of thermally conductive films is an exciting development in the field of thermal management, providing a reliable and efficient solution to improve thermal conduction and dissipate heat energy in electronic packaging systems.

2.2.1 Thermal conductivity

Thermal conductivity (TC) is a fundamental property that characterizes a material's ability to conduct heat in unit time, unit thickness and in unit gradient change in temperature.

$$k = Qd/A\Delta T$$

Where; k = Thermal conductivity, Q = Heat flux or energy in joules per second, d = Distance between two planes, A = Cross-sectional area, ΔT = Change in temperature.

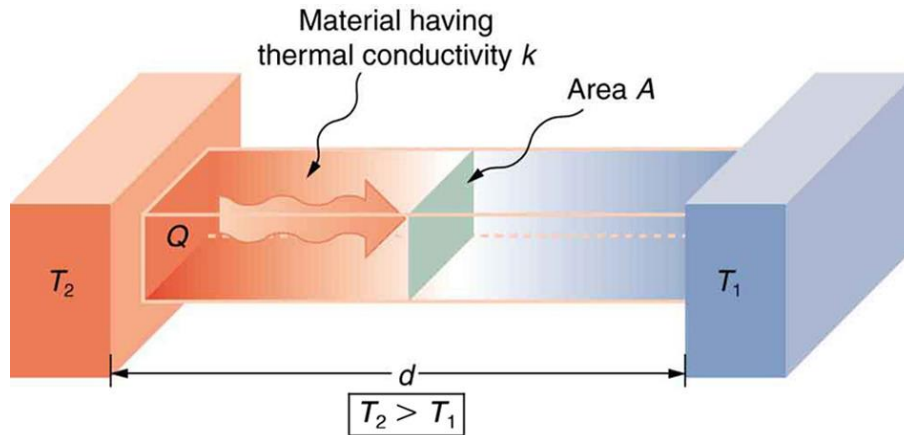


Figure 1: Illustration of heat conduction mechanism through any material. (Image Credit: Openstax College Physics)

Heat transfer can take place through various mechanisms, including radiation, convection, and conduction. It is well-established that, in most cases, thermal conduction serves as the predominant mode of heat transfer within solid materials. Thermal conductivity is the ability of an atom to

transfer its vibrational energy to adjacent atoms mainly through collisions, without changing the matter's state, and ultimately reach thermal equilibrium. From a fundamental perspective of quantum theory, this property is determined by many complex factors such as size, aspect ratio, thickness, alignment, and external temperature. Hence, this heat transfer is governed by the second law of thermodynamics, where it flows from high-temperature regions to lower-temperature regions [27-29]. TC is an intrinsic property of a material and is commonly measured in watts per meter Kelvin ($\text{W m}^{-1}\text{K}^{-1}$) using the International System of Units while the thermal resistance, which is the reciprocal of the thermal conductivity, is typically measured in Kelvin meters per watt (Km W^{-1}).

Before delving into the study of thermal conductivity in composites, it is essential to grasp the fundamental mechanisms underlying thermal conduction in crystalline materials. The materials known for their exceptional thermal conductivity, such as diamond, graphene, metals, silicon, and glass-ceramics, are characterized by a high degree of crystallinity. The pivotal role of crystalline structure in influencing thermal conductivity has been comprehensively elucidated by Toberer et al. [19] from a fundamental perspective. To provide insight into the fundamental aspects of thermal conduction [33], we employ **Figure 2** to illustrate the mechanism within a material possessing a crystalline structure.

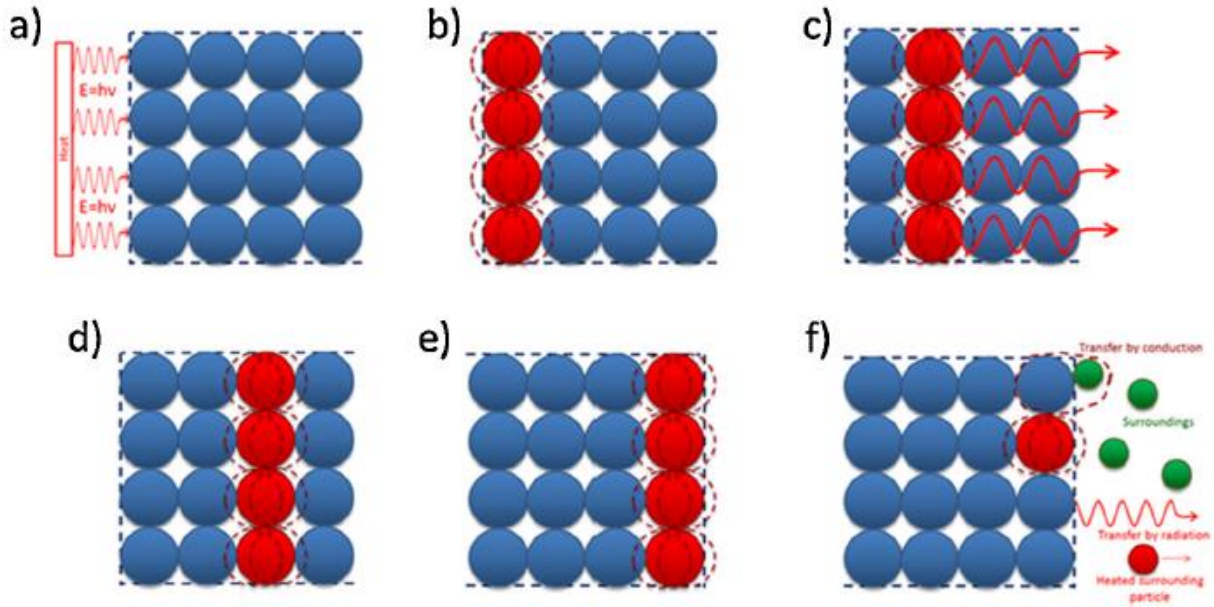


Figure 2. Thermal conductivity mechanism in a crystalline material. [32]

This simplification of the thermal conductivity mechanism within a perfectly crystalline, ordered, and rigid sample aids in visualizing the phenomenon:

- (a) Initially, thermal energy is conveyed to the surface atoms of the sample.
- (b) The surface atoms acquire vibrational energy.
- (c) Subsequently, the thermal energy of the surface atoms is transferred to adjacent atom(s) at a uniform rate, akin to a wave (depicted by red lines in the model of Figure 2).
- (d) The thermal energy then diffuses throughout the sample.
- (e) This thermal energy diffusion is characterized by a common vibrational mode, often referred to as a phonon, propagating throughout the entire crystal.
- (f) As heat reaches the opposite surface of the sample, it is subsequently partially disseminated through either conduction or radiation to the surrounding environment.

2.2.2 Mechanism of thermal conductivity in polymers

The heat diffusion mechanisms in polymers exhibit significant disparities between amorphous and crystalline polymers, as illustrated in **Figure 3**. In an amorphous and disordered polymer structure, unlike the compact lattice of a crystalline one, heat propagation follows a distinct pattern. Initially, thermal energy reaches a surface atom or monomer nearest to the heat source. Subsequently, this heat transfers to adjacent atoms and continues along this chain. Unlike the wave-like propagation observed in crystals, heat diffusion in polymers occurs at a much slower pace. This results in disordered vibrations and rotations of all atoms within the polymer, scattering them across neighboring chains.

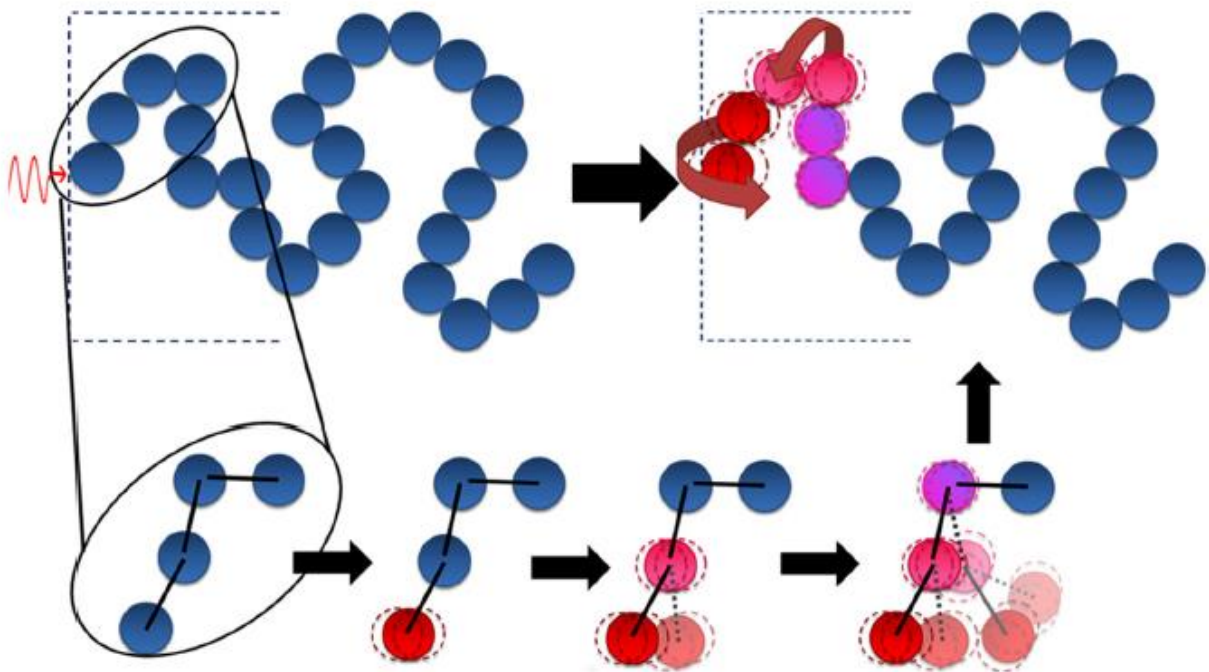


Figure 3. Thermal conductivity mechanism in an amorphous polymer. [32]

Figure 4 provides a visual representation of the contrasting thermal conductivity between excellent and poor thermal conductors, such as metals and polymers, based on their structural characteristics. To comprehend this disparity, we can liken these materials to Newton's pendulum.

A well-ordered Newton pendulum aptly symbolizes crystalline materials, while a disordered pendulum represents amorphous polymers. This depiction delves deeper into the vibrational behavior of particles within both structures. In an ordered structure (a), the initial vibration swiftly spreads to the opposite face. In contrast, the initial kinetic energy disperses primarily among the atoms in the disordered structure (b), resulting in vibrational motion for each particle.

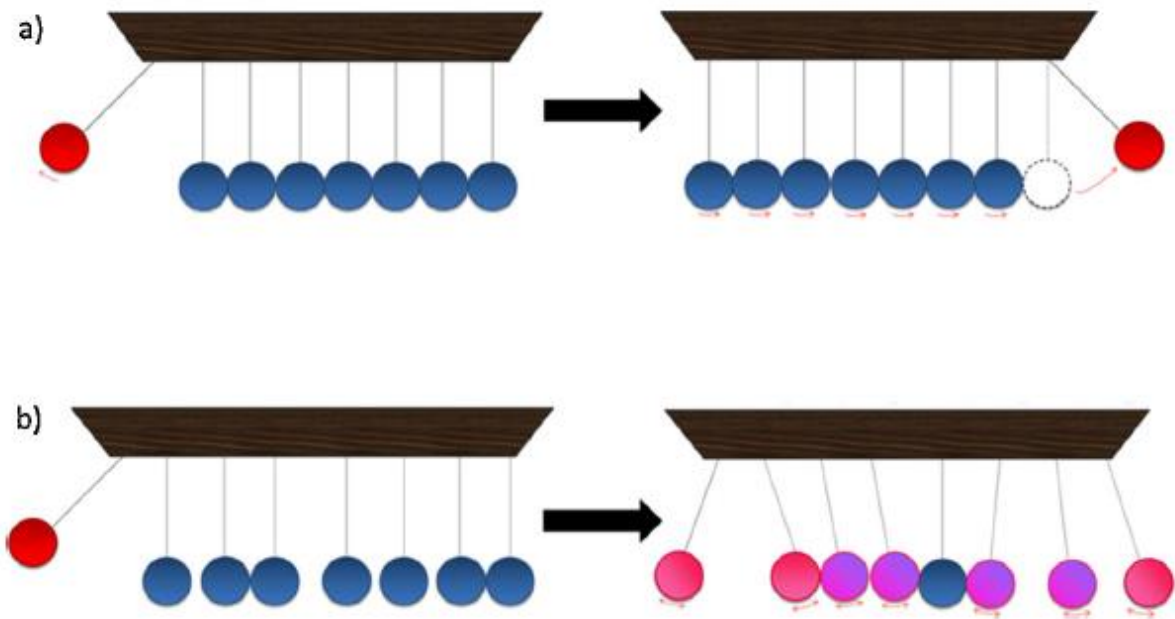


Figure 4. Schematic comparison by the Newton pendulum of thermal conductivity in crystalline materials (a) and polymers (b). [32]

Concerning thermal conductivity, it is logical to infer that a polymer's morphology is not conducive for efficient thermal conductivity by conduction only, this is due to the amorphous characteristics of polymer. The amorphous nature of polymers can be likened to a combination of numerous defects that impede heat transfer. Polymer chains lack the organization found in crystals, hindering the rapid transmission of thermal energy across the polymer sample. Amorphous polymers, such as epoxy resins, lack a single directional orientation and exhibit more random alignment, contributing to what we describe as "thermal resistance" – a term encompassing all phenomena

that impede thermal conductivity and slow the diffusion of heat. Additionally, fundamental factors like anharmonicity, varying particle sizes, and binding energy further account for the weak thermal conductivity exhibited by polymers.

2.2.3 Mechanism of thermal conductivity in polymer composites

One of the most promising ways to improve the TC of amorphous organic materials is to incorporate highly thermally conductive fillers into the insulating polymer matrix. However, calculating the TC of filler/polymer composites can be highly complex because it depends on several factors, including the filler network, filler structure(aspect ratio and size), filler dispersion, filler alignment, interfacial thermal conductance, and the intrinsic thermal conductivity of the filler[20]. Since, the thermal conductivity of the polymer composites is dominated by the filler, it is crucial to optimize these parameters during the processing of thermally conductive polymer systems. In terms of filler network, a continuous and integrated filler network can accelerate heat flow and transfer with less phonon scattering, as depicted in **Figure 5(a)**. In contrast, a discontinuous network would result in a large amount of phonon scattering at the filler/matrix interface due to the acoustic mismatch between different atoms, as illustrated in **Figure 5(b)**. Hence, in order to enhance the thermal conductivity of polymeric composites, it is essential to optimize the filler structure, including its size and aspect ratio, and the filler dispersion. So, therefore, by arranging the fillers to form a thermally conductive network in the polymer matrix, the thermal conductivity can be substantially improved and thus, the correct optimization of filler parameters and its network in polymer plays a crucial role in improving the thermal conductivity of filler/polymer composites.

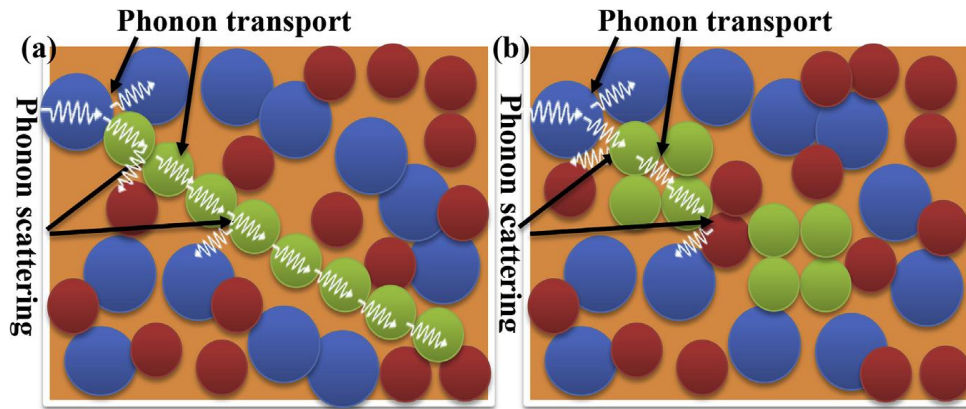


Figure 5. (a) Thermal conduction mechanism in the crystalline polymer nanocomposites with a continuous filler network; and (b) thermal conduction mechanism in crystalline polymer nanocomposites with a discontinuous filler network. Here, the crystalline fillers are represented by the green balls whereas, the others represent the polymer atoms [142]. (Reprinted with permission from Elsevier, copyright 2019)

2.2.4 Role of Interface

The interface plays a pivotal role in determining the overall properties of thermally conductive polymer composites, setting them apart from alloys. It acts as a crucial barrier for thermal conduction, influencing heat transfer across interfaces. This interface is distinct in its nature, representing a nanometer-scale phase with varying structures contingent upon the dispersed phase, i.e., the thermally conductive fillers. This interface phase, often referred to as the interface layer, consists of several distinct parts:

1. **Original Contact Area:** This is where the polymer matrix initially comes into contact with the thermally conductive fillers.
2. **Solid Solution Layer:** This layer forms through the diffusion process between the polymer matrix and the thermally conductive fillers.

3. **Surface Coating Layer:** Introduced by surface treatments of the thermally conductive fillers and serves various purposes.

As a result of these complexities, the chemical composition and structures at the interface are intricate. The interface's roles and effects are primarily manifested in three key aspects:

1. **Transfer Effect:** The interface serves as a bridge between the polymer matrix and the thermally conductive fillers, ensuring the continuity of these components. This facilitates the efficient transfer of properties between them.
2. **Blocking Effect:** A well-designed interface can hinder crack propagation and mitigate stress concentration, enhancing the overall mechanical integrity.
3. **Scattering and Absorption Effects:** The interface possesses the capability to scatter and absorb various waves, including light waves, sound waves, and thermoelastic waves.

When it comes to thermal conduction in polymer composites, phonon scattering at the interface results in substantial heat loss as heat flux traverses it. This decrease in thermal conductivity (λ) due to the interface is commonly referred to as Kapitza thermal resistance. This thermal resistance primarily hinges on the molecular forces between the polymer matrix and the thermally conductive fillers. The strength of these molecular forces directly influences the thermal conduction process, particularly the coupling effect between the thermally conductive fillers and phonons. Depending on the types of molecular forces involved, this interaction can be categorized into van der Waals forces, covalent bonds, and non-covalent bonds.

2.3 Thermally conductive three-dimensional (3D) framework materials

Thermally conductive three-dimensional frameworks have recently been developed for their usage in thermal management applications with their sort out characteristics. These frameworks are expected to yield significant findings for their use in thermal management, particularly as

TIMs, TMMs, phase-change materials, and thermally conductive structures such as 3D framework, foams, and sponges. Typical 3D networks include the segregation of thermally conductive 1D and 2D fillers in a polymeric system to attain respective properties.

Thermally conductive 2D filler-based 3D frameworks are a type of composite material that are designed to achieve high thermal conductivity with the material, composed of two-dimensional (2D) filler materials, such as boron nitride and graphene that are integrated into a three-dimensional (3D) framework. The resulting structure is highly porous with changeable porosity, with a large surface area-to-volume ratio, which allows for efficient transfer of heat. In terms of 2D filler networks, Carbon-based 3D framework with hierarchical anisotropic architectures are the most commonly used structures in the field. These 3D frameworks consist of a 3D framework in which the nanofiller is segregated, and the elements of this framework are composed of interconnecting nanosheets or nanofibers that are frequently aligned or oriented. This approach is aimed at achieving unique properties such as low density, high porosity, and super elasticity[34-36]. Typically, this self-organized 3D structuring is created by a phase-separation process, such as freeze-drying [37,38], or by other means of segregation[39]. Researchers have been focusing on constructing highly porous 3D-skeleton structures with aligned thermally conductive fillers such as graphene and boron nitride[40]. These porous microstructures aid in the infiltration and intercalation of inserted polymer chains, resulting in increased thermal conductivity of the entire 3D framework [19,39]. However, the challenge of achieving both high thermal conductivity and high electrical insulation values remains. Despite this challenge, further investigation into thermally conductive 3D structures could lead to the development of low-cost, highly thermally conductive components that are easier to fabricate and scale up than conventional phase-change and thermal interface materials, reshaping the electronics industry.

2.3.1 Thermally conductive aerogel 3D scaffold structure

3D framework are exceptional materials that have a perfect 3D interconnected design, characterized by tenuous networks of nanosheets or filaments. These materials are typically manufactured using various techniques such as sol-gel, freeze-drying, and phase-separating and drying techniques [35,38,41-44]. 3D framework possesses physical properties such as an extraordinarily high specific surface area, great flexibility, low density, variable tunable porosity, low dielectric constant, and low thermal conductivity. The advantageous physical features of 3D framework make them highly promising for a variety of applications. They can be used as adaptable absorbent materials [45], for electromagnetic shielding [46], thermal insulation [47], and as wearable pressure-sensing materials [48]. Furthermore, 3D framework can be modified into highly thermally conductive 3D structures with excellent electrical insulation, making them highly suitable for use in thermal management in the electronics industry as thermal interface materials or phase-change materials [38,43,49-51]. Currently and in the future, the focus with the researchers is on developing several types of thermally conductive 3D aerogel frameworks, including epoxy-infiltrated or cellulose-based composite 3D framework, carbonaceous and boron nitride nanomaterials, and fibrous materials as fillers materials. These materials are being investigated to improve the thermal conductivity of 3D framework and make them suitable for a range of applications. Ongoing research and development in this area will likely lead to further improvements in their thermal and electrical properties, expanding their potential applications even further.

The development of three-dimensional (3D) graphene-based monoliths has been the subject of numerous research attempts, with the aim of meeting the requirements of thermal interface materials (TIMs) that have both high in-plane and through-plane thermal conductivity (TC)

[39,52,53]. Such monoliths have been fabricated from 2D graphene materials, in the form of 3D framework with a honeycomb-like structure, to overcome the high anisotropy of horizontally or vertically oriented graphene materials[54-56]. In addition to their use as TIMs, 2D graphene materials have also been investigated for their potential as phase-change materials where, graphene foam or aerogel has been developed as thermal switch materials, with the transition of graphene from being thermally conductive to thermal insulating being utilized in applications [57]. Moreover, the use of graphene 3D aerogel framework as hybrid materials with metals has also been under investigation [58].

The formation of self-organized 3D structures is commonly achieved through a phase-separation process, such as freeze drying, or through other forms of segregation. By employing a directed process, such as a thermal gradient or an external force field, including gravitational, magnetic, or electrical fields, anisotropic 3D architectures can also be created [59]. During the structuring process, 2D particles self-align and orientate themselves to form the walls of the resulting 3D structure, facilitated by surface tension, van der Waals, or other forces. As a result, a highly directed graphene aerogel with a hierarchical structure and specific direction is created. The aligned graphene sheets may fully exploit their intrinsic in-plane thermal conductivity, producing a highly efficient thermal conduction network compared to randomly distributed graphene sheets in isotropic 3D framework. Several techniques have been employed to produce such structures, such as hydrothermal reduction and aligning graphene oxide (GO) nanosheets by freeze drying, followed by graphitization at 2800°C, as demonstrated by Wenya et al. [36]. In this study, the resulting 3D graphene networks were impregnated with silicone rubber (**Figure 6**) and instead of van der Waals forces, the researchers proposed that the nearby graphene sheets were joined by chemical covalent bonding. Hence, through vacuum impregnation and high-pressure treatment,

the graphene was thoroughly reduced, and the defects were completely removed while previous studies on the graphitization of graphene had mainly focused on removing the oxygen-containing functional groups and utilizing van der Waals forces for connecting adjacent graphene sheets [60].

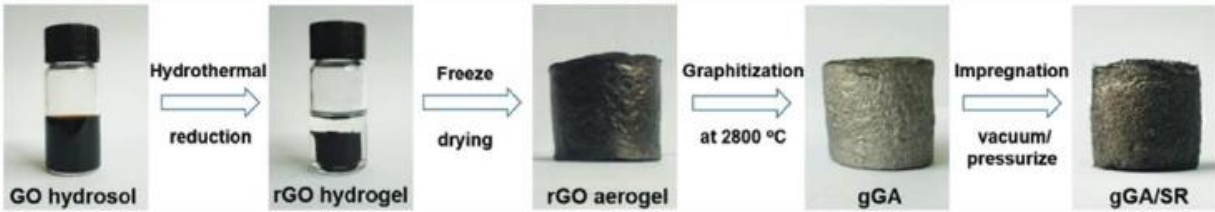


Figure 6. Fabrication process of graphene/silicone-rubber-based thermally conductive aerogel. (Reprinted with permission from John Wiley and Sons, copyright 2019). [36]

In summary, the development of 3D graphene-based monoliths for use as TIMs and phase-change materials has been the subject of extensive research. The use of thermally conductive polymers to fill the porosity of these materials has been shown to significantly improve their TC and mechanical stability. Ongoing research in this area is expected to yield further improvements and applications for these materials in various fields.

In recent years, an easy and scalable method for fabricating thermally conductive 3D-framework polymer composites has been reported through in-situ fabrication of a connected conducting composite network [61-63]. In this procedure, a monolith framework is created by first precoating polymer powders with a thermally conductive filler, and then hot-pressing and compressing them. For instance, Lin's group fabricated graphene/polymer composites by coating graphene on polymer powder first, then drying and hot-pressing it to form a 3D scaffold structure [64](See **figure 7**) . This creates a continuous graphene-conducting polymer matrix network that can be employed with most thermoplastic polymers, such as polyethylene (PE), polypropylene (PP), polyvinyl alcohol (PVA), and polyvinylidene. The researchers achieved a TC of ~ 0.8 W/mK at 5 wt.% filler loading of graphene in PP. **Figure 7** shows that the TC of PP composites with graphene

network connections, built in situ, was far more substantial than those of composite materials with randomly displaced/positioned graphene in a PP polymer. This method thus, allows for distinctive composite structures with superior properties to be formed. Using this method, Wang's team developed a highly organized 3D CNTs/polystyrene composites framework for achieving high thermal conductivity (TC)[65]. By coating the polystyrene (PS) particles with multi-walled carbon nanotubes (MWCNTs) and subjecting them to compression and heat-treatment processes, a 3D CNT interconnected structure was created in the polystyrene matrix. The composites displayed a continuous phase structure of the PS phase and MWCNT network, incorporating an intact, uniform, and well-defined 3D network of MWCNTs.

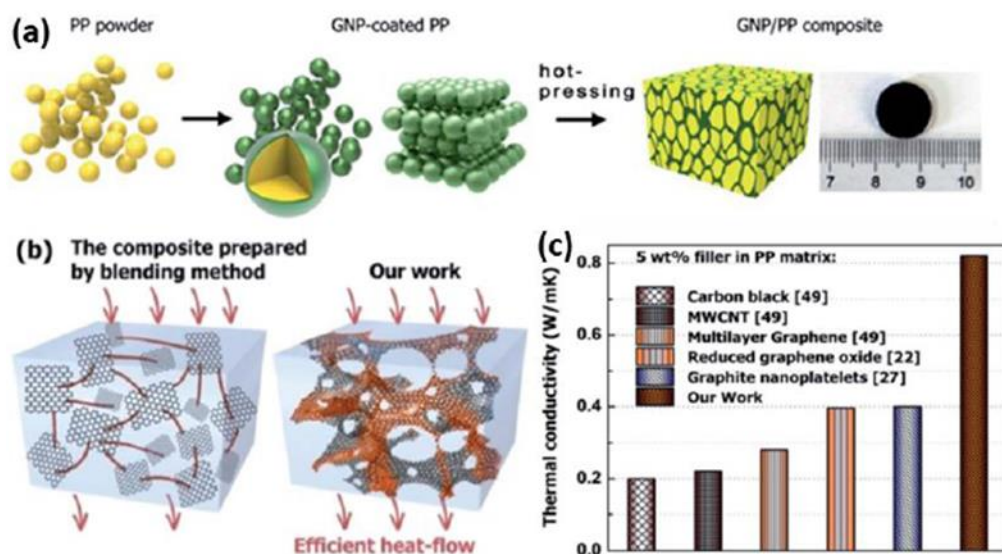


Figure 7. Schematics of the fabrication process of GNP/PP framework composites. (a) Fabrication of GNP-coated / PP composites; (b) Diagram comparing effective thermal conduction through a network of connected graphene to that through dispersed graphene; (c) Comparison between the TC values of these composites and randomly dispersed filler composites with the TC of GNP/PP composites (Reprinted with permission from Royal Society of Chemistry, copyright 2017) [64]

Boron nitride (BN), another type of 2D material, has gained considerable attention in the development of thermally conductive 3D framework, either as a BN/polymer cake framework or as an infiltrated structure with an external polymer[66-68]. BN can be exfoliated into boron nitride nanosheets (BNNS), which are 2D nanosheet structures that possess remarkable thermal conductance characteristics. These nanosheets have a graphene-like crystal structure and exhibit exceptional mechanical stability and high thermal conductivity ranging from (600 to 2000 W/mK). Additionally, they have a low coefficient of thermal expansion, excellent electrical insulation, antioxidative properties, and high thermal stability. The utilization of boron nitride (BN) as a thermally conductive aerogel has gained considerable attention in recent years due to its unique characteristics. A 3D interconnected network structure based on BN nanosheets can improve the thermal transfer efficiency per unit mass (i.e., TC) and provide an ideal material for a range of applications as discussed before. Hence, to enhance the TC of BN 3D framework, researchers have explored the use of boron nitride nanosheets (BNNs) in composite structures. Wang et al. [69] fabricated BN/cellulose nanofiber (CNF) composite structures and varied the BNNs content in the CNF. They fabricated the paper using two methods: simple blending and the aerogel 3D-skeleton approach. The aerogel-based nano-paper demonstrated an improvement in TC (1.68 W/mK) compared to the blended nano-paper (0.87 W/mK) with 50 wt% BNNs loading, as illustrated in **Figure 8a**. The higher TC of the 3D framework could be attributed to the BN nanosheets spreading more uniformly inside the cellulose matrix compared to the paper-blending process. Compressing the porous 3D framework reduced the amount of trapped air bubbles/pores, allowing for better phonon transfer inside the composite system, as the boron nitride nanosheet contacts are closer together. The volume electrical resistivity of the BNNs/CNF nano-paper ($3.8 \times 10^{14} \Omega \text{ cm}$) (**Figure 8d**) was also found to be higher than that of pure CNF ($2.6 \times 10^{14} \Omega \text{ cm}$), indicating the material's

potential as an electrical insulator. Moreover, the 3D framework demonstrated high strength, low thermal expansion coefficient, and environmental friendliness, making them ideal for a range of applications. **Table 1** shows the detailed information about the research work done on thermally conductive 3D framework/foams in recent years with respect to increase in TC at low or optimum filler loading concentrations where polymer is utilized as matrix material for the bridging effect in terms of enhancement of thermal conductivity and when there is a need to change or tune electrical resistivity.

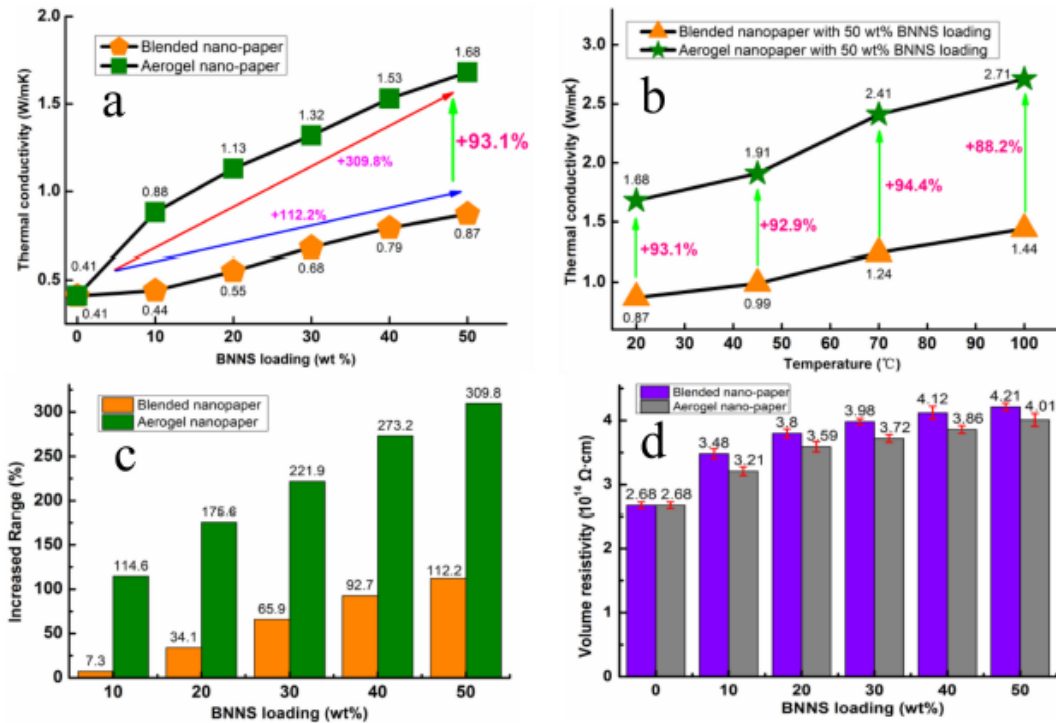


Figure 8. Blended nano-paper vs. aerogel nano-paper: **(a)** thermal conductivities with different BN loading content; **(b)** thermal conductivities at elevated temperatures with BN loading content of 50wt.%; **(c)** 3D framework' composite enhancement factor; **(d)** electrical volume resistivity[69].

Table 1. Thermal conductivities of various 3-D frameworks mentioned in the literature. Data is taken from my article published in Polymers [39]

Polymer matrix	Filler loading	Type of 3-D structure	Thermal conductivity, W/mK (Through-plane)	Thermal conductivity, W/mK (In-plane)	Technique for measuring thermal conductivity	References
Polydimethylsilo- xane (PDMM)	11.62 wt.% Graphene	Graphene foam	1.62	28.77	Laser flash	[70]
-----	Density of graphene aerogel 150.49 mg cm ⁻³	Graphene 3D framework films	0.7	53.56	Laser flash	[42]
Paraffin wax	-----	Polyamic acid/ graphene oxide aerogel	2.68	8.87	Laser flash	[71]
-----	5 wt.% graphene	Graphene 3D framework	-----	4.28	Laser flash	[72]
-----	100 wt.% boron nitride nanosheets	Boron nitride 3D framework	-----	25.2	-----	[73]
Polyethylene glycol	-----	boron nitride 3D framework	-----	0.67	Laser flash	[74]
Poly vinyl alcohol	0.12 wt.% boron nitride nanosheets	Boron nitride/polyvinyl alcohol hydrogels	-----	0.68	Transient plane source method	[75]
Poly vinyl alcohol	67.7 wt.% boron nitride	Boron nitride/polyvinyl alcohol 3D framework	1.1	10.04	Laser flash	[76]
Cellulose nanofiber	50% wt.% boron nitride	Boron nitride (BN)/cellulose nanofiber 3D framework	-----	2.71	Laser flash	[77]
Polydimethylsiloxane (PDMS)	3.32 wt.% reduced graphene oxide (rGO)-cellulose	Reduced graphene oxide (rGO)/cellulose polydimethylsiloxane	-----	0.65	Laser flash	[78]

Cellulose	33wt.% Boron nitride/cellulose	Boron nitride–nanosheet/cellulose nanofiber aerogel	-----	0.57	Hot wire transient method	[79]
Parrafin wax	1.23 vol. % graphene	Ultrathin-graphite foams	-----	3.44	Steady state method	[80]
Polydimethylsiloxane (PDMS)	25.4 wt. % boron nitride	boron nitride/PDMS	-----	1.5	Laser flash	[67]
Polyvinyl alcohol	66 wt.% boron nitride	BN/PVA aerogel cake composite	0.61	0.76	Laser optical thermal scanner	[20]

2.3.2 Epoxy Infiltrated 3D framework

Various strategies and fabrication methods have been developed by the researchers for the augmentation of TC in 3D framework as discussed in the prior section. Other than this, scientists developed another strategy to increase TC with the use of thermoset polymers like epoxy resins. The highly porous structure of 3D framework was utilized for our own benefits with the infiltration of TC epoxy inside it. The self-assembled hierarchical 3D filler networks with porosity can be fabricated as segregated or highly segregated structures containing large backfill space/voids in the matrix system. However, due to their large porosity, the TC of 3D monoliths is extremely low. In order to fill the porosity, pores are impregnated with thermally conductive polymers with the aim is fill the air gaps with conductive long chains and construct thermally conductive pathways or channels inside for continuous phonon propagation, resulting in an increase in TC. This also though, provides higher mechanical stability without the collapse of the structure. For instance, substantial research work has been done on the infiltration of polymers in the graphene foams/3D framework [40,60,81,82]. In one of the studies, highly thermally conductive 3D structures were

developed by infiltrating epoxy resin (EP) into graphene-based frameworks, resulting in the creation of polymeric nanocomposites with increased phonons transport characteristics. The high thermal conductivity of these structures was due to the strong connectivity of graphene planes with the chains of polymers. To achieve this, Weng et al. employed a simple yet effective process, which involved thermal-shock exfoliation of a graphene oxide sheet, followed by the self-polymerization of silanol inside the resulting graphene frameworks (GFs) [83]. The self-polymerization of silanol resulted in the surface modification of graphene by the silanol group (see **figure 9**). The silanol group then underwent a chemical reaction, leading to the conversion of silanol into siloxane, which cross-linked with the graphene frameworks to form siloxane networks (SGF) with a $-\text{Si}-\text{O}-\text{Si}-$ molecular network structure through self-polymerization. The resulting GFs were compressed, and the films generated a microporous honeycomb structure with pore sizes varying from several to tens of micro-meters, which was comprised of horizontally aligned and locally attached graphene sheets. This unique structure allowed for the effective and efficient transport of phonons and electrons, resulting in a highly anisotropic, continuous network.

To create the EP/SGF composite, the epoxy resin was infiltrated into the GF and compressed to remove any voids and create a denser structure for enhanced thermal conductivity, followed by thermal curing. The siloxane molecules in the composite system were able to immobilize the graphene sheets in the epoxy matrix, thereby reducing the thermal resistances in the composite and constructing siloxane molecular bridges inside the GF structure. Consequently, the in-plane and through-plane thermal conductivity (TC) values of the EP/SGF composites with a GF loading concentration of 20.2 wt.% reached 54.2 and 1.62 W/mK, respectively, due to improved GF quality and significantly decreased inter-sheet and interfacial resistances. Furthermore, the porosity of these 3D framework could be modified, resulting in different structural densities and varying

amounts of filler in the final 3D composite material. These findings are crucial for the development of advanced materials with superior thermal conductivity, which have significant applications in thermal management, electronic devices, and energy storage systems.

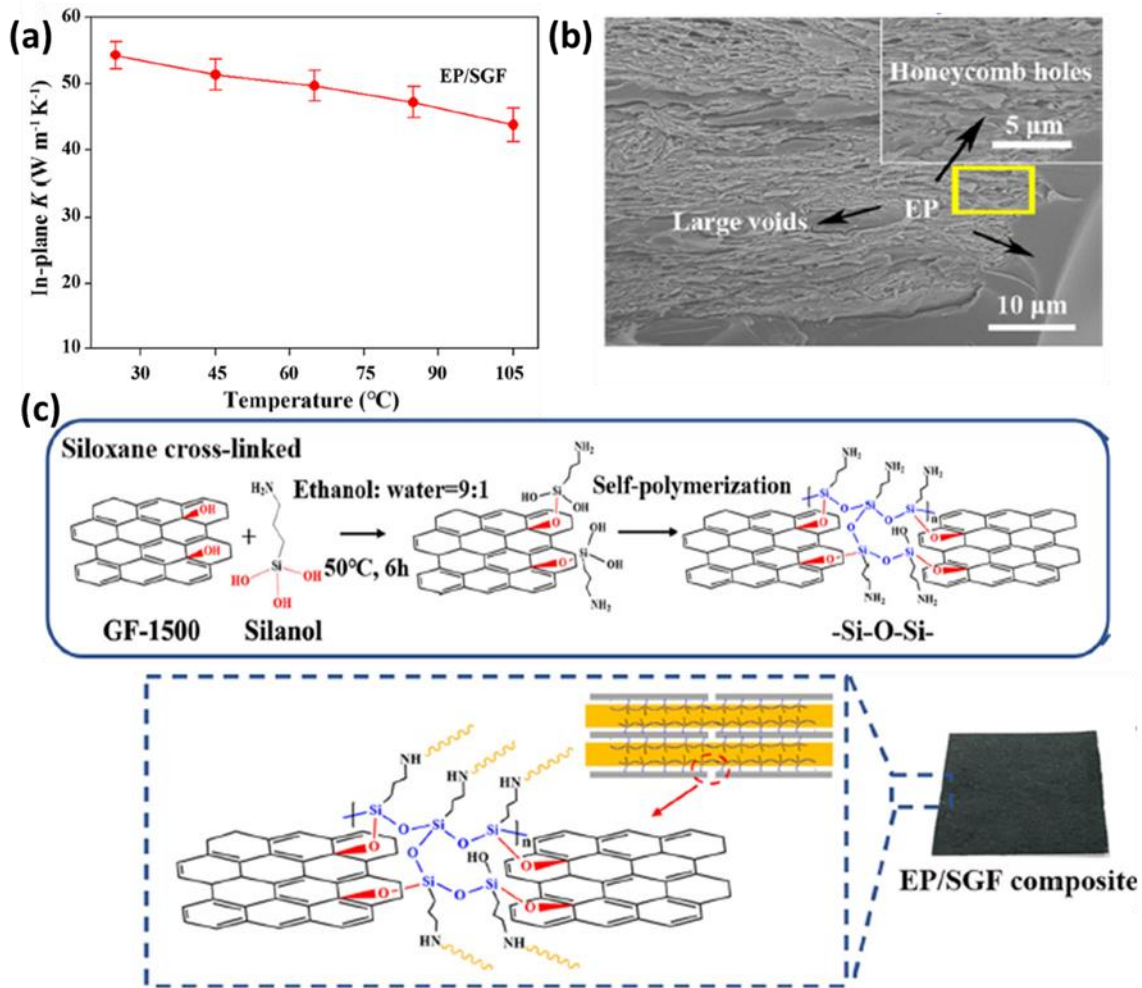


Figure 9. (a) Thermal conductivity as a function of temperature for EP/SGF composite at a loading concentration of 20.2 wt.% graphene; (b) Cross-sectional SEM image of EP/SGF. The inset shows EP-filled honeycomb holes [83]; (c) Schematic diagram for synthesizing EP/SGF composites (Reprinted with permission from Springer, copyright 2021).

2.4 Thermally conductive polymer films/papers

As an alternative to traditional thermal interface materials (TIMs), thermally conductive films have gained significant attention in recent times. These films are being increasingly preferred over their counterparts owing to their unique properties and suitability for various applications. Typically, these thermally conductive thin films are referred to as adhesive tapes, composed of thermoplastic, elastomer or other adhesive polymers, and offer a clean alternative solution to the existing thermal interface materials. As the demand for slimmer products with high-performance heat dissipation characteristics increases, highly thermally conductive films/papers have become an urgent requirement for the electronic industry. These films possess excellent characteristics such as high thermal conductivity, enhanced mechanical properties, electrical insulation, good flame retardancy, and ease of usage and durability for extended periods [84-88]. The exceptional flexibility of these films with high thermal conductivity make them ideal candidates for use in the electronics industry as thermal interface materials and an alternative to traditional TIMs. Thanks to their unique features, these films are becoming increasingly popular for various applications in the electronics industry. These applications include LED lighting, circuit, and power transformer bonding, connecting heat sinks, power transistors, integrated circuit packaging, thermal management of batteries, and in plasma displays [84,89-91]. As a result, thermally conductive films are gaining rapid popularity over conventional TIMs whereas, the overall, the use of thermally conductive films offers an excellent solution for high-performance heat dissipation characteristics and the urgent demand for slimmer products with powerful features as per the requirements of the electronics industry. These films, though possess unique properties such as high thermal conductivity, ease of usage, and durability, making them an ideal alternative to traditional TIMs

for various applications in the electronics industry. Typically, papery/film-like thermally conductive composites reported in literatures can be categorized into three types;

- (i) Polymer composites/nanocomposites,
- (ii) Carbonaceous materials with/without polymers,
- (iii) Carbon/ceramic materials.

Hence, these paper-like films are an advanced version of conventional thermal heat spreaders/thermal interface material with thickness ranging from mm to μm altogether.

In my dissertation, I will focus on polymeric based composite films with incorporated TC fillers. Typically, the thermal conductivity of conventional paper and plastics are relatively low, 0.03W/mK and 0.23W/mK, respectively, for their use as substrates in portable electronic systems [92,93]. Therefore, the need to design and fabricate papers and thin films with higher thermal conductivity is of great importance. Usually in most cases, solely graphene based thermal papers/films exhibit the highest thermal conductivity but they are not thought of promising materials when used in real based applications due to their brittleness and electrical conduction[94]. Hence, to solve this issue, polymers are introduced alongside the filler material to mitigate the weakness. Among the polymers; Cellulose, Polyimide (PI), natural rubber (NR) are considered important for practical applications.

Polyvinyl alcohol (PVA) is often utilized as a polymer matrix for thermally conductive composite films with several different fillers. Boron nitride (BN), also known as “white graphene”, is widely used in thin films/papers with PVA as matrix [95,96] as it has tremendous potential for thermal management applications due to its inherent high thermal conductivity combined with high electrical resistance. In one such case, 30 wt% of BN was used with PVA as a matrix to achieve thermal conductivity as high as 18.63 W/mK. The preparation method included ball

milling technique, directional freeze-drying, and electrospinning with hot-pressing in the later stages [96]. Most recently, the incorporation of 90 wt% content of surface-modified BN in PVA resulted in an escalation of thermal conductivity value to 120 W/mK, which is nearly about 100 times greater than of the pure PVA film[91]. The fabrication method was based on simple (Vacuum assisted filtration) VAF technique employed with the formation of layer-by-layer laminated nanostructures. Thus, very high thermally conductive films can be prepared by carefully varying the experimental conditions and BN-PVA weight ratio.

Biomimetic approaches generally offer more significant advantages over conventional. They provide high thermal conductivities with better mechanical properties and better electrical insulation characteristics. Besides, the functionalization of fillers could also lead to an increase in thermal conductivity in polymer composites. To make use of the aforementioned benefits, researchers motivated by the microstructure of natural nacre, fabricated a composite paper consisting of the hybrid of silver nanoparticles (Ag), boron nitride nanosheets (BNNS), and silicon carbide nanowires (SCNW) with PVA matrix [97]. Various samples of the functionalization of Ag on BN and Ag on SCNW as BNNS–Ag and SiCNW–Ag dispersions were homogenously mixed into the PVA aqueous solution. Subsequently, the mixtures were filtrated at slow pace to form free standing thermally conductive composite papers. The schematic diagram of the preparation of the samples is depicted in **Figure 10**. By experimenting with different weight and mole ratios, the best in-plane thermal conductivity achieved of these composite papers was 21.7 W/mK with a high filler loading concentration, when the weight ratio of BNNS–Ag to SiCNW–Ag was 85:10. In another study in this direction, BN were modified by silica nanoparticles to make a composite with PVA matrix. With the use of the Vacuum assisted filtration (VAF) technique, they observed the in-plane thermal conductivity of SiO₂@exfoliated h-BN/PVA composites to be 13.88 W/mK due

to the formation of a nacre-like structure. Moreover, BN functionalization also improved the storage modulus and the glass transition temperature[98]. In another research reported, by dispersing 10-50 wt.% of cellulose nanocrystal (CNC) as solid loading in PVA, bulk isotropic CNC-PVA films were prepared. These films exhibited an elevated in-plane thermal conductivity of 3.45 W/mK, which is relatively better than the thermal conductivity of conventional flexible substrates being used [99]. Hence, based on these reports, it can be concluded that thermal conductivity of PVA based composite films can be significantly enhanced by careful optimization of supporting composite material's loading concentration and surface functionalization.

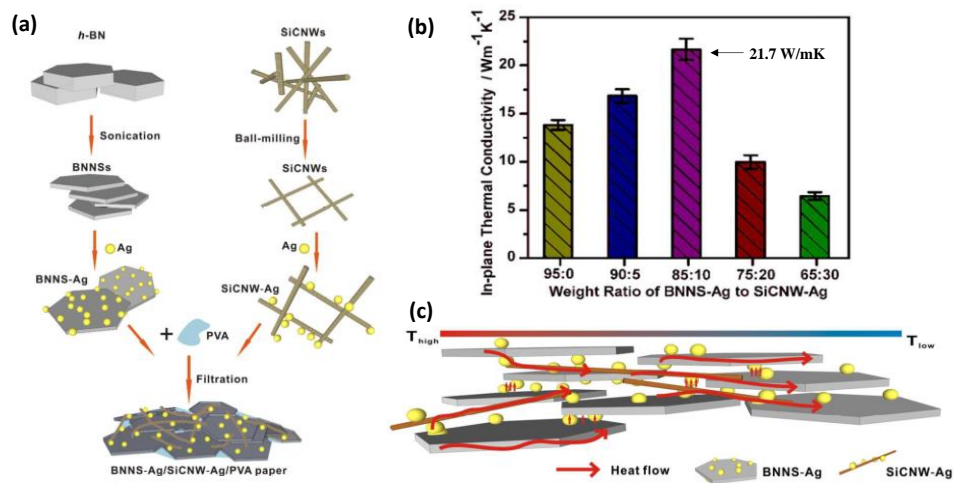


Figure 10. (a)Preparation procedure;(b) In-plane thermal conductivity;(c) Proposed mechanism model of thermal conduction in BNNS-Ag/SiCNW-Ag-PVA composite film. (Reprinted with permission from [97] Copyright (2020) American Chemical Society).

Typically, researchers in the past few years focused on the incorporation of higher filler loading concentrations inside the polymeric systems for the fabrication TC films/papers (see **Table 2**). In terms of achieving higher TC, the films display good reasonable TC but the mechanical stability and flexibility of the films are compromised. At certain concentration, the films become more

prone to brittleness and hence, these films could no longer be beneficial for TMMs or TIMs for practical industrial usage. So, therefore, to address this conundrum, we manage to employ low filler loadings < 10 wt.% inside polymeric system to sustain the flexibility required for thermal management-based applications (See **chapter 4**). The idea is to gain maximum TC at such low filler loading content without sacrificing the necessary flexibility. In regard to this, some researchers managed to fabricate thermally conductive polymer films with the use of low filler loading concentrations and managed to achieve high TC and simultaneously achieved flexibility (See **table 3**). The low filler loading approach has several advantages over high filler loading methods, where a large amount of graphene is added to the polymer matrix. Firstly, it allows for a more homogenous dispersion of graphene in the polymer matrix, which results in better thermal conductivity. High filler loading can lead to agglomeration of graphene particles, which can cause a reduction in thermal conductivity. Secondly, the low filler loading approach is cost-effective as the amount of graphene required is minimal. This makes the method more practical for industrial applications where cost is a significant factor. However, the use of low filler loading can also have limitations. The increase in thermal conductivity is not as significant as in high filler loading methods, which can limit the applications of these composites. Hence, researchers are finding an optimum loading filler concentration in which they can increase the TC to a maximum level and to essentially carefully balance the amount of graphene added to the polymer matrix to achieve the desired thermal and mechanical properties.

Table 2. Thermally conductive polymer composites films based on higher filler loading concentrations.

Polymer composites films	Filler content, wt.%	Thermal conductivity, W/mK	References
BNNS/PVA	94	6.9	[100]
BNNS/PVA	90	120	[26]
BNNS/PDDA	90	212.8	[21]
f-BNNS/CNF	70	30.25	[101]
BNNS/GO	95	29.8	[102]
BNNS–OH	100	58.3	[103]
CMC/SiC@Ag	>65	34	[104]
SiC@Ag/BNNS@Ag/PVA	95	21.7	[105]
PDA@BNNS/CNC	94	40	[106]
BNNS/TPU	95	50.3	[107]
F-graphene/PVA	93	61.3	[108]

Table 3. Thermally conductive polymer composites films based on lower filler loading concentrations.

Polymer composites films	Filler content	Thermal conductivity, W/mK	References
AgNPs@GNPs/PVA	10 wt%	8.45	[109]
RGO/PVA	5 wt%	4.00	[110]

RGO@carbon nitride	10wt%	6.08	[111]
RGO/Silicon rubber	2.53 wt%	2.03	[112]
GNP/PS	9.2 wt%	0.90	[113]
Polyimide/SiCNWs-GSs	7 wt%	0.57	[114]
BNNS-graphene framework/polyamide-6	1.6 wt + %/6.8 wt %	0.891	[115]

2.5 Conclusion

Numerous research endeavours have been dedicated to the development of polymeric materials that exhibit thermal conductivity, enabling their application in industries where efficient heat dissipation is of paramount importance. Achieving high thermal conductivity has been accomplished by incorporating higher filler loadings of thermally conductive (TC) fillers into the polymer matrix. However, this approach is not suitable for industrial use due to the detrimental effects it has on mechanical properties, such as stiffness, and its high cost. Conversely, researchers have shifted their focus towards utilizing lower TC filler loadings within polymers. Despite their efforts, they have been unable to achieve a comparable level of high thermal conductivity as that obtained with higher filler loadings. Consequently, there is a need to develop an optimal TC filler loading range for thermoset, thermoplastic, and elastomer-based polymers, which would enable a significant enhancement in thermal conductivity without compromising the mechanical properties. This development holds immense potential for industrial applications, as it would provide an ideal balance between thermal conductivity and material performance.

The upcoming chapters of my thesis showcase the experimental work conducted during my PhD, taking into account the limitations highlighted in the literature review. Throughout my research, I

focused on creating thermally conductive polymeric ceramic 3-D framework structures, also known as aerogels, employing various fabrication techniques like VAF, followed by meticulous polishing and compression to eliminate any potential presence of bubbles or air voids. Remarkably, I achieved high thermal conductivity without the need for polymer infiltration. While the 3-D structure polymer composite displayed commendable thermal conductivity and excellent electrical insulation properties, it did have certain drawbacks. Notably, it lacked mechanical flexibility and relied on relatively high filler loadings by weight. Consequently, I embarked on the development of thermally conductive polymeric thin films that addressed these concerns. These films feature optimized thickness, low filler loadings in the polymer matrix, exceptional mechanical flexibility, and outstanding thermal conductivity, making them exceptionally well-suited for use as thermal interface materials (TIMs) in the electronic industry. Conversely, when exploring under-filled materials as thermal management materials (TMMs), carbon nanotube (CNTs) based epoxy composites emerged as a promising avenue. These composites are characterized by very low filler loadings by weight, and they offer a combination of high thermal stability, elevated glass transition temperatures, and essential thermal conductivity. These attributes are crucial for electronic chips, enabling them to withstand mechanical stress even when exposed to temperatures near 100°C.

Chapter 3. Thermally Conductive Self-Assembled 3D BN-Based PVA Framework Nanocomposites

3.1 Introduction

This chapter discusses the increasing importance of thermal management in electronic devices due to miniaturization and integration and is based on my article published in *Polymers* [20]. The accumulation of heat reduces the dependability and performance of electronics, so the development of new materials with greater thermal conductivity is necessary. The passage specifically focuses on the study of continuous segregated thermally conductive filler networks, which have been found to be more effective at increasing thermal conductivity than random filler distributions [20]. Furthermore, it explains the importance of fabricating continuous heat conduction pathways and the characteristics of polymers that lead to higher thermal conductivities.

Thermal transfer efficiency is a critical factor when it comes to achieving high thermal conductivity in composite materials. The thermal transfer efficiency per unit mass is affected by interfacial thermal resistance, which means that this efficiency is greater in three-dimensional (3D) interconnected networks compared to two-dimensional (2D) or one-dimensional (1D) structures. This has been demonstrated in various studies, where the thermal transfer efficiency of 3D networks was found to be greater than that of 2D or 1D structures[116,117]. As a result, a 3D interconnected network is advantageous for achieving a high thermal transfer efficiency per unit mass, which in turn leads to an improvement in thermal conductivity. For instance, by putting together boron nitride nanosheets (BNNSs) in a 3D network structure, it is possible to create a material with 3-D skeletons frameworks with a high thermal transfer efficiency per unit mass. This makes it an effective way to improve the thermal conductivity of the material. In summary, a 3D

interconnected network structure is advantageous for achieving high thermal transfer efficiency per unit mass, which in turn improves the thermal conductivity of the material. Putting BNNSs together in a 3D network structure is an effective way to create a thermally conducting polymer composite material with high thermal transfer efficiency per unit mass.

3.2 Research objectives

The objectives of this research work are:

1. To fabricate 3D skeleton frameworks of boron nitride (BN) and polyvinyl alcohol (PVA) using varying stoichiometric ratios and weight loading filler concentrations.
2. To identify the optimum BN filler concentration in the thermoplastic PVA polymeric 3D system.
3. To utilize vacuum-assisted filtration (VAF) technique to self-assemble the fillers within the PVA matrix and to investigate this effect on the thermal conductivity of the polymer composites in both in-plane and through-plane directions.
4. To compare the thermal conductivity of the BN/PVA 3D framework composite with that of the pure PVA matrix.
5. To evaluate the potential of the 3D polymer composite as a unique material due to its high thermal conductivity of the BN/PVA framework without impregnation by any external polymer.
6. To check the values of electrical resistivity at various stoichiometric ratios of BN/PVA so that they can be tuned for specialized electronic applications.

3.3 Experimental

3.3.1 Materials

Boron Nitride (BN) powders with an average particle size of 10 μm , Polyvinyl alcohol (PVA) with an MW of 31,000–50,000, 98% hydrolyzed, and Diethyl glycol (DEG) were purchased from Sigma Aldrich Co., Ltd. (Burlington, MA, USA). None of the chemicals were further purified before usage.

3.3.2 Methodology

For the preparation of 15 wt.% PVA solution, PVA powder was dissolved in distilled water at a temperature of 105 °C with continuous magnetic stirring for a period of 1 hour. Following this, the PVA solution was mixed with 10 wt.% of Diethyl glycol (DEG) by stirring for 2 hours at 105 °C. For the synthesis of BN suspensions, different weight percentages of BN were dissolved in distilled water by mixing for 30 minutes via magnetic stirring, followed by a 3-hour bath sonication. Once the desired amount of BN suspension was obtained, it was added dropwise into the existing PVA suspension, followed by mixing for 1 hour at 105 °C. The resulting mixture was then poured onto a vacuum-assisted filtration technique machine. After filtration, the suspensions of PVA-BN 3D framework were dried at room temperature for 1 hour, followed by overnight heating at 60 °C and then vacuum drying for 2 days. Using the vacuum-assisted filtration technique, samples of PVA-BN 3D frameworks with densities of approximately 0.1 g/cm³ were fabricated with various BN to PVA ratios (9:1, 9:3, 2:1) following the aforementioned procedure. After that, the samples were polished well with the surfaces were smoothened. **Figure 1** provides a graphical representation of this process.

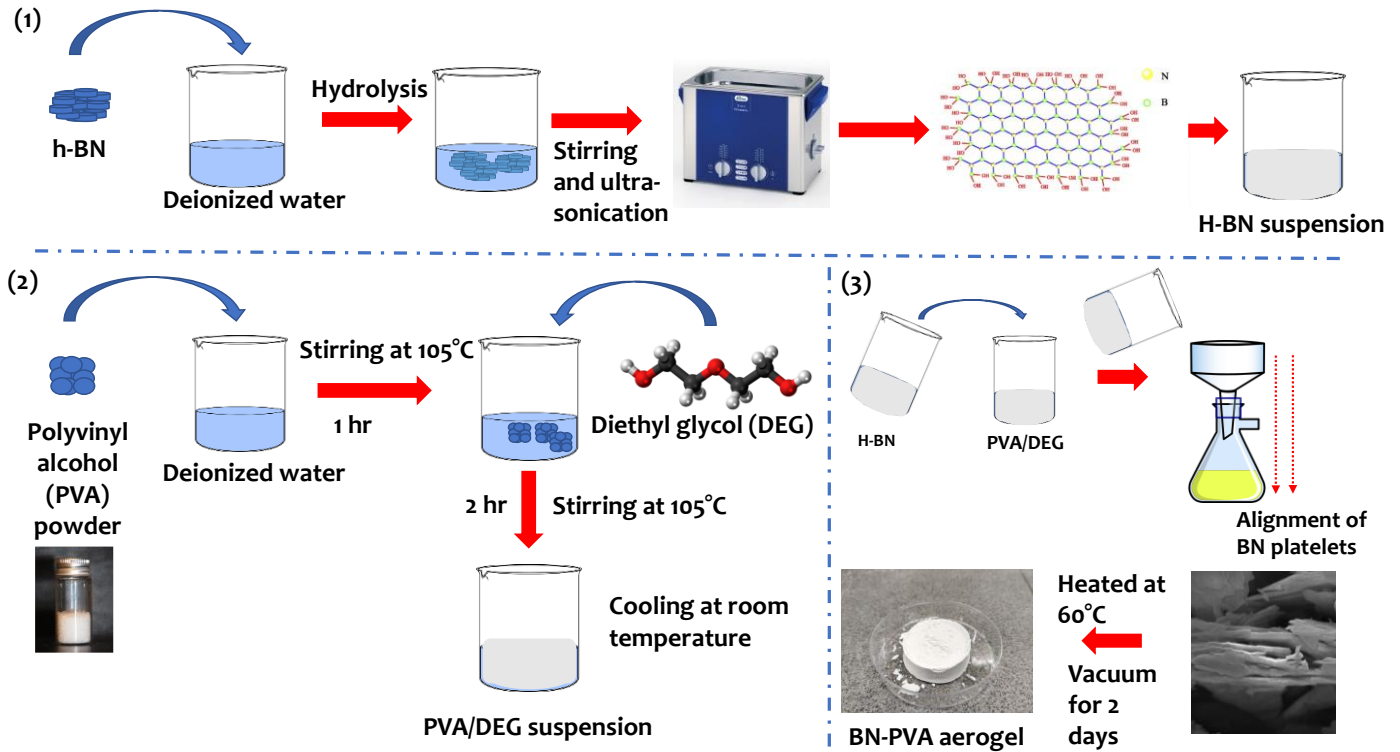


Figure 1: Schematic of the preparation of BN/PVA 3D framework.

Additionally, the corresponding bonding schematics are presented in **Figure 2**. Diethylene glycol (DEG) in polyvinyl alcohol (PVA) is commonly used as a plasticizer or binder in the synthesis of boron nitride/polyvinyl alcohol (BN/PVA) 3D framework. The bonding between DEG and PVA is primarily based on the covalent bonding between the interaction of hydroxyl group of PVA and DEG through ester linkage (See schematics) [118]. The diethylene glycol groups on the PVA molecules have a strong affinity for the hydroxyl groups on the BN surface. This type of covalent bonding results in the strong interactions between the PVA and BN, leading to a stable and robust aerogel framework. Thus, the PVA molecules form a cross-linked network within the BN/PVA aerogel framework, providing mechanical stability to the material. These interactions can thus, lead to a stable and robust cake framework that exhibits excellent thermal and electrical properties.

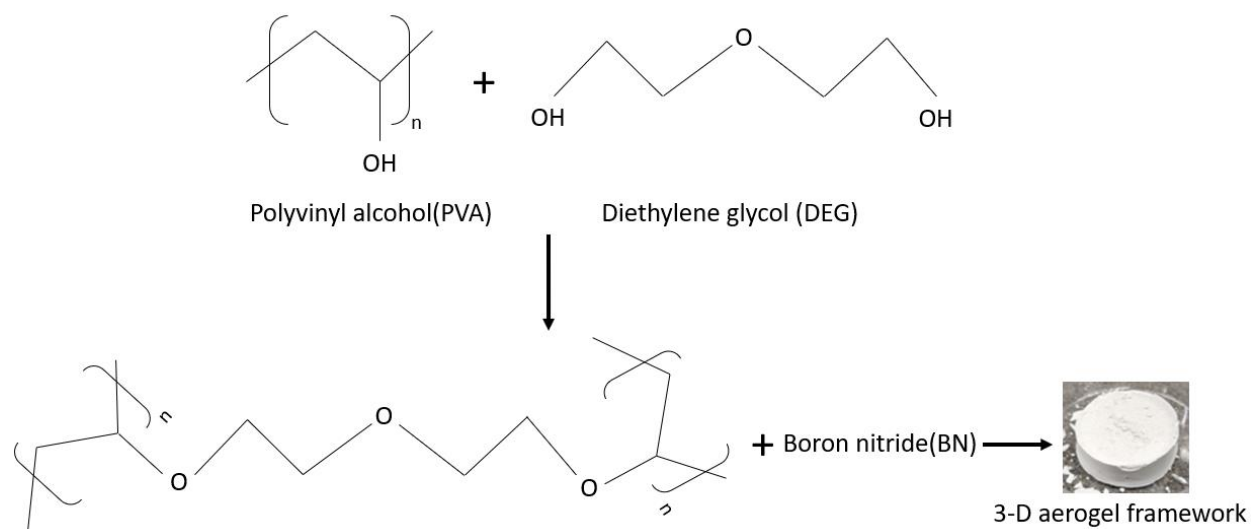


Figure 2. Schematics of the bonding of DEG cross-linked PVA on BN in BN/PVA 3D frameworks.

3.3.3 Characterizations

Scanning electron microscope (Thermo Scientific™ Helios G4 PFIB) working at an accelerating high voltage allowed to observe the microstructure of 3D framework while energy dispersive spectrometer (EDS) was used for the analyses of the elemental composition. The 3D framework surfaces were carefully sputtered with gold particles prior to image observation. Water contact angle (WCA) was measured at room temperature using an optical contact angle analyzer to determine the wettability of the specimens. An adhesive tape was used to adhere the 3D framework to a glass coverslip, and then 5 μL of deionized water was poured on the surface as an indicator for the WCA measurements. Each sample had at least three measurements, from which the average WCA values were determined. The functional groups on BN were identified by Fourier transform infrared (FTIR) spectrometry (Spectrum One, Perkin-Elmer, USA) in reflective mode. The observation was carried out within a wavenumber range of 4000–450 cm^{-1} for 10 scans per sample

reading. The electrical volume resistivity of materials was tested using the Keithley 6517B and 8009 resistivity test fixtures (Tektronix, USA). The in-plane and out-of-plane TCs of the samples were measured using a laser optical thermal scanner[119]. Testing was conducted on the cubic samples (surfaces polished) with the dimensions of (30×30×30) mm and in this TC measuring technique, a flat surface of a specimen is heated by a focused, movable, and continuously operating optical heat source mounted with an array of three infrared temperature sensors, as described in [120]. The optical head, which houses the heat source and infrared sensors, moves at a constant speed relative to the sample, allowing the heater and sensors to follow scanning lines while keeping a constant spacing. Optical scanning method provides the TC measurements with both precision and accuracy of 2% (at confidential level of 0.95) accounting for heterogeneity and anisotropy of materials under studying. Thermal stability measurements of materials were studied by the Simultaneous Thermogravimetry –Differential Scanning Calorimetry analyzer STA 449 F3 Jupiter coupled with Quadrupole Mass Spectrometer QMS 403 D Aëolos. XRD measurements were observed on Aeris Benchtop X-Ray Diffractometer with Malvern Panalytical Radiation of Cu K(alpha) 1,54060 Å, step size 0,005° and range of 2 θ from 5°-85°. Perkin Elmer Lambda 1050 UV-vis-NIR spectrometer was employed to obtain optical spectrum.

3.4 Results and discussion

In this section, we present and discuss the results of our study on the fabrication of BN/PVA 3D framework with varying concentrations of BN filler and PVA polymer.

3.4.1 Fourier-transform infrared (FTIR)

Fourier-transform infrared (FTIR) spectroscopy was used to identify the formation of hydrogen bonds between the hydroxyl groups of PVA and surface hydroxyl groups of

BN nanosheets. The results from FTIR analysis, as shown in **Figure 3**, demonstrate two distinct absorption peaks at 1366 cm^{-1} and 814 cm^{-1} which correspond to the stretching and deformation vibrations of B-N bonds, respectively, and are commonly observed in the spectrum of BN. However, a small peak at 2904 cm^{-1} close to 2926 cm^{-1} suggests the possible presence of impurities of C-H on the basal ends of BN. On the other hand, for BN-PVA 3D framework, four bands were observed at 3484 cm^{-1} , 2904 cm^{-1} , 1435 cm^{-1} , and 970 cm^{-1} , which are attributed to O-H stretching mode, C-H, C-O-H, and C-O bonds, respectively. The vibration of the O-H bond confirms the presence of surface hydroxyl groups on BN nanosheets by PVA. Furthermore, after the formation of BN- PVA 3D framework, the O-H bond around 3484 cm^{-1} is observed with the broadening of the C-O bond at 970 cm^{-1} . These changes indicate the formation of hydrogen bonds between the hydroxyl groups of PVA and surface hydroxyl groups of BN nanosheets.

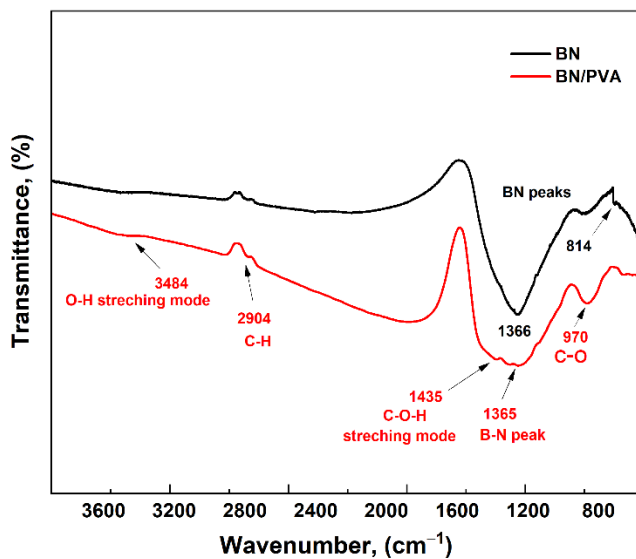


Figure 3. FTIR spectra of PVA aerogel and BN- PVA aerogel.

3.4.2 Energy dispersive spectrometer (EDS)

Energy dispersive spectrometer (EDS) was used for the analyses of the elemental composition of BN and BN/PVA frameworks. The 3D framework surfaces were carefully sputtered with gold particles prior to image observation. The elemental content of pure BN and BN/PVA composites showed a trend (**Figure 4**). The EDX spectra revealed that the peaks of C and O were slightly enhanced rather than remaining unchanged, indicating that the oxygenous and carbon groups were preserved. In comparison to pure fillers, the atomic composition of the BN/PVA composite reveals greater carbon and oxygen concentration. As demonstrated in **Tables 1** and **2**, the O atomic ratio increased from 3.7 to 6.7 percent, while the C atomic ratio increased from 3.50 to 15.1 percent respectively.

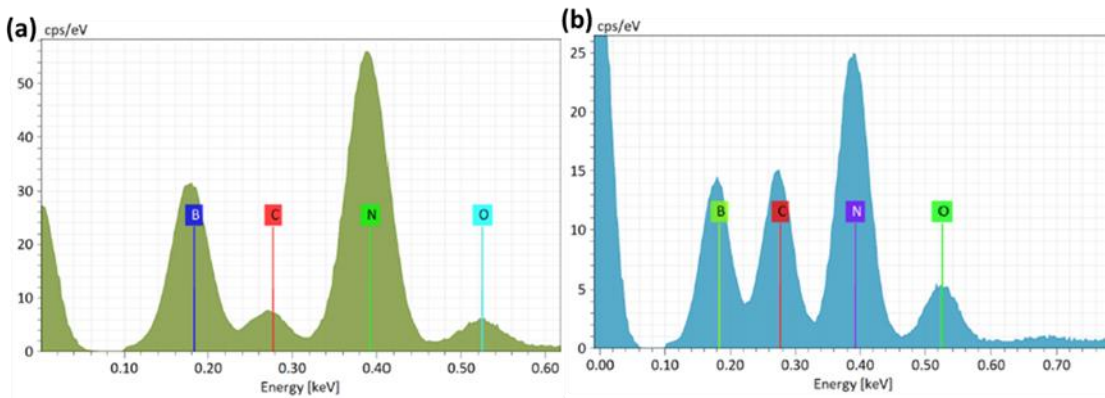


Figure 4. EDX analysis of pristine h-BN and h-BN/PVA composites

Table 1. Elemental composition of pure BN.

Pristine BN			
Element	At.No	Mass (%)	Atom (%)
Nitrogen	7	53.92	48.47
Boron	5	38.10	44.38
Oxygen	8	4.63	3.65
Carbon	6	3.34	3.50

Table 2. Elemental composition of BN/PVA composite.

BN/PVA composite			
Element	At.No	Mass (%)	Atom (%)
Nitrogen	7	45.40	40.99
Boron	5	31.84	37.25
Oxygen	8	8.42	6.66
Carbon	6	14.34	15.10

3.4.3 Optical contact angle analyzer

The water contact angle (WCA) was measured at room temperature using an optical contact angle analyser to determine the wettability of the specimens. An adhesive tape was used to adhere the 3D framework to a glass coverslip, and then 5 μ L of deionized water was poured on the surface

as an indicator for the WCA measurements. Each sample had at least three measurements, from which the average WCA values were determined.

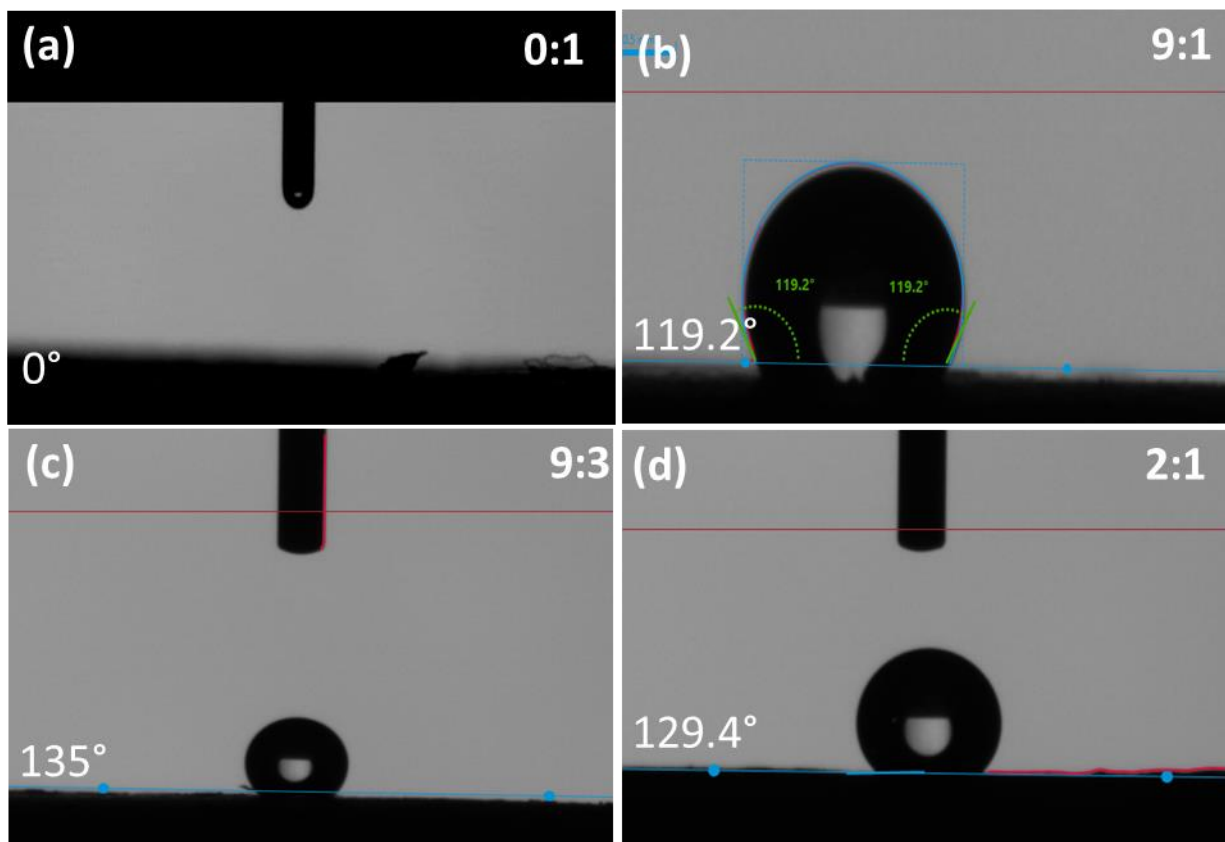


Figure 5. The WCA of PVA 3D framework and BN- PVA 3D framework with different BN to PVA ratios; (a) 0:1; (b) 9:3; (c) 9:1; (d) 2:1.

Studying the wetting behaviour of materials is crucial for applications related to thermal management. Hydrophilic thermal interface materials may not be effective due to their tendency to absorb moisture. Pristine PVA, for instance, are hydrophilic in nature and can absorb water drops. Therefore, it is important to modify the 3D framework to improve their hydrophobicity and protect themselves from moisture absorption. In this context, boron nitride (BN) was studied to modify PVA 3D framework and improve their hydrophobicity. Varying concentrations of BN in PVA (9:3, 9:1, and 2:1) were investigated to achieve the desired hydrophobic surface. The rich

hydroxyl groups of the PVA aerogel (without BN) have a strong water adsorption capacity, leading to a water contact angle (WCA) of 0°. However, by adding BN to the PVA 3D framework, the WCA increased significantly to 135°, 119.2°, and 129.4°, respectively, for the three different BN:PVA ratios. These results indicate that the BN- PVA 3D framework exhibit a hydrophobic surface (as shown in **Figure 5**). The segregated structure of PVA 3D framework with BN is a promising approach to improve their thermal management performance. By reducing moisture absorption, the modified 3D framework can maintain their structural integrity and help in enhancing their thermal conductivity. The improvement in hydrophobicity achieved by incorporating BN is attributed to its low surface energy and the formation of a barrier layer on the surface of the 3D segregated BN/PVA structure.

In summary, the segregated structure of PVA 3D framework with BN is a promising approach to improve their hydrophobicity and protect them from moisture absorption. The results of the study indicate that BN-PVA 3D framework exhibit a hydrophobic surface, with the WCA increasing significantly compared to pristine PVA 3D framework. This approach has potential for enhancing the thermal management performance of 3D framework and reducing their susceptibility to damage.

3.4.4 Morphology of 3D framework by scanning electron microscopy (SEM)

The SEM images in **Figure 6b-f** reveal that abundant BN nanoplatelets are adsorbed onto the surface of each other via π - π - stacking, in contrast to the pure BN-agglomerated cluster shown in **Figure 6a**. The phenomenon of self-assembly of BN platelets within the PVA polymer contributes significantly to the improvement in the physical attributes of the BN/PVA-based polymer composite system, including thermal conductivity (discussed in the next section). These self-assembled BN platelets within the PVA matrix can be seen clearly in **figure 6d-e** creates a

thermally conductive pathway for the transfer of heat from one BN platelet to another within the polymer matrix. These segregated BN/PVA structure may have reduced the interfacial thermal resistance (also called Kapitza resistance) between the filler and the polymer matrix interface, resulting in an increase in thermal conductivity. While the vacuum-assisted filtration technique initiates the fabrication of this 3D structure, we believe that the platelet self-assembly is the main contributor to the increase in TC in 3D skeleton albeit the fact that the inherent TC of BN is ~ 600 W/mK, which also contributes immensely in augmenting the TC of this 3D structure. These findings suggest that the self-assembly of BN nanoplatelets inside PVA polymer is a promising strategy to develop high-performance polymer composites with enhanced thermal conductivity.

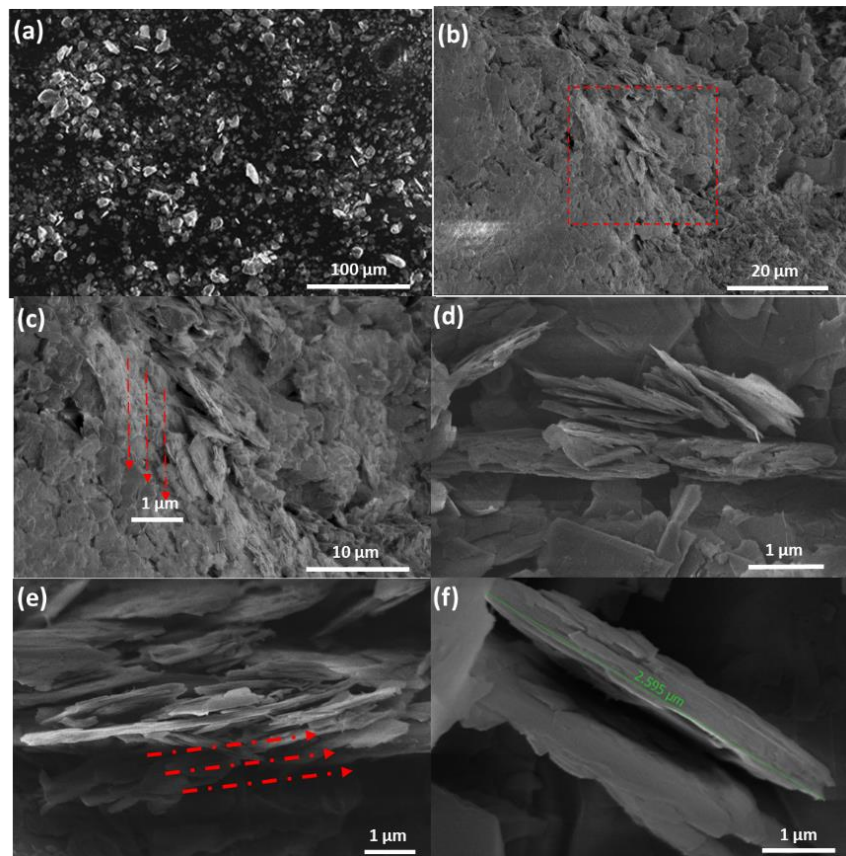


Figure 6. SEM of (a) pristine h-BN Powder; (b-f) Self assembled BN: PVA (2:1) composites at different magnifications.

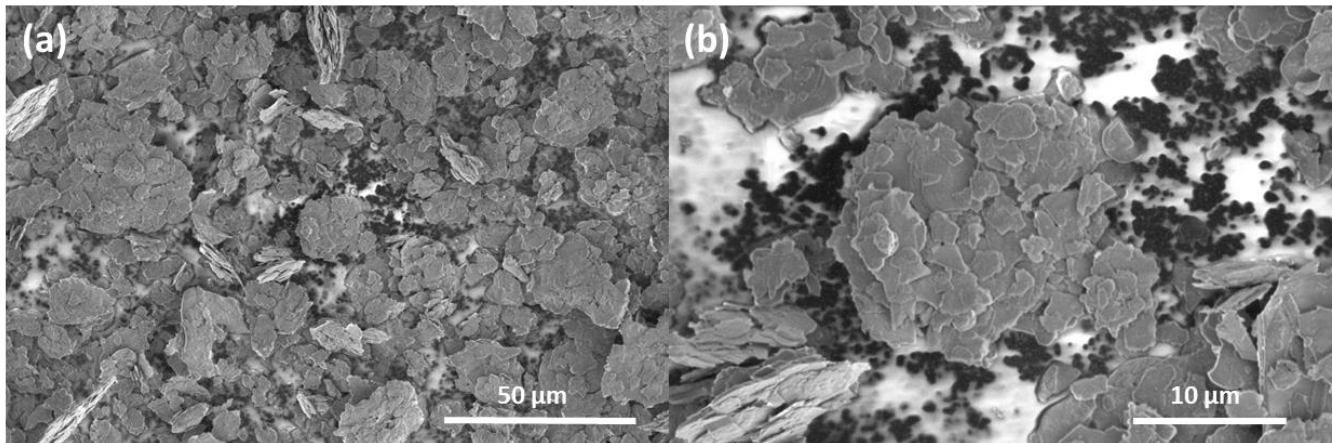


Figure 7. SEM image of agglomeration and clustering of BN platelets in BN: PVA (9:1) aerogel-based 3D structure.

3.4.5 Thermal conductivity

Thermal conductivity (TC) measurements were conducted on the BN/PVA composites to evaluate their thermal management properties. The TC of PVA and BN-PVA based 3D framework with varied stoichiometric ratios is shown in **Figure 8**. The highest reached TC of the BN-PVA based 3D framework is around 0.76 W/mK (in-plane) and 0.61 W/mK (out-of-plane) with the ratio of BN/PVA as (2:1), which is significantly higher than the TC of pure PVA 0.15 W/mK. Of course, the thermal conduction, which results from ordered heat conducting channels, benefits from the self-assembled BN flakes in PVA polymer system. The addition of BNNS to the PVA is known to strengthen the covalent bond interaction in the molecular structure, resulting in a considerable increase in TC. The PVA-DEG-BNNS cross-link interaction (as shown in **figure 2**) would close the gap and connect the adjacent BNNSs, resulting in a considerable reduction in the interface thermal resistance and an increase in TC [110]. The morphology of BN platelets as shown in SEM images with self-assembling of BN in a PVA polymer system created a segregated BN filler-based PVA thermal channel. Other factors such as homogenous mixing, vacuum drying, and polishing

the samples may have closed the gap between adjoined thermally conductive BN fillers in a closed segregated structure facilitating the reduction in interfacial thermal resistance. Correspondingly, BN/PVA-based 3D framework with a stoichiometric ratio of (9:1) also exhibited an increase in the TC but did not achieve the same increase in TC in comparison to (2:1) in spite of higher BN content. Our idea behind investigating high BN:PVA ratios was to minimize the usage of low TC PVA, replacing it with a higher inherent TC of BN. This high filler content often leads to brittleness of the composite, and our 3D framework (9:1) showed brittleness. The failure of the BN-PVA (9:1) structure to demonstrate a high TC 3D structure could be due to different factors. This decrease in TC might be the result of a nearly 90% increase in BN content in the PVA polymer, which causes the agglomeration and clustering of BN platelets (see SEM image in **Figure 7**). The agglomeration, in turn, causes an increase in interfacial thermal resistance, which lowers the TC. Hence, the enhancement in TC is limited due to the poor interfacial interaction between the filler and the polymer, the lack of polymer to create thermally conductive bridges in-between BN particles and agglomerates, and, as the result, the construction of a poor thermally conductive adjacent network. On the other hand, In the intermediate case of a stoichiometric ratio BN-PVA (9:3), a considerable increase in TC was observed when the BN content in the PVA polymer reached ~ 66%. Due to possible good uniform dispersion of BN inside PVA and homogenous mixing, BN-PVA showed good TCs in both planes. Hence, a strategy to obtain thermally conductive 3D framework with an optimum stoichiometric ratio was introduced where TC depends not only on the BN content, but also on its structuring in the nanocomposite and on the possibility of transfer of heat from particle to particle and polymer bridges. Dropping the BN content to a ratio of (2:1), we did not observe a significant change in TC relative to (9:3), as shown in **Figure**

8, the fact demonstrating that high TC depends not as much on the BN content but on the optimal ratio and structuring on the nano-level.

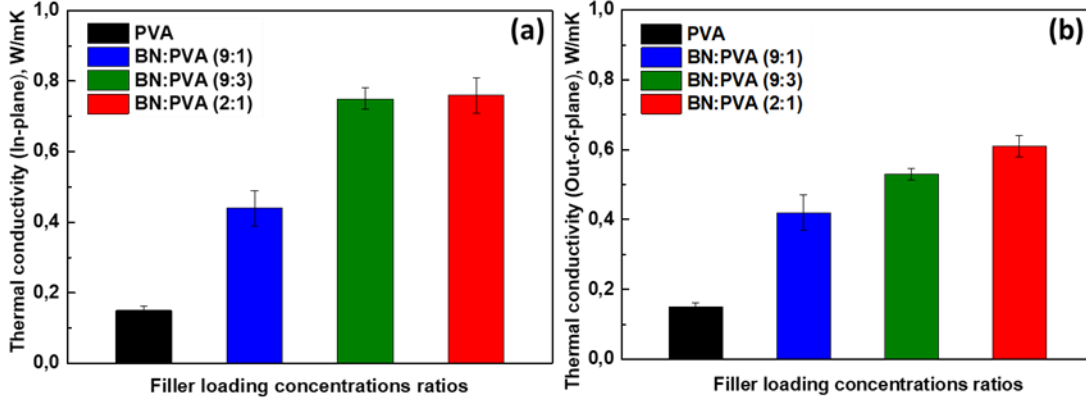


Figure 8. In-plane (a); and (b) out of plane thermal conductivity of pristine PVA and h-BN/PVA composites.

3.4.6 X-ray Diffraction (XRD)

The self-assembly of BN within PVA in a segregated BN/PVA 3D framework was further evaluated by XRD to further provide evidence of change of orientation of fillers to some extent by self-assembly (**Figure 9**). To explain this, pristine BN exhibit sharp diffraction peaks of (002), (100) and (004) at $2\theta = 26.6^\circ$, 41.3° and 55.2° respectively, whereas PVA shows its diffraction peaks of (101) at $2\theta = 19.5^\circ$. Notably, when observing XRD pattern of the BN: PVA composites, with the ratio of (2:1), we see that the diffraction peaks of (100) and (004) are disappeared and the

intensity of (002) peak is reduced, which results from the horizontal random orientation of the BN platelets induced by VAF technique [66].

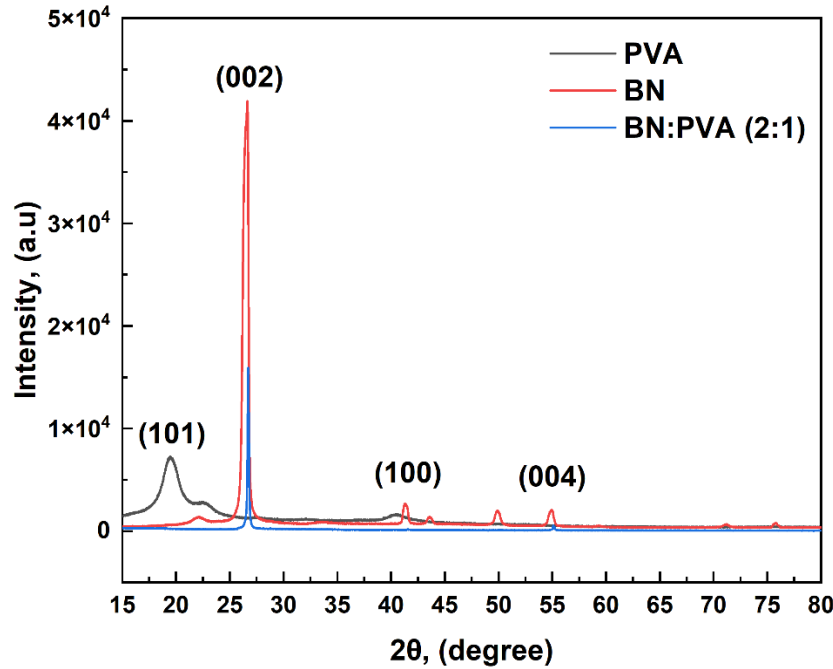


Figure 9. XRD pattern of BN/PVA composites.

3.4.7 Electrical resistivity

In the context of thermal management applications in the electronic industry, it is crucial for composite materials to exhibit high electrical resistivity. **Figure 10** illustrates the electrical volume resistivity of neat PVA and its nanocomposites. Neat PVA, as an electrical insulator, has a volume resistivity of approximately $8.93 \times 10^{11} \Omega \text{ cm}$. However, the incorporation of BN into PVA matrix leads to an enhanced electrical resistivity due to the intrinsic electrical insulating property and large bandgap of BN. This wide bandgap of approximately 5.5 eV of BN is attributed to its insulating nature. Hence, upon creating a segregated 3D structure in the PVA matrix, BN particles act as barriers to the flow of electric charge, impeding electrical conductivity and elevating electrical resistivity. This enhancement in electrical resistivity is contingent on the BN:PVA ratio,

whereby higher ratios engender reduced electrical conductivity and augmented electrical resistivity. The incorporation of BN into PVA imparts electrical insulating properties to the resultant composite, rendering it desirable for various applications, including thermal management of electronic devices. For instance, with BN:PVA ratios of (9:1) and (9:3), the volume resistivity was found to be as low as approximately as ca. $1 \times 10^{14} \Omega \text{ cm}$ and ca. $3 \times 10^{14} \Omega \text{ cm}$, respectively. Whereas, BN: PVA with a stoichiometric ratio of (2:1) nearly increases the electrical insulation characteristics of neat PVA with an electrical resistivity of $\sim 1 \times 10^{15} \Omega \text{ cm}$. Therefore, for all four cases, electrical resistivity values lie well within the high-insulation range, indicating the straightforward applicability of the 3D framework for TIM implementations in electronics industry.

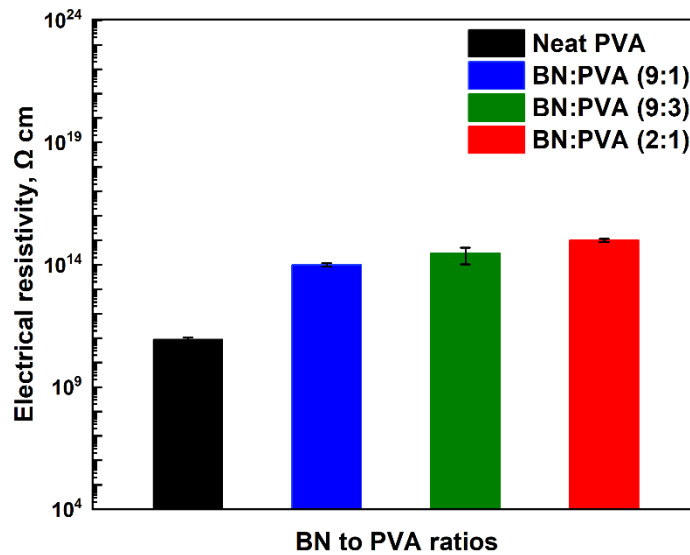


Figure 10. Electrical resistivities of pristine PVA and h-BN/PVA composites.

3.4.8 Thermogravimetric Analyzer (TGA)

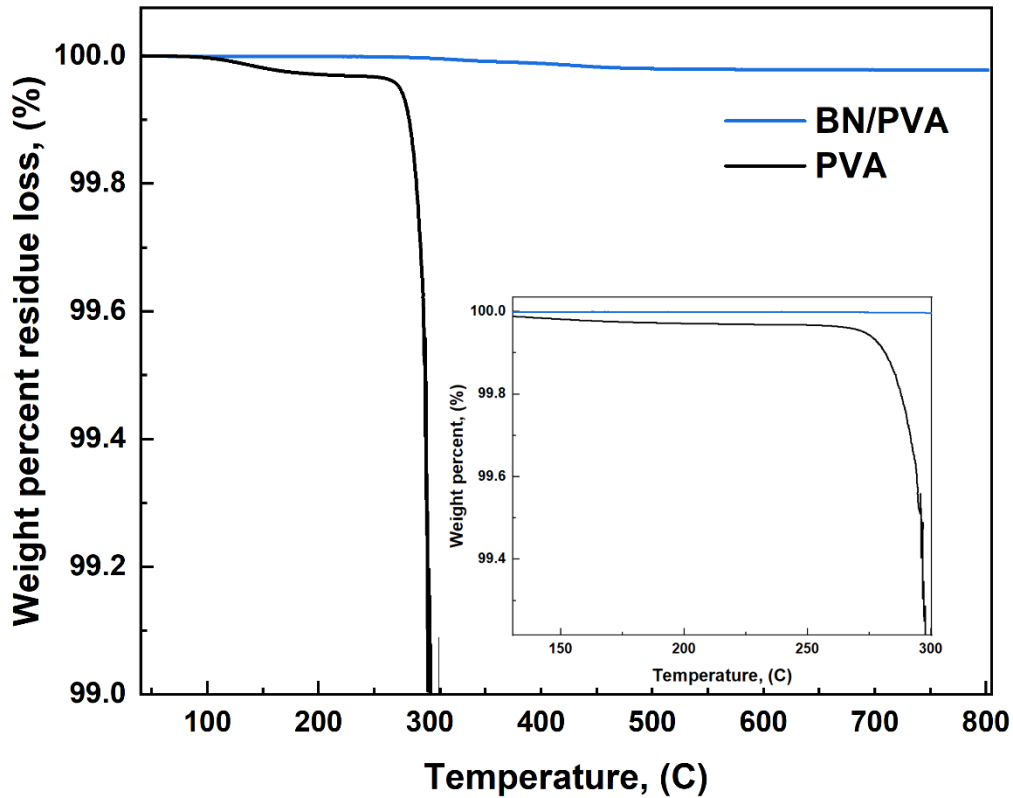


Figure 11. TGA curves of PVA and BN/PVA nanocomposites

The thermal stability of composite materials is a crucial factor in their suitability for thermal management applications in the electronic industry. In this regard, the BN/PVA cake frameworks exhibit exceptional thermal stability, as demonstrated by their ability to withstand temperatures up to 800°C without any signs of degradation. In stark contrast, the neat PVA material undergoes full degradation at a much lower temperature of 300°C. Even for comparison at 1% degradation temperature, BN/PVA composite doesn't degrade at all while neat PVA reached the temperature of 295°C. This remarkable difference in thermal stability is attributed to the presence of BN in the

composite material. BN possesses high thermal stability, which is attributed to the strength and stability of its covalent bonds. Therefore, when BN is incorporated into the PVA matrix to make segregated type structure, the resulting composite material inherits the thermal stability of BN, resulting in the remarkable thermal stability of the BN/PVA framework. Moreover, the BN/PVA composite material does not show any signs of degradation even at temperatures as high as 800°C, indicating its suitability for high-temperature applications. This underscores the importance of the incorporation of BN into polymer matrices to enhance their thermal stability and make them suitable for a wide range of applications in the electronic industry.

Table 3. Data derived from TGA curves of nanocomposites at 1% degradation temperature.

Filler content, (wt%)	$T_{1\%}$ (°C)
Neat PVA	295
BN/PVA	Doesn't degrade till 800

3.5 Conclusion

A facile technique was employed to construct a three-dimensional (3D) Polyvinyl alcohol (PVA)/aligned boron nitride (BN) 3D framework nanocomposite framework with outstanding performance. As compared to the pure PVA matrix (thermal conductivity 0.15 W/mK), self-assembled BN/PVA 3D framework composite exhibited outstanding in-plane and out-of-plane thermal conductivities of 0.76 W/mK and 0.61 W/mK, respectively. Hence, we employed a strategy to acquire a TC 3D composite with an optimum stoichiometric ratio, unaffected by the BN content, but with its structuring dependency on the nanocomposite framework with the possibility of efficient phonon transfer from particle to particle and bridging effect of polymer to segregated filler network. In our study, the comparative analysis demonstrated that the highest TC

was achieved not at the highest BN content, but in the range of BN-PVA stoichiometric ratios where the better self-structuring of filler and matrix material occurred. Furthermore, the composites demonstrated good hydrophobicity in water, high thermal stability, and a high electrical resistivity of at least $1 \times 10^{15} \Omega \text{ cm}$. As a result of their outstanding properties, these nanocomposites offer a wide range of potential applications in packaging and electronics for thermal management applications.

Within this chapter, my research efforts were primarily dedicated to the creation of thermally conductive polymeric ceramic 3-D framework structures, commonly referred to as aerogels. This endeavor involved the utilization of fabrication techniques, with a notable focus on Vacuum Assisted Filtration (VAF). Following this, a process of meticulous polishing and compression was employed to meticulously eliminate any potential presence of bubbles or air voids. Remarkably, this approach resulted in the attainment of impressively high thermal conductivity, all achieved without the need for polymer infiltration. While the 3-D structure polymer composite proved to be a significant breakthrough, offering commendable thermal conductivity and exceptional electrical insulation properties, it was not without its limitations. One prominent drawback was its inherent lack of mechanical flexibility, which restricted its utility in certain applications. Additionally, this composite relied on relatively high filler loadings by weight, further necessitating refinement. Therefore, my research focus has now shifted towards the development of more advanced thermally conductive polymeric thin films designed to address these limitations. These thin films are meticulously engineered to possess several key attributes, including optimized thickness, low filler loadings within the polymer matrix, good mechanical flexibility, and outstanding thermal conductivity. These combined characteristics render them exceptionally well-suited for

deployment as TIMs within the electronic industry, where the demand for effective heat management and reliable performance is paramount.

Chapter 4. Thermally conductive reduced graphene oxide polymer films

4.1 Introduction

The intensifying problem of electronic device failure due to excessive heat generation has necessitated the development of high-performance thermal interface materials that can rapidly dissipate thermal energy. In light of the constant advancements in the electronic industry, particularly in the realm of cellular devices, tablets, and computers, it is crucial to produce substrates that possess high thermal conductivity and reduced thickness to ensure optimal thermal performance, extended lifespan, and heightened reliability. In lieu of traditional thermal interface materials, thermally conductive films have emerged as a promising alternative. These films offer a clean, effective solution for high-performance heat dissipation, meeting the urgent need for slimmer products with powerful features demanded by the electronic industry.

4.2 Research objectives

1. Successful reduction of graphene oxide (GO) with diethylene glycol (DEG)
2. Fabrication of DEG-GO/PVA flexible films via facile synthesis method which is economically viable and to attain high thermal conductivity.
3. Trend of change of thermal and electrical properties of GO/PVA films with the use of different low to optimum filler loading concentrations.
4. Use of optimized reduced GO/PVA flexible films as an alternative of traditional TIMs that uses higher filler weight loading in their polymeric system for their usage in TMM or TIMs for industry.

4.3 Experimental

4.3.1 Materials

Graphene oxide (GO) with an average particle size of 100 nm, Polyvinyl alcohol (PVA) with an MW of 31,000–50,000, 98% hydrolyzed, and Diethyl glycol (DEG) were purchased from Sigma Aldrich Co., Ltd. (Burlington, MA, USA). None of the chemicals were further purified before usage.

4.3.2 Methodology

The reduced graphene oxide films were fabricated by the process described in figure 1, including self-assembly, graphitization, and mechanical pressing in the end.

4.3.2.1 Reduction of graphene oxide (GO)

Reduction of graphene oxide (GO) were achieved through a hydrothermal process at high temperatures using DEG as a plasticizer. Specifically, 0.4 g of GO was mixed with 2 g of DEG in 80 mL of H₂O and stirred for 4 hours at 120°C, followed by sonication for 10 minutes. The resulting solution was then filtered under vacuum, and the resulting GO powder was heated overnight at 80°C to achieve the desired reduced GO. Hence, the reduced GO is termed as DEG-GO.

4.3.2.2 Preparation of polymer composite films

A 15% Polyvinyl Alcohol (PVA) solution was prepared using distilled water to achieve a uniform dispersion of PVA powder. The PVA powder was dissolved in the distilled water at 105°C for 1 hour with continuous magnetic stirring. Once the PVA solution was prepared, 10 weight percent of DEG was added and stirred for an additional 2 hours at 105°C. For synthesis of graphene suspensions, different weight percent in grams are dissolved in distilled water and allowed to for 3-hours bath sonication. Subsequently, the desired quantity of graphene suspension was introduced

into the pre-prepared PVA suspension. The resulting mixture was stirred for 1 hour at 105°C, following which it was poured onto silicon molds or glass petri plates. The prepared suspension was subjected to a drying process at 60°C for a duration of 48 hours, followed by transferring the resulting films to a desiccator containing silica gel. The desiccator facilitated the removal of any remaining moisture. Subsequently, the films were subjected to compression using a pressing machine at a force of 10 kilonewtons for a duration of 5 minutes, resulting in a highly flexible and smooth film. This compression process effectively eliminated any bubbles present within the film, resulting in a flattened and uniform structure as shown in the picture below.

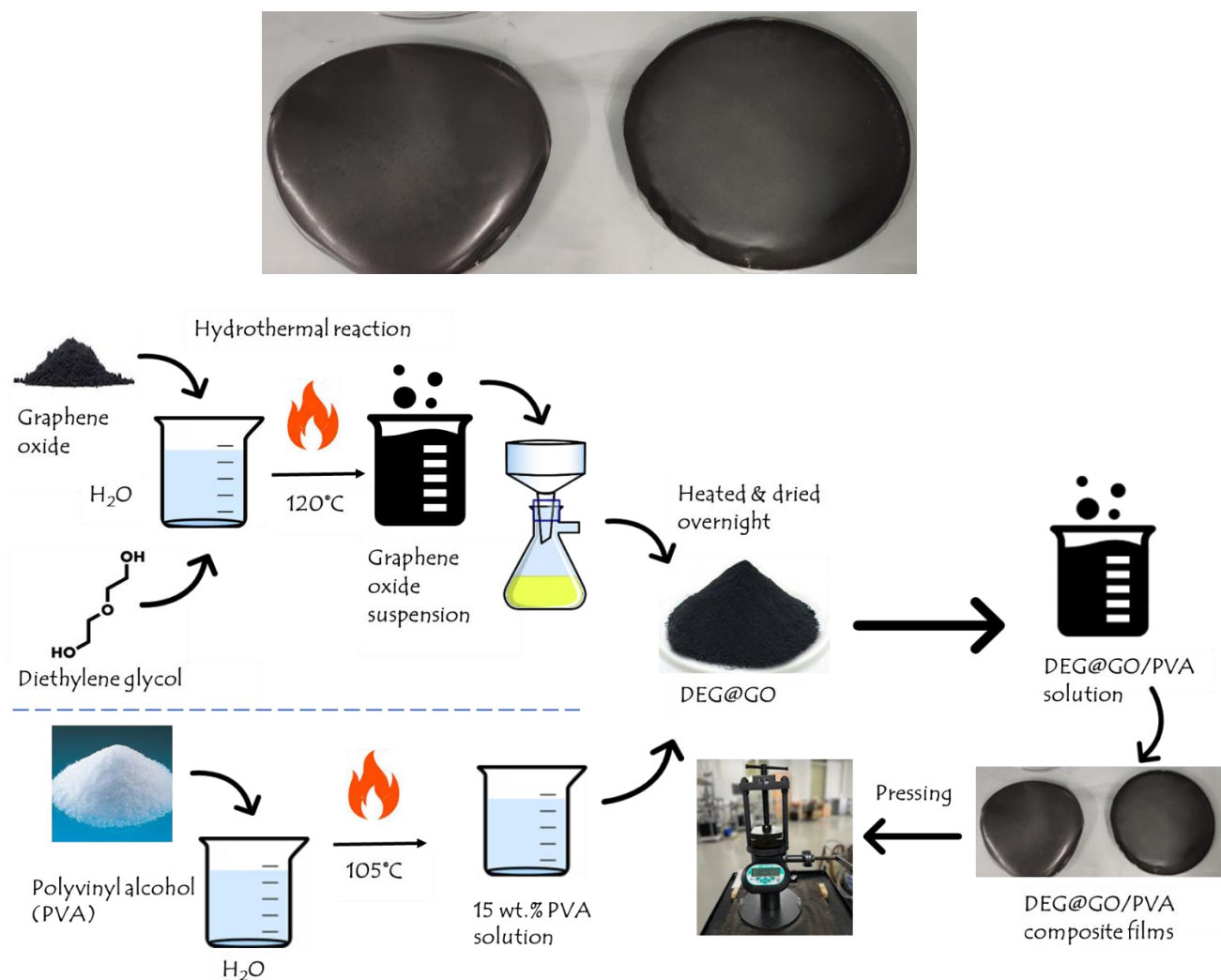


Figure 1. Schematic showing the fabrication process of DEG-GO/PVA composite films.

4.4 Results and Discussion

In this section, we will discuss the techniques and the results that are used to study the reduction of GO by treating it with DEG and discuss the results of our study on the fabrication of flexible GO/PVA and DEG-GO/PVA films.

4.4.1 Reduction of graphene oxide (GO)

Evidences, that support the reduction of GO by treating it with DEG are as following:

4.4.1.1 Fourier-transform infrared (FTIR)

The Fourier-transform infrared (FTIR) spectra of both powder graphene oxide (GO) and the reduced GO layers were obtained and presented in **Figure 2**. Analysis of the FTIR spectrum revealed the presence of several absorption peaks that correspond to specific functional groups. Two absorption peaks were observed at 3534 cm^{-1} and 3501 cm^{-1} , which are attributed to the presence of hydroxyl groups (O-H). The existence of these hydroxyl groups is further supported by the observations from Energy-dispersive X-ray spectroscopy (EDS) mentioned later in the section. Additionally, the FTIR spectrum showed peaks at 2875 cm^{-1} and 2853 cm^{-1} , which are associated with the asymmetric and symmetric stretching vibrations of CH_2 bonds, respectively. There was a slight broadening of the peak related to the CH_2 bonds for DEG-GO, which can be attributed to the reduction of pristine GO by diethylene glycol (DEG). The observed peak broadening is likely due to the removal of oxygen-containing functional groups and the restoration of sp^2 carbon bonds in GO, resulting in a more graphitic structure. Overall, the FTIR analysis provides valuable information about the functional groups present in the GO and DEG- GO layers, which is crucial for understanding the chemical properties and behavior of these materials.

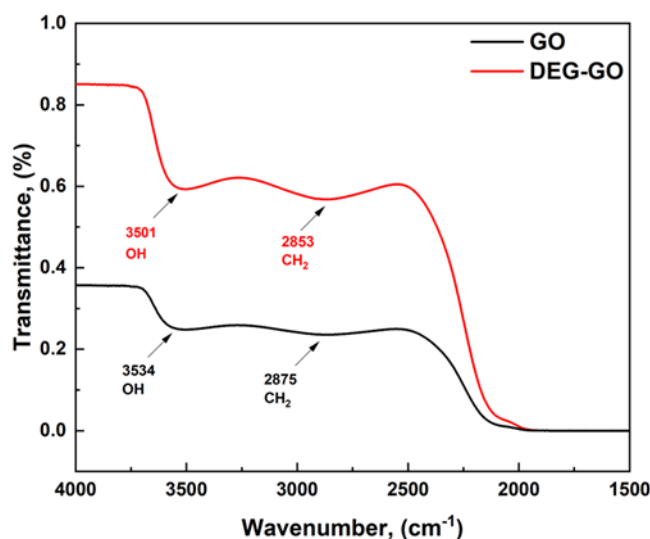


Figure 2. FTIR spectra GO and of DEG treated GO.

4.4.1.2 UV-Visible spectroscopy

The UV-Visible spectroscopy observations were carried out to investigate the optical properties of the powder samples, including GO and reduced GO. As shown in **Figure 3**, the absorption spectrum of GO exhibited an absorption band centered around 212 nm, which is likely associated with the $\pi \rightarrow \pi^*$ transition of the C–C bonds of graphitic carbon. Another shoulder peak at less than 300 nm is linked to the $n \rightarrow \pi^*$ transition of the C=O bonds. The observed peaks are characteristic of the electronic structure of GO, where the π electrons of the graphitic carbon and oxygen-containing functional groups interact with UV-Visible light, leading to electronic transitions. After the reduction process by diethylene glycol (DEG), the absorbance of the entire spectrum was found to increase. Furthermore, there was a peak shift at ~ 220 nm from 212 nm, which suggests the change in the electronic structure of GO. The complete elimination of the shoulder peak linked to the $n \rightarrow \pi^*$ transition of the C=O bonds in the DEG treated GO spectrum further supports the reduction of GO. This reduction is associated with the removal of oxygen-containing functional groups, leading to a significant change in the electronic and optical

properties of GO. Overall, the UV-Visible spectroscopy observations provide valuable insights of GO.

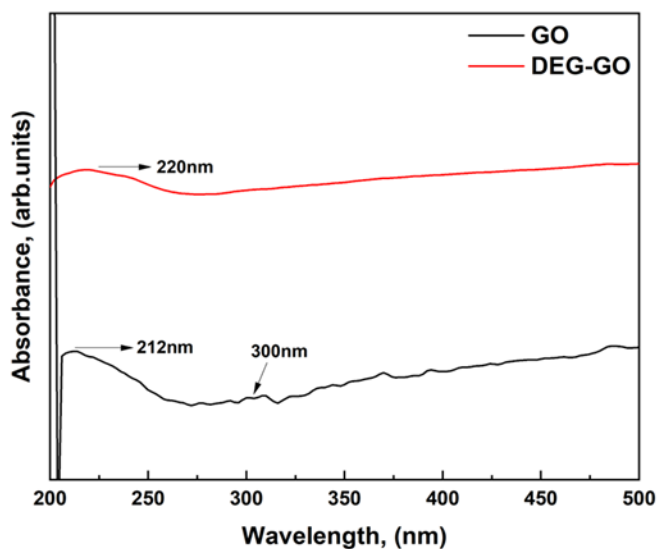


Figure 3. UV-Vis spectra of GO and DEG treated GO.

4.4.1.3 Raman spectroscopy

The characterization of GO and its modified form with the reduction with DEG was carried out using Raman spectroscopy. The Raman spectrum of GO and DEG-GO was obtained, and it was observed that the typical Raman spectrum of GO comprises three distinctive bands namely D, G, and 2D bands. The G bands correspond to the in-plane stretching vibrations of sp^2 -hybridized carbon atoms in graphitic structures, while the 2D band arises from the second-order scattering of the D band. The D band represents the defects and disorder of the graphene structure, which are correlated to the presence of vacancies and grain boundaries.

The Raman spectrum of GO and DEG-GO are shown in the **Figure 4** with the first-order D peaks at 1345 cm^{-1} and 1348.3 cm^{-1} and the G peaks arising from the in-plane stretching vibration of C=C sp^2 carbon bonds which appeared at 1577.2 cm^{-1} and 1570.5 cm^{-1} respectively. The D-band identifies crystalline material disorders and defects correlated to vacancies and grains[121]. Here,

the thickness of GO layers varies, as it is shown in the change of G peak's shift in terms of their position. The intensity of D band relative to G band as I_D/I_G ratio was associated with the number of defects concentration present in the graphene oxide structures. Hence, after the reduction, the I_D/I_G ratio of DEG- GO is reduced, which clearly shows the decrease in OH functional groups and defects in comparison to pure GO.

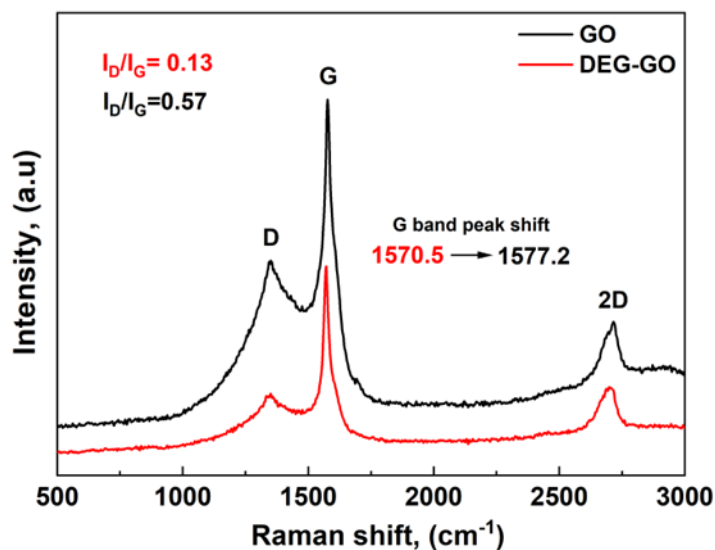


Figure 4. Raman spectra of GO and DEG-GO.

4.4.1.4 Transmission electron microscopy (TEM) and Energy dispersive spectrometer (EDS)

The morphology, microstructure and element information for graphene flakes were obtained by Transmission electron microscopy (TEM) and Electron Diffraction Spectroscopy (EDS). EDS is a useful technique for analyzing the atomic composition of materials. The results of EDS analysis in this study showed that the successful reduction of GO flakes by the treatment with DEG (see **Figure 5 and 6**). The carbon peaks in DEG-GO were significantly enhanced compared to pure GO. The atomic composition analysis revealed that the DEG-GO sample had a higher concentration of carbon and lower concentration of oxygen compared to pure GO, indicating a successful reduction process. The O atomic ratio decreased from 9.22% to 1.22% while the C

atomic ratio increased from 90.78% to 98.38%. These changes suggest in the reduction of the oxygen functional groups and the enhancement of carbon groups on GO flakes. Moreover, the morphology of GO flakes can be easily seen at a very high magnification in the TEM image (see **figure 6c**). Here, pure GO flake exhibited several graphene oxide sheets with randomly dispersed impurities like S on it. These impurities are present there, most probably because of the use precursors when synthesizing GO via hummer's method whereas the presence of Cu in the EDS compositional analysis graph is due to the Cu grid where the graphene specimens were placed.

In comparison to TEM imagery of pristine GO, reduced GO displayed simultaneously areas of quite thinner graphene flakes combined with areas of superimposed stacked hexagonal graphene rings (see **Figure 7a**) which is completely absent for GO when observed. These thinner graphene flakes as shown in TEM are in accordance with the reduced thickness of graphene sheets as enumerated later in the AFM images whereas, the well-defined diffraction spots by selected area diffraction patterns (SAED) in **figure 7b** proves some level of crystalline structure inside DEG treated reduced GO which can be beneficial when dealing with increasing thermal conductivity in a composite system.

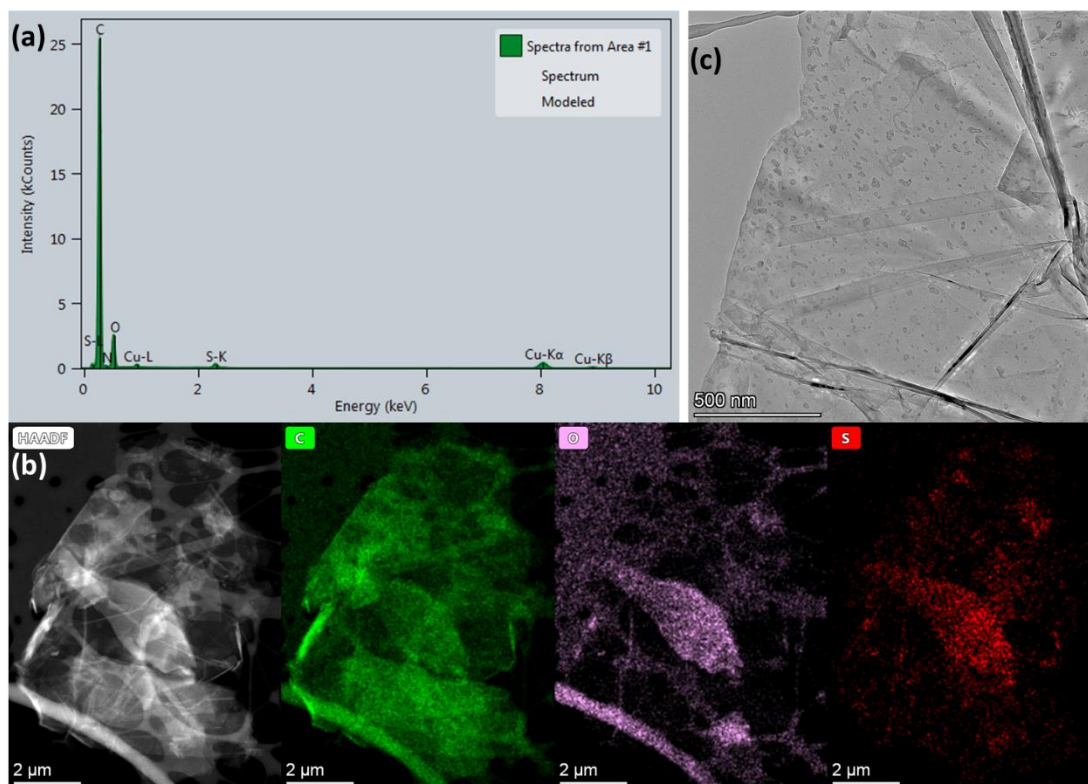


Figure 5 (a, b): EDS compositional analysis of pristine GO and STEM-EDX elemental mapping images of C, O and S present in GO flakes (c) TEM characterization of GO flakes at high resolution

Table 1a: Elemental composition of pure GO

Pristine GO						
Element	At. No	Mass (%)	Atom (%)	Atomic error (%)	Mass error (%)	error
Carbon	6	88.08	90.78	3.51	2.11	
Oxygen	8	11.92	9.22	1.88	2.41	

Table 1b: Elemental composition of DEG-GO

DEG-GO						
Element	At. No	Mass (%)	Atom (%)	Atomic error (%)	Mass error (%)	error
Carbon	6	98.38	98.78	0.65	0.43	
Oxygen	8	1.62	1.22	0.25	0.33	

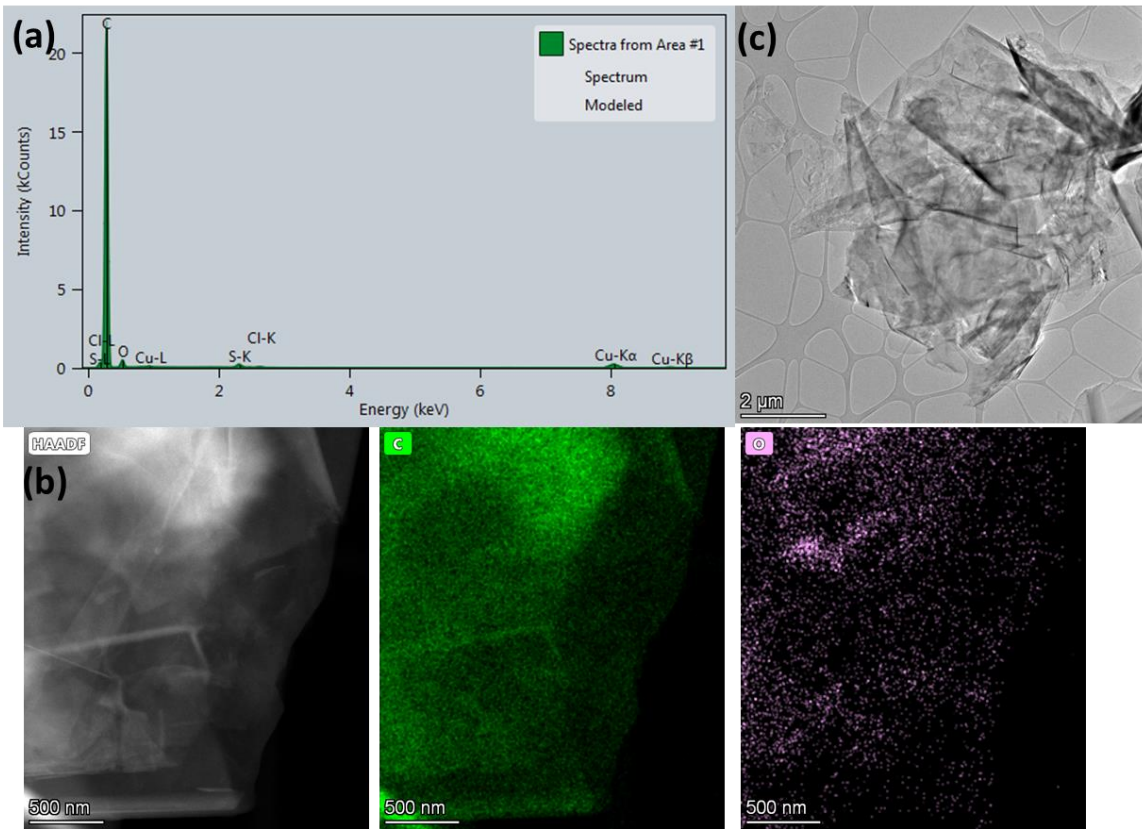


Figure 6(a, b): EDS compositional analysis of reduced GO and STEM-EDX elemental mapping images of C and O present in reduced GO flakes (c) TEM characterization of GO flakes at high resolution

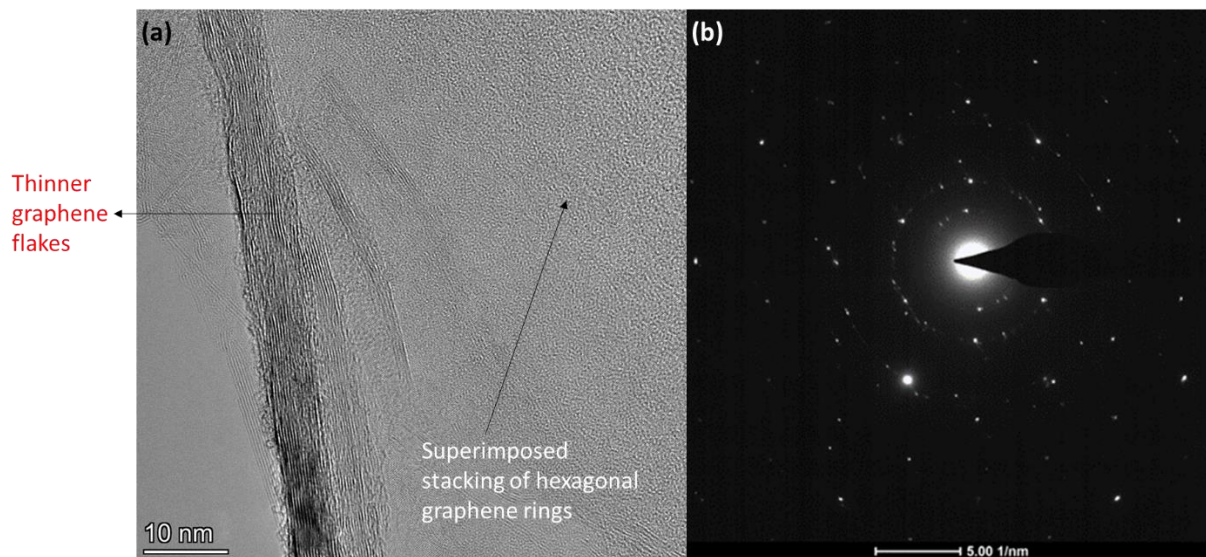


Figure 7 (a): High resolution image of DEG-GO by HRTEM; **(b)** SAED pattern of DEG-GO

Hence, these findings are in agreement with the results obtained from other characterization techniques used in this study. The UV-Visible spectroscopy results showed a peak shift at ~220 nm from 212 nm, indicating the reduction of GO by DEG. The Raman spectroscopy results demonstrated a decrease in the number of defects and OH functional groups in DEG-GO compared to pure GO. Overall, the EDS results provide further evidence for the successful reduction of GO by DEG, and the reduction process resulted in the enhancement of carbon groups and the decrease in oxygen functional groups. These findings highlight the potential of DEG-GO as a promising material for various applications.

4.4.1.5 Scanning electron microscope (SEM)

The SEM images of pure GO and DEG-GO were presented in **Figure 8a and 8b**, respectively. The SEM image of pure GO shows a sheet-like structure with a rough surface, which is consistent with previous reports on GO morphology. However, the SEM image of DEG-GO reveals a different morphology compared to pure GO. DEG-GO exhibits a more compact and smoother surface, indicating a significant reduction in the number of defects and functional groups on the surface of GO due to the reduction process.

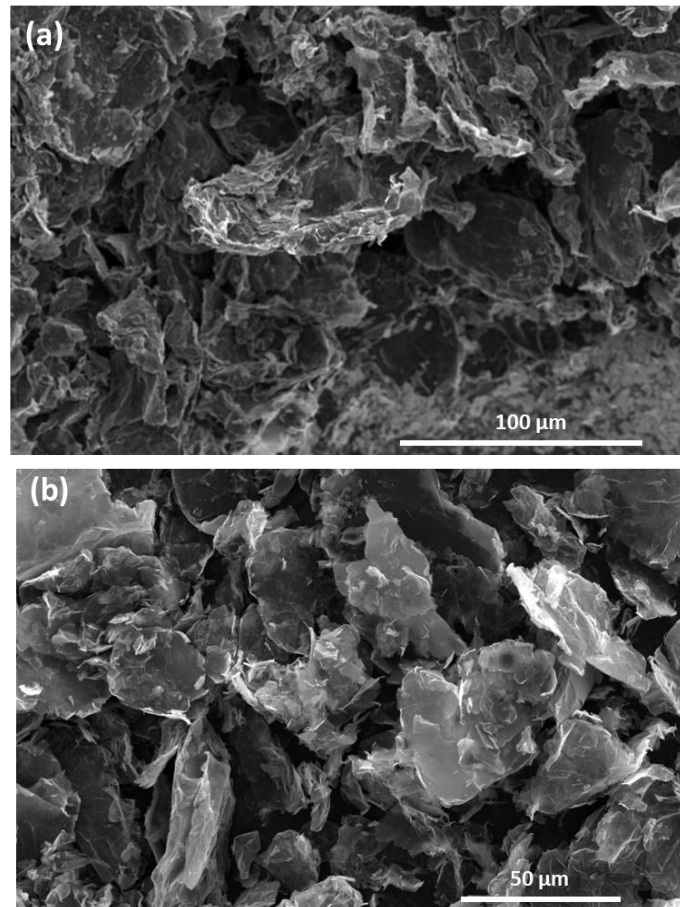


Figure 8. SEM images of (a) GO; (b) DEG-GO

These SEM images provide important information on the surface morphology of the samples, which is directly related to their physical and chemical properties. The morphology of GO is influenced by several factors, including the starting material, preparation method, and processing conditions. In the case of DEG-GO, the reduction process using diethylene glycol leads to the removal of some oxygen functional groups and defects, resulting in a smoother and more compact surface morphology.

4.4.2 PVA based polymer nanocomposite films

Pure GO and DEG-GO/PVA polymer films were fabricated with various filler loading concentrations or weight percentages of 1%, 2%, 5% and 10% GO and DEG-GO with PVA as polymer matrix. The films exhibited thickness of approximately 1mm with the diameter of around 8cm. Results from different characterization techniques (discussed in the later sections) exhibited good flexibility, thermal conductivity, thermal stability, tunable electrical resistivity and good wettability.

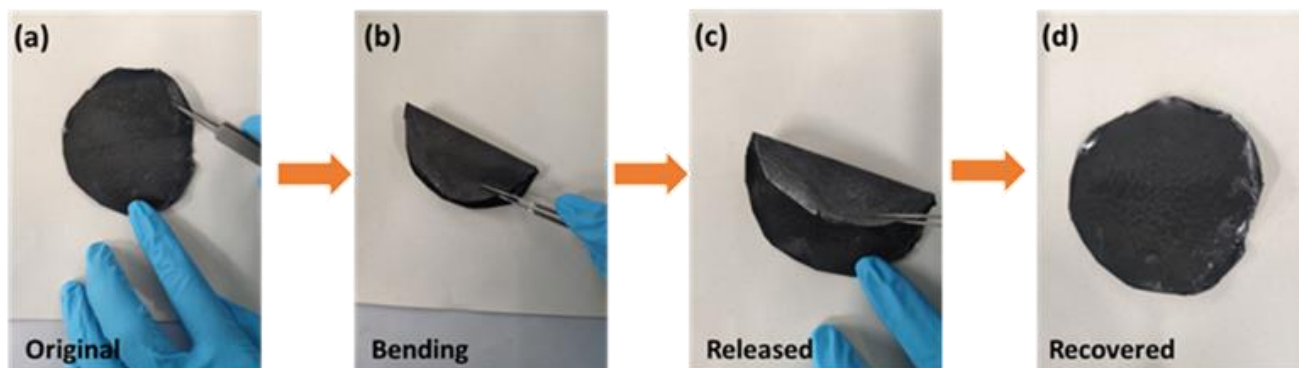


Figure 9. Flexibility of thermally conductive DEG-GO/PVA films.

4.4.2.1 Optical contact angle analyzer

The investigation of wetting behaviour in materials is critical for various applications, especially those related to thermal management. One of the significant considerations in thermal interface materials is their hydrophilic nature, which can significantly impact their effectiveness. Pristine

PVA films, for instance, have a high affinity to water, resulting in the absorption of water drops that may lead to reduced performance. Therefore, it is essential to understand the wetting behaviour of PVA and its composites with pure and reduced GO fillers. One promising approach to enhance the performance of thermal interface materials is by increasing their surface hydrophobicity. For this purpose, we observed an increase in the water contact angles (WCAs) from 35.89 to 72.13 degrees for the diethylene glycol reduced graphene oxide/PVA film is a clear indication of improved surface hydrophobicity, which is highly desirable for thermal management applications (See **figure 10 & 11**). A hydrophobic surface can prevent water condensation, thus reducing the risk of short circuits and corrosion in electronic devices. Compared to the PVA graphene oxide film, the DEG reduced GO/PVA film exhibits greater hydrophobicity and non-wettability, making it more suitable for hydrophobic thermal management applications. The higher contact angle observed in the DEG modified GO/PVA film is attributed to the presence of hydrophobic DEG molecules as surfactant, which could be present on the surface of graphene oxide. These molecules form a hydrophobic layer that inhibits the interaction between the film surface and water molecules, resulting in a higher contact angle and reduced surface energy and surface tension. This effect becomes more pronounced as the weight percentage of diethylene glycol reduced graphene oxide in the PVA matrix increases making the composite films partial non-wettable from being wettable, as shown in the experimental results below.

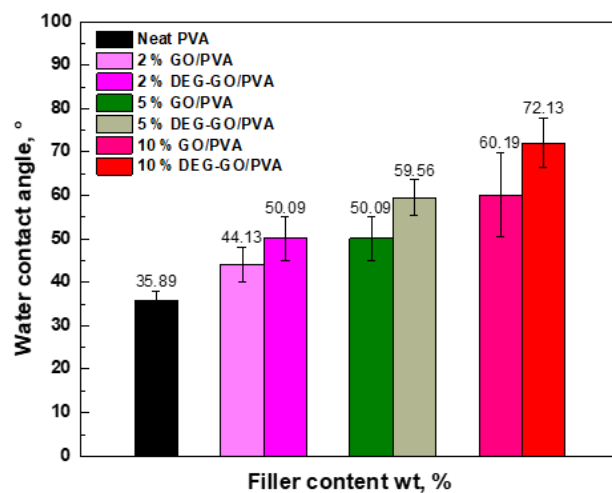


Figure 10. The WCAs of PVA and it's composite films.

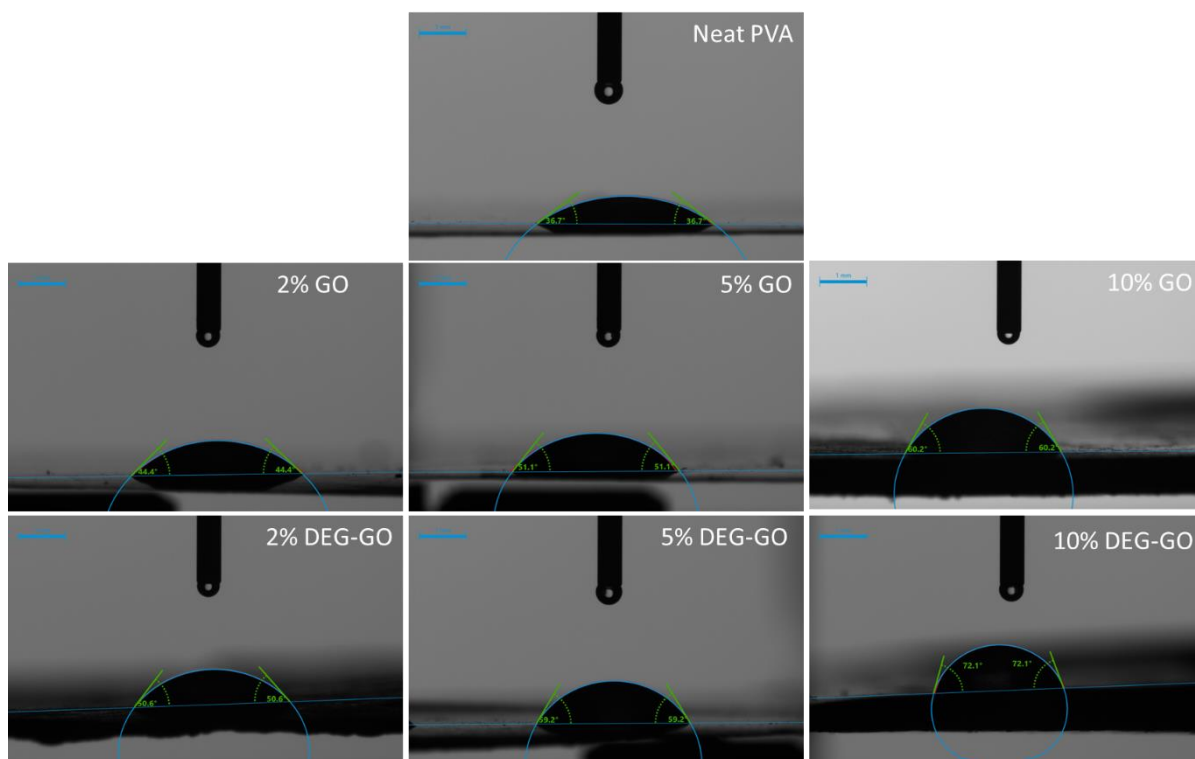


Figure 11. Pictorial representation of WCAs of PVA and it's composite films.

4.4.2.2 Atomic force microscopy (AFM)

In addition to the various pieces of evidence that support the reduction of graphene oxide (GO), we conducted atomic force microscopy (AFM) tests on both GO and DEG-GO PVA composite films. This analysis allowed us to delve deeper into the structural characteristics of these materials (see **Figure 12**). Initially, pure GO flakes exhibited an average thickness, that was measured to be around ca. $\sim 0.5 \mu\text{m}$. However, after the reduction process of GO with DEG and subsequent formation of DEG-GO sheets, notable changes were observed in their dimensions. The DEG-GO displayed an average thickness of $\sim 0.1 \mu\text{m}$ showcasing a significant decrease in the thickness compared to the original GO flakes.

The observed decrease in the thickness of the particles after the reduction process suggests that the introduction of DEG with GO was successful. This transformation could be attributed to the removal of most of the defects like functional groups attached on graphene oxide like hydroxyl and carboxyl molecules, making the graphene sheets in the flakes closer to each other and hence, resulting in the formation of much thinner DEG-GO flakes in PVA. To provide visual confirmation of these structural changes, AFM images were obtained and it allowed us to visualize the surface morphology and topography of the samples at nanoscale resolution. The images obtained from the AFM clearly displayed the decreased thickness and altered morphology of the DEG-GO compared to pure GO. Hence, by employing AFM analysis, we were able to corroborate the findings from other evidence and confirm the successful reduction process of GO with DEG as the reducing agent.

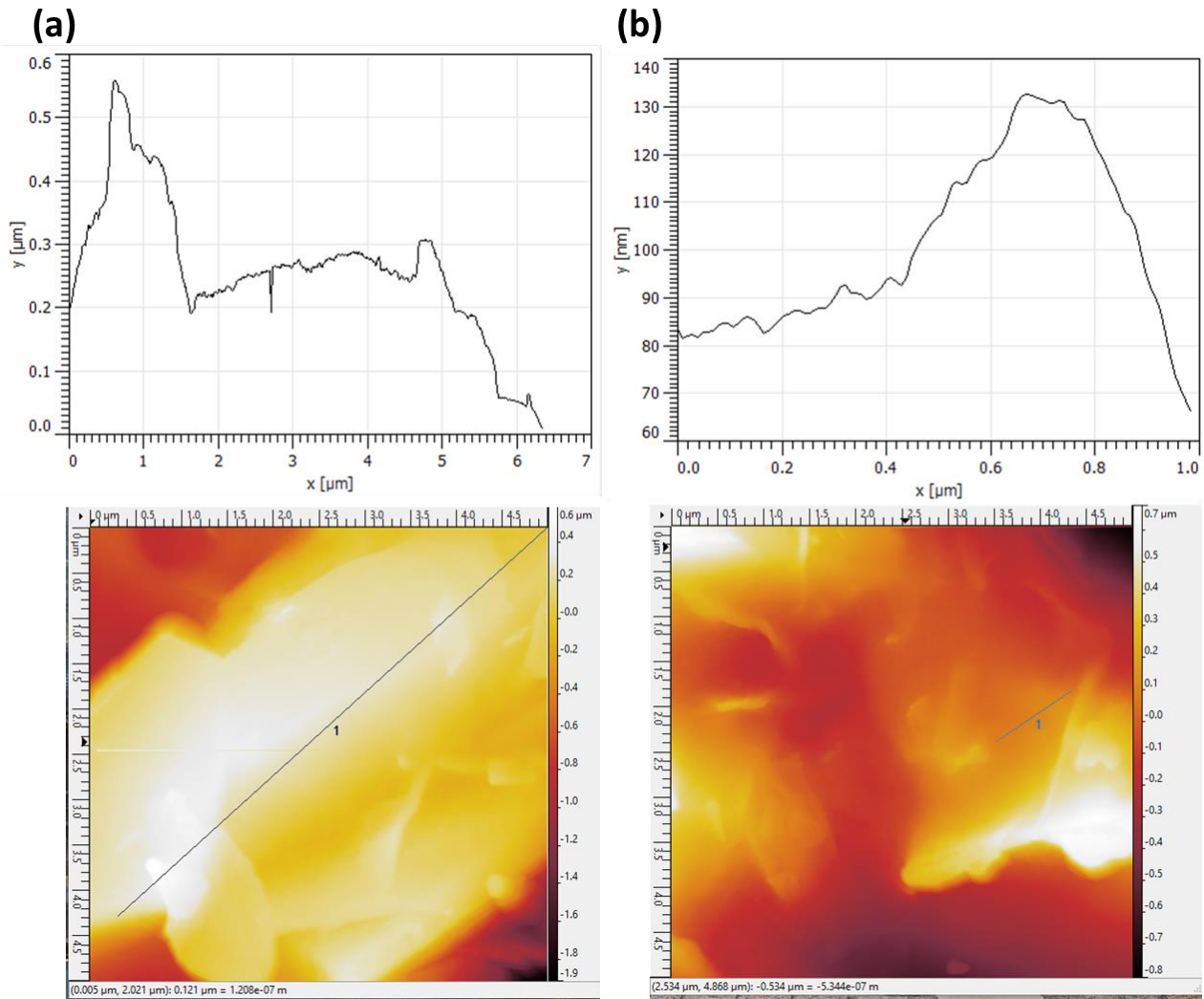


Figure 12(a): AFM analysis of pristine GO and; (b) DEG-GO in PVA.

4.4.2.3 Electrical resistivity

The electrical resistivity of PVA and its composites were investigated using the Keithley 6517B and 8009 resistivity test fixtures, as illustrated in **Figure 13**. While neat PVA served as an electrical insulator, exhibiting a volume resistivity of approximately $9.3 \times 10^{11} \Omega \text{ cm}$, the composites, containing various concentrations of GO and DEG-GO as filler material, demonstrated a decreasing trend in electrical resistivity. This decrease was primarily attributed to the high electrical conductivity of graphene as the filler material. Specifically, pure 10 wt. % GO/PVA

composites exhibited an electrical resistivity of approximately $9 \times 10^4 \Omega \text{ cm}$. However, DEG-GO/PVA films with the same filler loading demonstrated a slight decrease in electrical resistivity to approximately $8 \times 10^3 \Omega \text{ cm}$. This reduction in electrical resistivity could be attributed to the removal of -OH and -COOH groups from GO and the modification by DEG, which increased the C content, as mentioned in the EDS analysis. Other specimens with the pure and the reduced filler in PVA exhibited a similar trend as enumerated before. Therefore, these results indicate that the incorporation of GO and DEG-GO fillers can significantly affect the electrical resistivity of the PVA matrix, and the electrical conductivity of the composite can be tailored based on the concentration and type of filler material used. Thus, these findings provide valuable insights for the design and development of high-performance composite materials for electronic applications, particularly in thermal management.

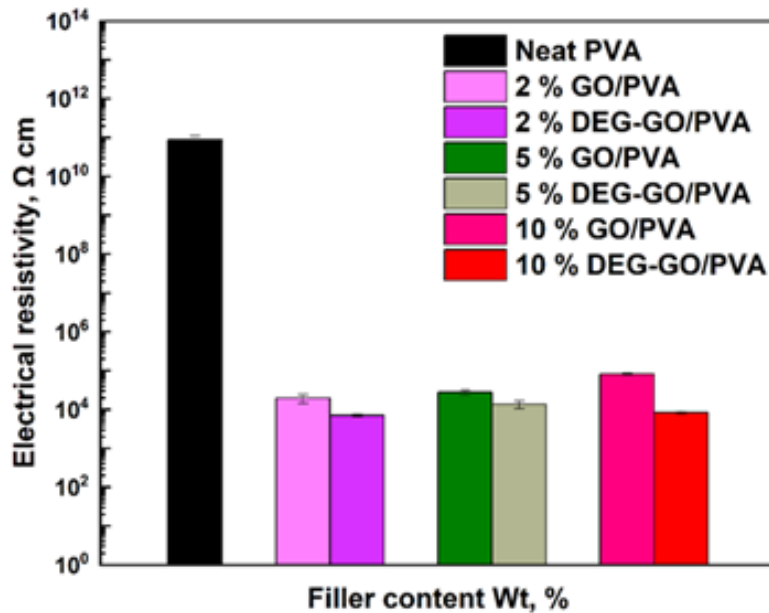


Figure 13. Electrical resistivity of GO/PVA composites

4.4.2.4 Thermal conductivity

Thermal conductivity of PVA and its composite films were characterized by the laser flash analysis (LFA) technique at room temperature conditions. An individual specimen taken to be tested, exhibited average thickness of ~ 1.3 mm and density of ~ 0.8 g/cm³. The results displayed that the highest increase in thermal conductivity is ca. 5.1 W/mK with just 10 wt.% DEG-GO based PVA films, as shown in **Figure 14**. Whereas, the pure GO flakes based PVA film with 10 wt.% filler loading also depicted a high thermal conductivity of ~ 4.63 W/mK. An enhancement in the thermal conductivity of DEG treated GO inside PVA matrix is substantial, even in the other weight fraction loadings as illustrated clearly in the figure. Hence, based on the observations we can say that the presence of DEG has endured this increase in the thermal conductivity and will discuss the possible mechanism in detail.

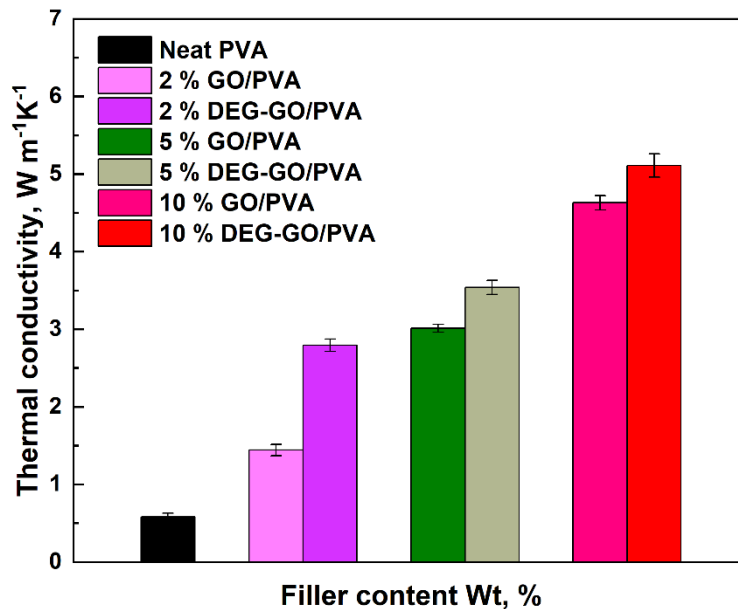


Figure 14. Thermal conductivity of GO/PVA composites.

DEG-treated GO can enhance the thermal conductivity in PVA films through several mechanisms:

- 1. Reduction of defects and functional Groups:** The DEG can lead to the reduction of defects and oxygen-containing functional groups on GO. These defects and functional groups tend to serve as heat scattering centers, impeding the smooth transfer of heat through the material. Through the process of reducing these scattering centers via reduction, the heat transport within the GO flakes in PVA is enhanced, leading to a notable increase in the material's thermal conductivity.
- 2. Superimposed stacking of graphene sheets:** Once the DEG treatment of GO induces the reduction process, it creates vacancies and results in the fulfilling and the overlapping of thinner graphene flakes with some regions of superimposed stacking of sp² graphene sheets into each other and self-assembly of DEG-GO sheets. This reduction also increased the crystallinity of graphene to some extent as enumerated before in SAED patterns leading to enhanced thermal conductivity.
- 3. Enhanced filler dispersion:** DEG also plays a role in enhancing the dispersion of GO flakes within the PVA matrix. It acts as a solvent and dispersant, effectively separating and dispersing the individual GO flakes, thereby preventing agglomeration[124]. A well-dispersed filler distribution ensures a continuous pathway for the heat conduction, enabling efficient thermal transport throughout the composite film.
- 4. Increased graphitic domains:** The reduction process that occurs during DEG modification promotes the restoration of conjugated sp² graphene networks in GO, resulting in increased graphitic domains (i.e., more C content as discussed earlier in EDS analysis). Graphitic domains possess higher thermal conductivity compared to the oxygen-

containing functional groups present in GO. As a result, the incorporation of DEG-reduced GO with increased graphitic domains enhances the overall thermal conductivity of the PVA film.

Collectively, these factors contribute to the enhanced thermal conductivity observed in PVA films containing DEG-reduced GO. The reduced defects, enhanced dispersion, and superimposed stacking of graphene sheets work together to facilitate the efficient heat transfer and improve the overall thermal conductivity of the composite film material.

4.5 Conclusion

In conclusion, the findings of this study have successfully demonstrated the enhanced thermal and electrical conductivity of flexible graphene oxide/polymer composite films through the reduction of graphene oxide fillers. By employing diethyl glycol as a reducing agent, the reduced fillers exhibited improved dispersibility and compatibility with the polymer matrix, thereby mitigating aggregation and fostering connectivity between graphene and polymer chains for the transfer of heat. The DEG-GO/PVA polymer films showcased remarkable thermal conductivity of approximately 5.1 W/mK at an optimal loading concentration of only 10 wt.%, as compared to the thermal conductivity of pure PVA film, which was approximately 0.45 W/mK. This heightened thermal conductivity is of utmost significance, particularly when considering the application of these films as TIMs, given that conventional industrial TIMs typically possess thermal conductivity values below 4 W/mK.

Furthermore, the DEG-treated composite films exhibited higher thermal conductivity compared to pure GO/PVA films. This can be attributed to the abundance of covalent bonds, reduced defects, and the bridging effect of the polymeric PVA with DEG-GO, which facilitates efficient heat transfer within the composite system. Additionally, the treatment of GO by DEG led to a reduction

in the electrical resistivity of the composite films. This improvement in both thermal and electrical properties hold significant potential for enhancing the performance of polymer-based materials, which find extensive applications in diverse fields such as electronics, energy, and aerospace.

Future studies can build upon these findings by optimizing the modification process and delving into the potential practical applications of reduced graphene oxide-based composites. By refining the fabrication techniques, researchers can strive to enhance the overall performance of these materials and explore their utilization in various real-world scenarios. The prospect of employing reduced graphene oxide-based composites holds promise for advancing the development of innovative solutions across multiple industries.

Chapter 5. CNT masterbatch based epoxy nanocomposites

5.1 Introduction

Carbon nanotubes (CNTs) have gained significant attention from researchers due to their exceptional properties, including high electrical and thermal conductivity, chemical and thermal stability, and high mechanical strength, making them ideal for various practical applications [125-127]. In particular, the incorporation of CNTs into thermoplastic and thermoset matrices to create percolation networks in polymer matrix nanocomposites enhances their mechanical and functional properties, such as electrical and thermal conductivity, and piezoresistive response [128,129]. The use of masterbatches, offer a unique method of introducing CNTs into polymer matrices, both on a research and industrial scale. They allow for the incorporation of nanoparticles into conventional composite production lines without major alterations, and they also provide an added layer of safety for handling and manufacturing, which takes away safety concerns associated with CNT/composite processing [129-132].

Previous research in the field of polymer nanocomposites using CNTs has primarily focused on mechanical and electrical properties, with few studies characterizing thermal properties. Therefore, in this study, we as researchers characterized the functional properties of masterbatch-based CNT reinforced epoxy nanocomposites in terms of electrical and thermal conductivity to evaluate their industrial applicability. We also investigated how the degree of dispersion and the manufacturing route of masterbatches affecting the properties of the nanocomposites. Understanding these factors is crucial in optimizing the properties of these nanocomposites for practical applications [133]. This chapter carries data from my article published in IEEE Xplore [133].

CNTs are well-known for their high thermal conductivity, which makes them ideal for improving the thermal properties of polymer nanocomposites [134-137]. The formation of a percolation network by CNTs within the polymer matrix allows for efficient thermal transport and results in a significant increase in the thermal conductivity of the nanocomposite, which can be controlled by varying the CNT loading and degree of dispersion[138]. Furthermore, the thermal conductivity of the nanocomposite can be tailored by controlling the orientation and alignment of the CNTs within the polymer matrix.

Apart from their high thermal conductivity, CNTs also exhibit tunable electrical resistivity, which can be adjusted by controlling their chirality and diameter. This intrinsic property of CNTs makes them ideal for enhancing the electrical conductivity of polymer nanocomposites. The addition of CNTs can lead to the formation of a percolation network, enhancing the electrical conductivity of the nanocomposite. This property can be exploited in various applications, such as in sensors, electromagnetic interference shielding, and energy storage devices [138].

In conclusion, the exceptional properties of CNTs, including their high thermal conductivity and tunable electrical resistivity, make them ideal for enhancing the functional properties of polymer nanocomposites. The effect of CNT loading, dispersion, and manufacturing route on these properties must be understood to tailor the properties of nanocomposites for specific applications.

5.2 Research objectives

The objectives of this work are to:

1. Characterize the electrical and thermal conductivity of masterbatch-based CNT reinforced epoxy nanocomposites to evaluate their industrial applicability for producing functional nanocomposites.

2. Investigate how the degree of dispersion of CNTs in the epoxy matrix affects the electrical and thermal conductivity of the nanocomposites.
3. Determine how the properties of the nanocomposites are dependent on the masterbatch manufacturing route when simple manufacturing techniques are used.
4. Understand the factors that optimize the properties of these nanocomposites for practical applications.

5.3 Experimental

5.3.1 Materials

In this study, we used three different industrial masterbatches to produce carbon nanotube (CNT)/epoxy nanocomposites at various weight percentages ranging from 0.5% to 2.0%. The details and name of each masterbatch used in the experiment are provided in Table 1.

Table 1: Various carbon nanotubes masterbatch particle detail.

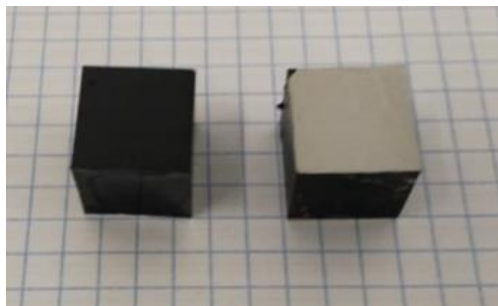
Name	Particle	Outer Diameter	Inner Diameter	Length	Aspect Ratio
MW1	MWCNT	10-30 nm	5-15 nm	2 μm and larger	60-1000
MW2	MWCNT	10-15 nm	5-15 nm	0.1-10 μm	6-1000
SW	SWCNT	1.6 \pm 0.4 nm	N/A	5 μm	2500-3200

5.3.2 Methodology

The nanocomposites were produced by diluting commercially available masterbatches and casting the resulting specimens. The desired weight percentages were 0.5%, 1.0%, and 2.0% wt, for MW1 (multiwalled carbon nanotubes 1), MW2 (multiwalled carbon nanotubes 2) and SW

(single walled carbon nanotubes) which were chosen to be close to, above, and well above the estimated percolation weight fraction, respectively. This study involved the utilization of three distinct masterbatches of carbon nanotubes (SW, MW1 and MW2) to create electrically and thermally conductive epoxy nanocomposites at varying weight percentages via a cost-effective, scalable processing method. Specifically, two of the masterbatches consisted of multi-wall carbon nanotubes (MWCNT) with comparable aspect ratios, while the third contained single-wall carbon nanotubes (SWCNTs) with a greater aspect ratio. Each masterbatch was manufactured via a distinct industrial processing technique.

To dilute the masterbatch, the required amount was weighed and added to pure epoxy resin. The mixture was homogenized using the ST 202 high-speed shear mixer at 500 RPM for 15 min, then further homogenized at 3000 RPM for 1 hour. The mixtures were ultrasonicated in four stages, each consisting of 15 min of ultrasonication time and a cool down period between stages of 5 min, to avoid overheating. Samples were then degassed under vacuum for 20 min in a degassing chamber. After degassing, hardener was added, and the mixture was mixed at 200 RPM for 10 min. The final step involved molding the samples in silicon molds for the required shape. The samples were cured at room temperature for 24 hours and then subjected to a post-cure heat treatment of 80 °C for 5 hours. Freekote NC770 was used as a debonder to ensure the easy release of samples from the molds. The thermal conductivity samples were prepared in the size of 1.5 cm × 1.5 cm × 1.5 cm,



while the electrical conductivity samples were in the size of 8 cm × 1 cm × 0.4 cm.



Electrical testing was conducted on five samples, whereas thermal testing was conducted on three samples.

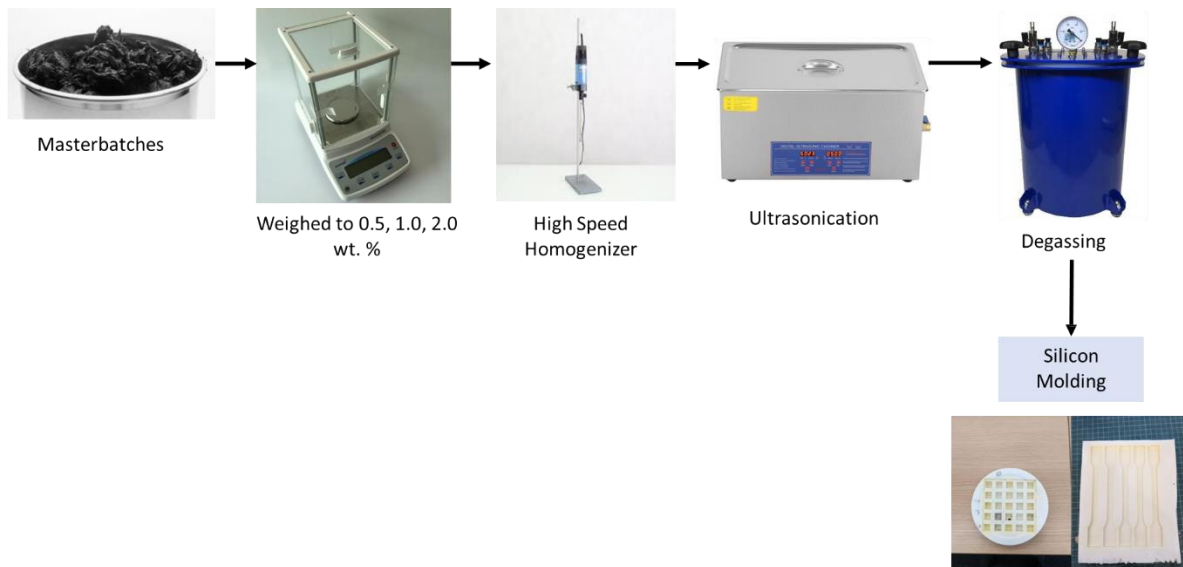


Figure 1. Schematic description of fabrication of CNTs/epoxy composites.

5.3.3 Characterization

The aim of this study was to determine the general dispersion degree of carbon nanotubes (CNTs) and to measure the electrical, thermal conductivity and thermal stability of the manufactured epoxy nanocomposites. Microstructural analysis was performed using the Thermo Scientific™ Helios G4 PFIB SEM on fractured thermal conductivity samples. The samples were coated with a layer of gold before imaging. Electrical conductivity measurements were obtained using the Keithley

DMM 6500, where a silver-based glue was applied to opposite faces to ensure proper contacts. The electrical conductivity was calculated using equations (1) and (2) with R being the resistance of the sample, ℓ being the distance between measurement probes, A being the cross-sectional area of the sample, ρ being the electrical resistivity of the sample, and σ being the electrical conductivity.

$$R = \rho l / A \quad (1)$$

$$\sigma = \frac{1}{\rho} \quad (2)$$

Thermal conductivity of the samples was measured using a Laser Optical Thermal Scanner on the rectangular samples mentioned earlier. Lastly, the thermal stability measurements were conducted using the Simultaneous Thermogravimetry – Differential Scanning Calorimetry analyzer STA 449 F3 Jupiter coupled with Quadrupole Mass Spectrometer QMS 403 D Aëolos.

5.4 Results and discussion

5.4.1 Microstructural Analysis

In the study, we performed microstructural analysis to investigate the dispersion of the carbon nanotubes (CNTs) in the nanocomposites via SEM images as shown in figure 2. We compared the dispersion of the CNTs in the composites made with two different multi-walled CNT masterbatches (MW1 and MW2) and a single-walled CNT masterbatch (SW). The results of the analysis showed significant differences in the dispersion of the CNTs between the composites made with the different masterbatches. The SW masterbatch, which was produced through a three-

roll milling process, showed the highest degree of homogeneous dispersion with relatively smaller, submicron-sized elongated bundles of CNTs. We attributed this to the high degree of dispersion and homogenization in the precursor material.

In contrast, the MW2 composites, which were produced through mechanical mixing, exhibited large ovular agglomerates with sizes ranging from 1-10 μm , along with smaller circular agglomerates. This led to a much lower degree of dispersion and agglomerate interconnectivity compared to the SW composites. The MW1 masterbatch, which was produced through extrusion, resulted in the largest agglomerates dispersed throughout the sample, ranging from 1-20 μm in size, but with better interconnectivity through smaller agglomerates. In the case of Single-Walled Carbon Nanotubes (SWCNTs), a discernible percolation network emerges within the epoxy resin system, comprising interconnected SWCNTs and SWCNT bundles. This network formation signifies a notable enhancement in thermal conductivity. However, in the case of Multi-Walled Carbon Nanotubes (MWCNTs), we observe the presence of ovular agglomerates, and huge vacant regions of epoxy resin as depicted in the SEM images in Figure 2. These images also clearly reveal the impregnation of epoxy resin into the spaces between MWCNTs. Unfortunately, the percolation networks formed by MWCNTs in other regions are not sufficiently well-structured to yield a significant increase in thermal conductivity like we see in SWCNTs.

Overall, these findings suggest that the processing technique used to produce the masterbatch has a significant impact on the dispersion and interconnectivity of the CNTs in the resulting nanocomposites. This information can be valuable in optimizing the manufacturing process of electrically and thermally conductive nanocomposites for various applications.

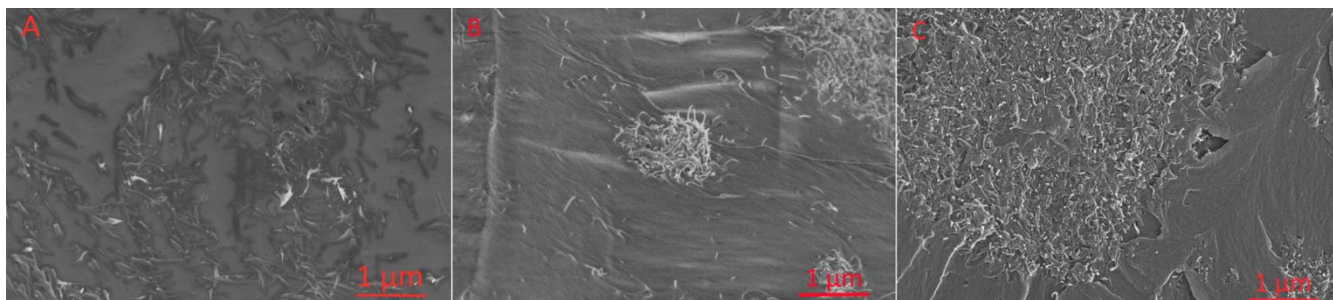


Figure 2. SEM imagery of (A) SW, (B) MW2 and (C) MW1. All images are from samples with 2 % wt. CNTs at 65,000X magnification.

5.4.2 Electrical resistivity

Electrical resistivity of various epoxy composites was measured with the results of the observations indicating that as the weight percentage of carbon nanotubes (CNTs) increased, all materials exhibited a trend in decrease in electrical resistivity (see **Figure 3**). Among the samples, the SW nanocomposites, which had the highest degree of dispersion, exhibited the lowest electrical resistivity at all weight percentages, specifically at 2 wt.% SW carbon nanotubes, it displayed an ultra-low electrical resistivity of 2.23 Ω cm. On the other hand, the dispersion effects were more evident in the MW1 and MW2 samples in terms of electrical resistivity, with the MW1 samples displaying higher electrical resistivity at all weight percentages due to superior masterbatch processing. Additionally, the differences in performance between MW1 and MW2 samples are believed to be due to different microstructures resulting from the masterbatch processing techniques employed. In conclusion, the results of the study demonstrated the importance of proper dispersion of CNTs in the preparation of nanocomposites with desirable electrical properties with SW outperforming MW1 and MW2 as shown in **figure 3**. Furthermore, the study highlights the impact of the masterbatch processing technique on the microstructure and performance of the final nanocomposite product. The low electrical resistivity of CNTs in epoxy resin makes the material suitable for several applications such as under-filled materials, and electronic packaging. In these particular applications, the CNT-filled epoxy resin composite can be used in underfilled material

where a slurry of thermally conductive CNT-filled epoxy resin (uncured) can be impregnated within the gaps of substrate (e.g., motherboard in computers) and the chip which will be then cured at room temperature after 24 hours, and provide a thermally and electrically conductive pathway for electronic components. Concisely, the low electrical resistivity of CNTs in epoxy resin makes them an excellent choice for applications where high electrical conductivity is required.

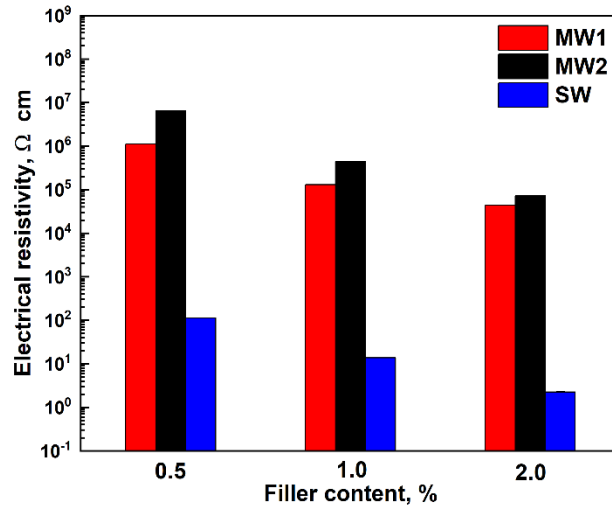


Figure 3. Electrical resistivity vs. weight % of CNTs added. All variances $\leq 15\%$.

5.4.3 Thermal conductivity

Thermal conductivity measurements were conducted on the rectangular samples as mentioned earlier, using a Laser Optical Thermal Scanner. The results as showed in **figure 4** that all the samples exhibited an increase in thermal conductivity with an increase in weight percentage of CNTs. The SW nanocomposites showed the highest thermal conductivity at all weight percentages due to their relatively uniform dispersion. The elongated shape of the SWCNTs, which have a superior aspect ratio compared to MWCNTs, provided a better thermal conduction channel between the CNTs and the polymer. The TC enhancement factor for the 2.0% SW nanocomposite was particularly high, at approximately 172%, due to the homogeneous mixing of CNTs within

the polymer matrix. This resulted in more efficient heat conduction from a much larger thermal channel of connected SWCNTs, which greatly contributed to the augmentation of thermal conductivity up to ~ 0.5 W/mK. SW with a superior aspect ratio of 2500–3200 perhaps provided better extended dimensionality and a large contact area owing to its 2D structure, henceforth, creating a better interface and decreasing the overall interfacial thermal resistance between the epoxy resin polymer. Thus, this cylindrical structure of SW carbon nanotubes with a larger diameter of $\sim 5\mu\text{m}$ of length provided an effective channel for the transfer of heat in the polymer resin system.

In contrast, the MW1 and MW2 nanocomposites did not exhibit a significant rise in thermal conductivity, which could be attributed to their lower aspect ratios and weaker dispersion. Overall, the thermal conductivity differences between the MW nanocomposites were less pronounced, with both MW1 and MW2 showing very similar values for all weight percentages tested (0.5% = 0.2 W/mK, 1.0% = 0.21 W/mK, 2.0% = 0.22 W/mK). The differences in thermal conductivity between the different types of nanocomposites are attributed to their respective microstructures, which are influenced by the processing techniques used to produce the masterbatches.

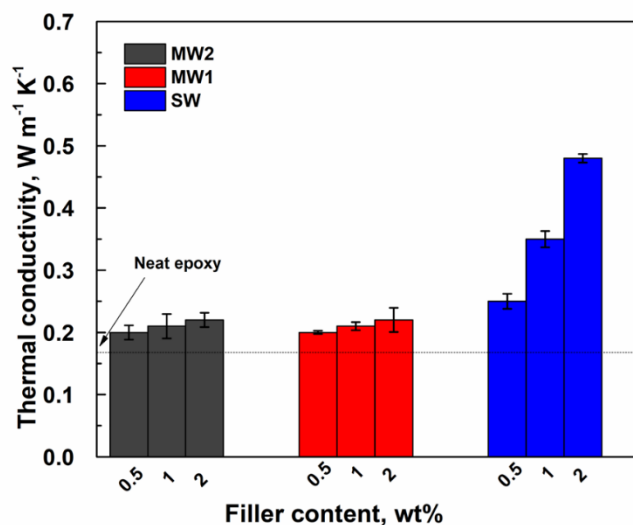


Figure 4. Thermal conductivity of epoxy nanocomposites

5.4.4 Thermal stability

The results of the study showed that all SW (single-walled) composites exhibited an improvement in thermal stability as the weight percentage of carbon nanotube (CNT) fillers increased. This was shown in **Figure 5a, b** that as the filler loading increased, the temperature at which 10 wt.% loss occurred also increased. For example, the addition of 1 wt.% fillers caused an increase in temperature of around 18 °C, while the addition of 2 wt.% fillers caused an increase of around 35 °C compared to neat epoxy resin. The reason for this improvement in thermal stability can be attributed to the uniform dispersion of high aspect ratio carbon nanotubes in the SW composites. This facilitates the formation of a percolated network that provides better thermal conduction channels[139], enabling the passage of heat over longer distances without transitions from particle to particle. This improved thermal conductivity is also attributed to better interfacial interaction with the matrix, making the composites thermally stable and robust at elevated temperatures [137,140].

On the other hand, MW1 and MW2 composites did not exhibit a significant increase in thermal stability (See **Table 1**). The addition of 2 wt.% MW fillers only resulted in an increase in temperature of around 16 °C and 17 °C at 10 wt.% loss, respectively. The probable causes for this were weaker dispersion and agglomeration of fillers when considering the microstructures.

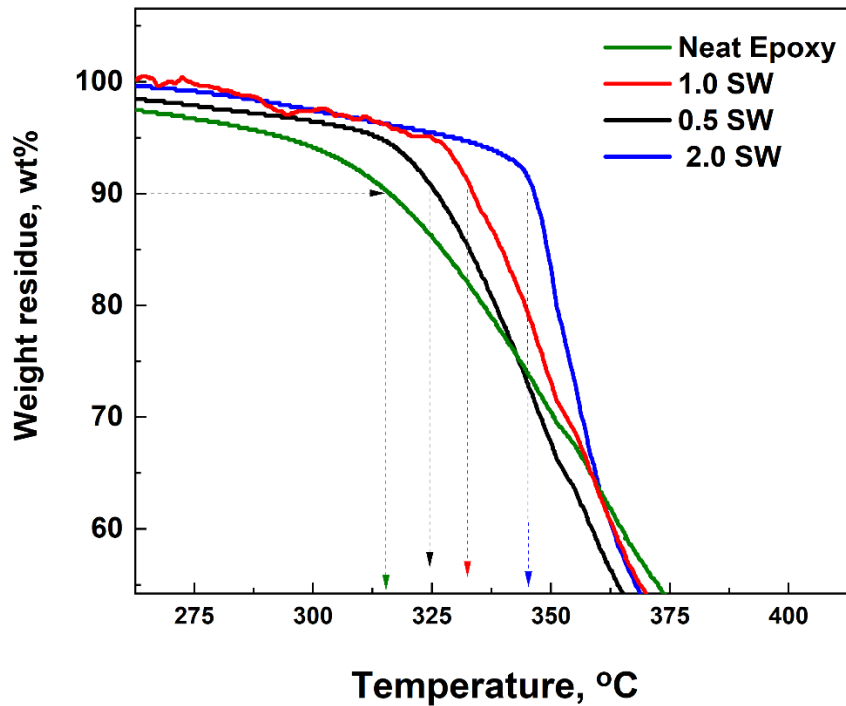


Figure 5. Thermogravimetric analysis (TGA) of SW/epoxy composites with various loading contents with thermal stability of specimens at 10 % thermal degradation temperature.

Table 1. Thermal stability of CNTs/epoxy composites with T10% is referred to as the temperature at 10% degradation of material.

Nanocomposite	T_{10%} (°C)
Plain epoxy	316
0.5 SW	326
1.0 SW	334
2.0 SW	347
0.5 MW1	319
1.0 MW1	327
2.0 MW1	332
0.5 MW2	318
1.0 MW2	326
2.0 MW2	333

5.4.5 Differential scanning calorimetry (DSC) analysis

The results of the differential scanning calorimetry (DSC) analysis show that the addition of carbon nanotubes (CNTs) to the epoxy matrix caused an increase in glass transition temperature (T_g) for all the nanocomposites, as shown in **Figure 6**. The T_g values were determined by calculating the tangents on the heat flow curve and are presented in **Table 2**. The highest enhancement in T_g was observed for the 2.0 wt.% SW composites, which showed an increase from around 81 °C (plain epoxy) to approximately 102 °C. This significant enhancement in T_g is attributed to the strong interfacial interaction between the SWCNTs and the epoxy, which reduces the segmental mobility of the polymer chains[141]. In contrast, the MW1 and MW2 nanocomposites did not show as significant an increase in T_g compared to the SW samples.

Furthermore, the increase in T_g for the SW composites was higher than that observed for MW1 and MW2 (although the measurement error needs to be considered). These results suggest that the SWCNTs are more effective in enhancing the T_g of the epoxy matrix due to their superior aspect ratio and uniform dispersion, which promotes a more efficient reinforcement effect.

Table 2. DSC values for the nanocomposites

Nanocomposite	Glass transition temperature (T_g, C°)
Neat epoxy	81
0.5 SW	93
1.0 SW	95
2.0 SW	102
0.5 MW1	89
1.0 MW1	91
2.0 MW1	92
0.5 MW2	85
1.0 MW2	93
2.0 MW2	97

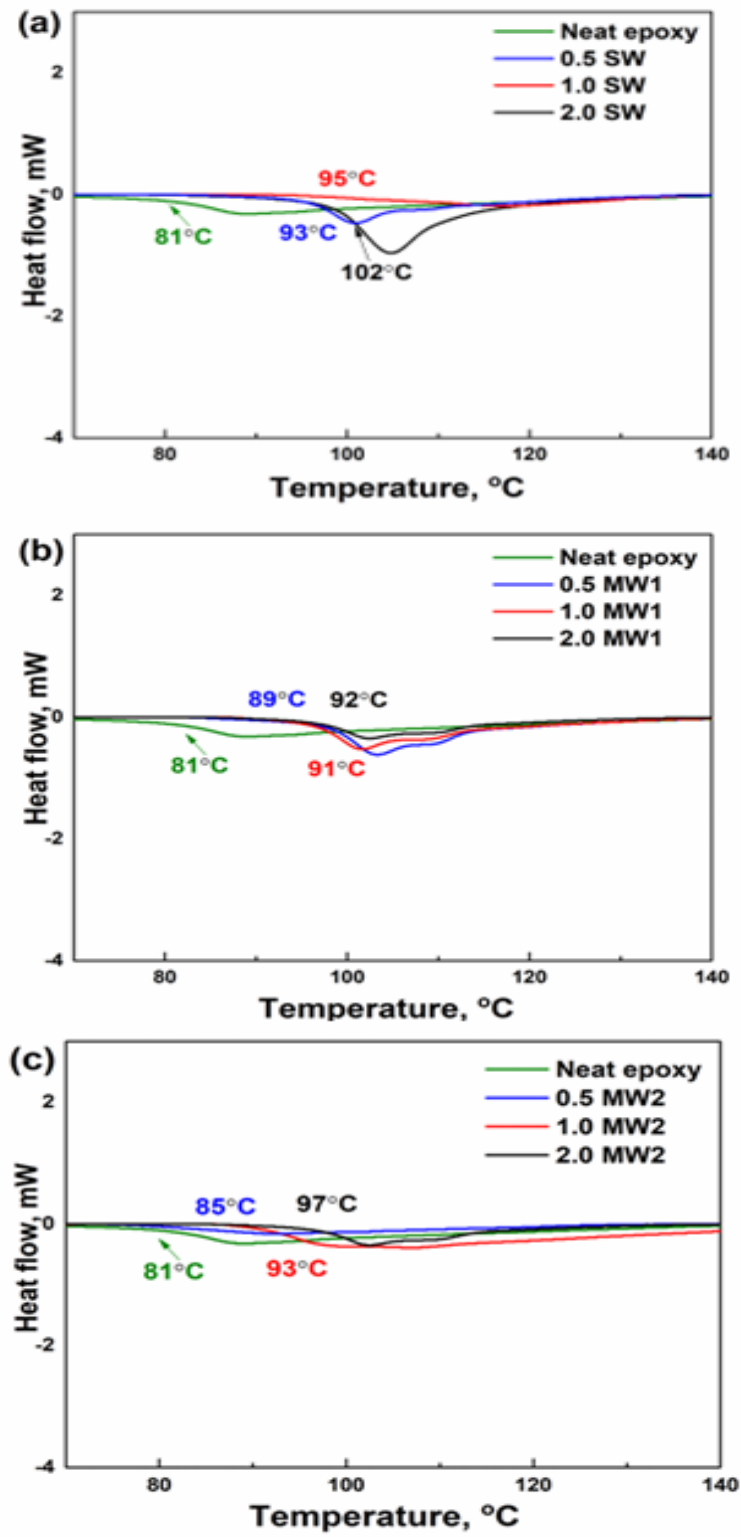


Figure 6. The DSC curves of (a) SW, (b) MW1 and (c) MW2 nanocomposites

5.5 Conclusion

In conclusion, the present study aimed to develop electrically and thermally conductive epoxy nanocomposites using three masterbatches of carbon nanotubes (CNTs) at different weight percentages. The masterbatches were produced industrially using different processing techniques, and the functional properties of the produced nanocomposites were found to be directly related to the particle dispersion and masterbatch production route. The nanocomposites produced with better masterbatch production technology, i.e., single-walled carbon nanotubes (SWCNTs), exhibited better dispersion compared to those produced using less effective production techniques, i.e., multi-walled carbon nanotubes (MWCNTs).

The SWCNT nanocomposites showed higher electrical and thermal conductivity values compared to MWCNT samples, with electrical resistivity reaching as low as of $2.23 \Omega \text{ cm}$ and thermal conductivity reaching $0.48 \text{ Wm}^{-1} \text{ K}^{-1}$ at 2.0% wt. In contrast, MWCNT samples showed much higher electrical resistivity values between $4.41 \times 10^4 \Omega \text{ cm}$ and $7.29 \times 10^4 \Omega \text{ cm}$ and thermal conductivity values of $0.22 \text{ Wm}^{-1} \text{ K}^{-1}$ at the same weight percentage. The superior performance of SWCNT samples was attributed to the higher aspect ratio of the SWCNTs and their uniform dispersion, resulting in the generation of a percolated network facilitating better thermal and electrical conductivity.

Furthermore, the glass transition temperature and thermal stability of the nanocomposites followed the same trend as electrical and thermal conductivity, with higher dispersion degrees, weight percentages, and aspect ratios resulting in higher values. It was observed that the resulting composites displayed microstructures dependent upon the quality of the masterbatch production

route when simple production methods were utilized, which cannot decrease agglomerate size beyond the method employed during masterbatch production.

In summary, this study has successfully demonstrated that masterbatch based manufacturing can produce nanocomposites with the desired functional properties of thermal and electrical conductivity. The findings highlight the importance of selecting the appropriate masterbatch production technology and achieving good particle dispersion for the development of high-performance nanocomposites. Overall, CNT-epoxy composites are versatile materials that can be used in a wide range of applications that require both high electrical and thermal conductivity.

They can find their usage in industrial applications like transparent conductive films as these CNT-epoxy composites can be used as underfilled materials and to make transparent conductive films (TCFs) that are used in touch screens, LCDs, and solar cells. The high electrical conductivity of CNTs ensures efficient charge transfer, while the high thermal conductivity ensures that the film does not overheat.

Chapter 6. Conclusion

This dissertation presents a comprehensive experimental investigation into the synthesis of thermally conductive polymer nanocomposites, with a focus on their application within the electronic industry in the industrial sector. Our research entailed the fabrication of a series of Thermal Interface Materials (TIMs) and underfilled materials, employing diverse thermally conductive filler materials in the form of two-dimensional (2-D) materials such as boron nitride and reduced graphene oxide, as well as one-dimensional (1-D) materials like single-walled and multi-walled carbon nanotubes (CNTs) into the set of various polymers. Enhancement of the thermal conductivity of the composites requires homogeneous dispersion of the thermally conductive fillers within the polymer composites, which can be achieved by using a complex of various techniques, including self-assembly of the fillers within the polymers, reducing the filler materials, and utilizing the most suitable mixing methods

The findings of our study can be summarized as follows:

1. Throughout the experimentation process, we emphasized on making the production of TIMs more cost-effective for industrial applications. As a result, we carefully considered loading concentrations of fillers ranging from low (0.5% to 10%) to optimum levels (66%), facilitating their incorporation into more affordable polymers like epoxy resin and PVA for the fabrication of thermally conductive polymer composites since the cost of these TC fillers like graphene, carbon nanotubes and boron nitride are very expensive.
2. Flexible thermally conductive polymer films with a remarkably low filler concentration (10 wt.% reduced graphene oxide) produced show an outstanding thermal conductivity of approximately 5.1 W/mK. This value surpasses the conventional thermal conductivity of TIMs typically employed in the industry, which typically ranges around 4.0 W/mK.

Optimization of thermally conductive polymer nanocomposites were achieved in contrast to the conventional TIMs which employed quite high filler loading concentrations. Consequently, polymer composite films based on DEG-GO/PVA can serve as a viable alternative to existing TIMs or TMMs

3. CNT-based epoxy composites exhibited a notably high thermal conductivity of 0.48 W/mK, achieved with a mere 2 wt.% SWCNT loading concentration. These composites are highly suitable for utilization as under-filled materials.
4. Three-dimensional (3-D) frameworks of thermally conductive 3D framework demonstrating isotropic thermal conductivity properties, namely, an elevated in-plane thermal conductivity of approximately 0.76 W/mK and an out-of-plane thermal conductivity of around 0.63 W/mK are fabricated thereby. Furthermore, these composites displayed excellent hydrophobicity in water, exceptional thermal stability, and a remarkably high electrical resistivity of at least $1 \times 10^{15} \Omega \text{ cm}$, making them ideal for applications requiring stringent electrical insulation within the industry.

In conclusion, this dissertation offers a comprehensive analysis of the experimental study conducted on the fabrication of thermally conductive polymer nanocomposites, shedding light on their potential applications within the industrial sector of the electronic industry. The significant advancements achieved in terms of thermal conductivity, cost-effectiveness, electrical conductivities, and their overall performance, making these materials highly promising for future implementation in relevant industrial settings.

Bibliography

1. Burger, N. Laachachi A. Ferriol M. Lutz M. Toniazzo V. Ruch D. Review of thermal conductivity in composites: mechanisms, parameters and theory. *Prog. Polym. Sci* 2016, 61, 1-28.
2. Jia, H.; Liang, L.-l.; Liu, D.; Wang, Z.; Liu, Z.; Xie, L.-j.; Tao, Z.-c.; Kong, Q.-q.; Chen, C.-m. A review of three-dimensional graphene networks for thermal management and electromagnetic protection. *New Carbon Materials* 2021, 36, 851-868, doi:10.1016/s1872-5805(21)60088-4.
3. Cui, Y.; Li, M.; Hu, Y. Emerging interface materials for electronics thermal management: experiments, modeling, and new opportunities. *Journal of Materials Chemistry C* 2020, 8, 10568-10586, doi:10.1039/c9tc05415d.
4. Yang, X.; Liang, C.; Ma, T.; Guo, Y.; Kong, J.; Gu, J.; Chen, M.; Zhu, J. A review on thermally conductive polymeric composites: classification, measurement, model and equations, mechanism and fabrication methods. *Advanced Composites and Hybrid Materials* 2018, 1, 207-230, doi:10.1007/s42114-018-0031-8.
5. Zhang, F.; Feng, Y.; Feng, W. Three-dimensional interconnected networks for thermally conductive polymer composites: Design, preparation, properties, and mechanisms. *Materials Science and Engineering: R: Reports* 2020, 142, 100580, doi:10.1016/j.mser.2020.100580.
6. Ji, T.; Feng, Y.; Qin, M.; Feng, W. Thermal conducting properties of aligned carbon nanotubes and their polymer composites. *Composites Part A: Applied Science and Manufacturing* 2016, 91, 351-369.
7. Li, A.; Zhang, C.; Zhang, Y.-F. Thermal conductivity of graphene-polymer composites: Mechanisms, properties, and applications. *Polymers* 2017, 9, 437.
8. Feng, C.-P.; Chen, L.-B.; Tian, G.-L.; Wan, S.-S.; Bai, L.; Bao, R.-Y.; Liu, Z.-Y.; Yang, M.-B.; Yang, W. Multifunctional thermal management materials with excellent heat dissipation and generation capability for future electronics. *ACS applied materials & interfaces* 2019, 11, 18739-18745.
9. Zhang, X.; Zhang, H.; Li, D.; Xu, H.; Huang, Y.; Liu, Y.; Wu, D.; Sun, J. Highly thermally conductive and electrically insulating polydimethylsiloxane composites prepared by ultrasonic-assisted forced infiltration for thermal management applications. *Composites Part B: Engineering* 2021, 224, 109207.
10. Owais, M.; Javed, M.H.; Akram, M.Z.; Paxton, W.F.; Akhatov, I.S.; Abaimov, S.G. Review—Recent Advances in Thermally Conductive Paper-Like Films. *ECS Journal of Solid State Science and Technology* 2021, 10, 033001, doi:10.1149/2162-8777/abea5b.
11. Hanafi, M.Z.M.; Ismail, F.S.; Rosli, R. Radial plate fins heat sink model design and optimization. In *Proceedings of the 2015 10th Asian control conference (ASCC)*, 2015; pp. 1-5.
12. Zhao, Y.; Zeng, X.; Ren, L.; Xia, X.; Zeng, X.; Zhou, J. Heat conduction of electrons and phonons in thermal interface materials. *Materials Chemistry Frontiers* 2021, 5, 5617-5638, doi:10.1039/D0QM01136C.
13. Lee Sanchez, W.A.; Li, J.-W.; Chiu, H.-T.; Cheng, C.-C.; Chiou, K.-C.; Lee, T.-M.; Chiu, C.-W. Highly thermally conductive epoxy composites with AlN/BN hybrid filler as underfill encapsulation material for electronic packaging. *Polymers* 2022, 14, 2950.
14. Wang, X.; Wu, P. Melamine foam-supported 3D interconnected boron nitride nanosheets network encapsulated in epoxy to achieve significant thermal conductivity enhancement at an ultralow filler loading. *Chemical Engineering Journal* 2018, 348, 723-731.
15. Sun, Z.; Li, J.; Yu, M.; Kathaperumal, M.; Wong, C.-P. A review of the thermal conductivity of silver-epoxy nanocomposites as encapsulation material for packaging applications. *Chemical Engineering Journal* 2022, 137319.
16. Li, T.; Zhang, J.; Wang, H.; Hu, Z.; Yu, Y. High-performance light-emitting diodes encapsulated with silica-filled epoxy materials. *ACS applied materials & interfaces* 2013, 5, 8968-8981.

17. Ma, H.; Gao, B.; Wang, M.; Yuan, Z.; Shen, J.; Zhao, J.; Feng, Y. Strategies for enhancing thermal conductivity of polymer-based thermal interface materials: a review. *Journal of Materials Science* 2020, doi:10.1007/s10853-020-05279-x.
18. Feng, C.P.; Wei, F.; Sun, K.Y.; Wang, Y.; Lan, H.B.; Shang, H.J.; Ding, F.Z.; Bai, L.; Yang, J.; Yang, W. Emerging Flexible Thermally Conductive Films: Mechanism, Fabrication, Application. *Nano-micro letters* 2022, 14, 127, doi:10.1007/s40820-022-00868-8.
19. Toberer ES, Baranowski LL, Dames C. Advances in thermal conductivity. *Annu Rev Mater Res* 2012;42:179–209.
20. Owais, M.; Shiverskii, A.; Sulimov, A.; Ostrizhiniy, D.; Popov, Y.; Mahato, B.; Abaimov, S.G. Scalable Fabrication of Thermally Conductive Layered Nacre-like Self-Assembled 3D BN-Based PVA Aerogel Framework Nanocomposites. *Polymers* 2022, 14, doi:10.3390/polym14163316.
21. Wu, Y.; Xue, Y.; Qin, S.; Liu, D.; Wang, X.; Hu, X.; Li, J.; Wang, X.; Bando, Y.; Golberg, D.; et al. BN Nanosheet/Polymer Films with Highly Anisotropic Thermal Conductivity for Thermal Management Applications. *ACS applied materials & interfaces* 2017, 9, 43163-43170, doi:10.1021/acsmi.7b15264.
22. Hu, Z.; Wang, S.; Chen, G.; zhang, Q.; Wu, K.; Shi, J.; Liang, L.; Lu, M. An aqueous-only, green route to exfoliate boron nitride for preparation of high thermal conductive boron nitride nanosheet/cellulose nanofiber flexible film. *Composites Science and Technology* 2018, 168, 287-295, doi:https://doi.org/10.1016/j.compscitech.2018.09.020.
23. Sun, J.; Yao, Y.; Zeng, X.; Pan, G.; Hu, J.; Huang, Y.; Sun, R.; Xu, J.B.; Wong, C.P. Preparation of boron nitride nanosheet/nanofibrillated cellulose nanocomposites with ultrahigh thermal conductivity via engineering interfacial thermal resistance. *Advanced Materials Interfaces* 2017, 4, 1700563.
24. Li, G.; Tian, X.; Xu, X.; Zhou, C.; Wu, J.; Li, Q.; Zhang, L.; Yang, F.; Li, Y. Fabrication of robust and highly thermally conductive nanofibrillated cellulose/graphite nanoplatelets composite papers. *Composites Science and Technology* 2017, 138, 179-185, doi:https://doi.org/10.1016/j.compscitech.2016.12.001.
25. Liang, Q.; Yao, X.; Wang, W.; Liu, Y.; Wong, C.P. A Three-Dimensional Vertically Aligned Functionalized Multilayer Graphene Architecture: An Approach for Graphene-Based Thermal Interfacial Materials. *ACS nano* 2011, 5, 2392-2401, doi:10.1021/nn200181e.
26. Wang, J.; Wu, Y.; Xue, Y.; Liu, D.; Wang, X.; Hu, X.; Bando, Y.; Lei, W. Super-compatible functional boron nitride nanosheets/polymer films with excellent mechanical properties and ultra-high thermal conductivity for thermal management. *Journal of Materials Chemistry C* 2018, 6, 1363-1369, doi:10.1039/c7tc04860b.
27. Kunova, O.; Kustova, E.; Mekhonoshina, M.; Nagnibeda, E. Non-equilibrium kinetics, diffusion and heat transfer in shock heated flows of N₂/N and O₂/O mixtures. *Chemical Physics* 2015, 463, 70-81, doi:https://doi.org/10.1016/j.chemphys.2015.10.004.
28. Zhang, X.; Sun, D.; Li, Y.; Lee, G.-H.; Cui, X.; Chenet, D.; You, Y.; Heinz, T.F.; Hone, J.C. Measurement of Lateral and Interfacial Thermal Conductivity of Single- and Bilayer MoS₂ and MoSe₂ Using Refined Optothermal Raman Technique. *ACS applied materials & interfaces* 2015, 7, 25923-25929, doi:10.1021/acsmi.5b08580.
29. Ren, L.; Pashayi, K.; Fard, H.R.; Kotha, S.P.; Borca-Tasciuc, T.; Ozisik, R. Engineering the coefficient of thermal expansion and thermal conductivity of polymers filled with high aspect ratio silica nanofibers. *Composites Part B: Engineering* 2014, 58, 228-234, doi:https://doi.org/10.1016/j.compositesb.2013.10.049.
30. Huang, C.; Qian, X.; Yang, R. Thermal conductivity of polymers and polymer nanocomposites. *Materials Science and Engineering: R: Reports* 2018, 132, 1-22, doi:https://doi.org/10.1016/j.mser.2018.06.002.
31. Xu, X.; Chen, J.; Zhou, J.; Li, B. Thermal Conductivity of Polymers and Their Nanocomposites. *Advanced materials* 2018, 30, e1705544, doi:10.1002/adma.201705544.

32. Burger, N.; Laachachi, A.; Ferriol, M.; Lutz, M.; Toniazzo, V.; Ruch, D. Review of thermal conductivity in composites: Mechanisms, parameters and theory. *Progress in Polymer Science* 2016, 61, 1-28, doi:<https://doi.org/10.1016/j.progpolymsci.2016.05.001>.
33. Tritt TM. *Thermal conductivity – theory, properties & applications*. New York: Plenum Publishers; 2004. p. 285.
34. Sun, H.; Xu, Z.; Gao, C. Multifunctional, ultra-flyweight, synergistically assembled carbon 3D framework. *Advanced materials* 2013, 25, 2554-2560.
35. Wu, Y.; Yi, N.; Huang, L.; Zhang, T.; Fang, S.; Chang, H.; Li, N.; Oh, J.; Lee, J.A.; Kozlov, M.; et al. Three-dimensionally bonded spongy graphene material with super compressive elasticity and near-zero Poisson's ratio. *Nature communications* 2015, 6, 6141, doi:10.1038/ncomms7141.
36. Zhang, W.; Kong, Q.Q.; Tao, Z.; Wei, J.; Xie, L.; Cui, X.; Chen, C.M. 3D Thermally Cross-Linked Graphene Aerogel–Enhanced Silicone Rubber Elastomer as Thermal Interface Material. *Advanced Materials Interfaces* 2019, 6, 1900147, doi:10.1002/admi.201900147.
37. Pan, D.; Dong, J.; Yang, G.; Su, F.; Chang, B.; Liu, C.; Zhu, Y.-C.; Guo, Z. Ice template method assists in obtaining carbonized cellulose/boron nitride aerogel with 3D spatial network structure to enhance the thermal conductivity and flame retardancy of epoxy-based composites. *Advanced Composites and Hybrid Materials* 2021, 5, 58-70, doi:10.1007/s42114-021-00362-6.
38. Lv, P.; Miao, H.; Ji, C.; Wei, W. Highly compressible graphene aerogel with high thermal conductivity along both in-plane and through-plane directions. *Materials Research Express* 2021, 8, 045608, doi:10.1088/2053-1591/abf8e4.
39. Owais, M.; Shiverskii, A.; Pal, A.K.; Mahato, B.; Abaimov, S.G. Recent Studies on Thermally Conductive 3D 3D framework/Foams with the Segregated Nanofiller Framework. *Polymers* 2022, 14, doi:10.3390/polym14224796.
40. An, F.; Li, X.; Min, P.; Li, H.; Dai, Z.; Yu, Z.-Z. Highly anisotropic graphene/boron nitride hybrid 3D framework with long-range ordered architecture and moderate density for highly thermally conductive composites. *Carbon* 2018, 126, 119-127, doi:10.1016/j.carbon.2017.10.011.
41. Rapisarda, M.; Malfense Fierro, G.P.; Meo, M. Ultralight graphene oxide/polyvinyl alcohol aerogel for broadband and tuneable acoustic properties. *Scientific reports* 2021, 11, 10572, doi:10.1038/s41598-021-90101-0.
42. Liu, Z.; Wang, Q.; Hou, L.; Liu, Y.; Li, Z. Ultralight, Ultraflexible, Anisotropic, Highly Thermally Conductive Graphene Aerogel Films. *Molecules* 2021, 26, doi:10.3390/molecules26226867.
43. Ahankari, S.; Paliwal, P.; Subhedar, A.; Kargarzadeh, H. Recent Developments in Nanocellulose-Based 3D framework in Thermal Applications: A Review. *ACS nano* 2021, 15, 3849-3874, doi:10.1021/acsnano.0c09678.
44. Cheng, Y.; Zhou, S.; Hu, P.; Zhao, G.; Li, Y.; Zhang, X.; Han, W. Enhanced mechanical, thermal, and electric properties of graphene 3D framework via supercritical ethanol drying and high-temperature thermal reduction. *Scientific reports* 2017, 7, 1439, doi:10.1038/s41598-017-01601-x.
45. Li, C.; Li, Z.; Qi, X.; Gong, X.; Chen, Y.; Peng, Q.; Deng, C.; Jing, T.; Zhong, W. A generalizable strategy for constructing ultralight three-dimensional hierarchical network heterostructure as high-efficient microwave absorber. *Journal of colloid and interface science* 2022, 605, 13-22, doi:<https://doi.org/10.1016/j.jcis.2021.07.054>.
46. Liang, L.; Han, G.; Li, Y.; Zhao, B.; Zhou, B.; Feng, Y.; Ma, J.; Wang, Y.; Zhang, R.; Liu, C. Promising Ti₃C₂T_x MXene/Ni Chain Hybrid with Excellent Electromagnetic Wave Absorption and Shielding Capacity. *ACS applied materials & interfaces* 2019, 11, 25399-25409, doi:10.1021/acsnano.9b07294.
47. Yang, F.; Yao, J.; Jin, L.; Huyan, W.; Zhou, J.; Yao, Z.; Liu, P.; Tao, X. Multifunctional Ti₃C₂T_x MXene/Aramid nanofiber/Polyimide 3D framework with efficient thermal insulation and tunable electromagnetic wave absorption performance under thermal environment. *Composites Part B: Engineering* 2022, 243, 110161, doi:<https://doi.org/10.1016/j.compositesb.2022.110161>.
48. Chen, X.; Liu, H.; Zheng, Y.; Zhai, Y.; Liu, X.; Liu, C.; Mi, L.; Guo, Z.; Shen, C. Highly Compressible and Robust Polyimide/Carbon Nanotube Composite Aerogel for High-Performance

- Wearable Pressure Sensor. *ACS applied materials & interfaces* 2019, 11, 42594-42606, doi:10.1021/acsami.9b14688.
49. Zhang, Q.; Chen, B.; Wu, K.; Nan, B.; Lu, M.; Lu, M. PEG-filled kapok fiber/sodium alginate aerogel loaded phase change composite material with high thermal conductivity and excellent shape stability. *Composites Part A: Applied Science and Manufacturing* 2021, 143, 106279, doi:https://doi.org/10.1016/j.compositesa.2021.106279.
 50. Zhang, C.; Huang, R.; Wang, P.; Wang, Y.; Zhou, Z.; Zhang, H.; Wu, Z.; Li, L. Highly Compressible, Thermally Conductive, yet Electrically Insulating Fluorinated Graphene Aerogel. *ACS applied materials & interfaces* 2020, 12, 58170-58178, doi:10.1021/acsami.0c19628.
 51. Yang, J.; Tang, L.-S.; Bao, R.-Y.; Bai, L.; Liu, Z.-Y.; Yang, W.; Xie, B.-H.; Yang, M.-B. Largely enhanced thermal conductivity of poly (ethylene glycol)/boron nitride composite phase change materials for solar-thermal-electric energy conversion and storage with very low content of graphene nanoplatelets. *Chemical Engineering Journal* 2017, 315, 481-490, doi:https://doi.org/10.1016/j.cej.2017.01.045.
 52. Zhao, H.Y.; Yu, M.Y.; Liu, J.; Li, X.; Min, P.; Yu, Z.Z. Efficient Preconstruction of Three-Dimensional Graphene Networks for Thermally Conductive Polymer Composites. *Nano-micro letters* 2022, 14, 129, doi:10.1007/s40820-022-00878-6.
 53. Wu, N.; Che, S.; Li, H.-w.; Wang, C.-n.; Tian, X.-j.; Li, Y.-f. A review of three-dimensional graphene networks for use in thermally conductive polymer composites: construction and applications. *New Carbon Materials* 2021, 36, 911-926, doi:10.1016/s1872-5805(21)60089-6.
 54. Zhang, X.; Yeung, K.K.; Gao, Z.; Li, J.; Sun, H.; Xu, H.; Zhang, K.; Zhang, M.; Chen, Z.; Yuen, M.M.F.; et al. Exceptional thermal interface properties of a three-dimensional graphene foam. *Carbon* 2014, 66, 201-209, doi:https://doi.org/10.1016/j.carbon.2013.08.059.
 55. Qin, M.; Xu, Y.; Cao, R.; Feng, W.; Chen, L. Efficiently controlling the 3D thermal conductivity of a polymer nanocomposite via a hyperelastic double-continuous network of graphene and sponge. *Advanced functional materials* 2018, 28, 1805053.
 56. Wang, Q.; Xiang, L.; Mei, D.; Xie, Y. Graphene 3D framework: Structure Control, Thermal Characterization and Thermal Transport. *International Journal of Thermophysics* 2020, 41, 155, doi:10.1007/s10765-020-02740-6.
 57. Du, T.; Xiong, Z.; Delgado, L.; Liao, W.; Peoples, J.; Kantharaj, R.; Chowdhury, P.R.; Marconnet, A.; Ruan, X. Wide range continuously tunable and fast thermal switching based on compressible graphene composite foams. *Nature communications* 2021, 12, 4915, doi:10.1038/s41467-021-25083-8.
 58. Pan, C.; He, P.; Wu, J.; Chen, N.; Wei, J.; Xu, T.; Shi, E.; Wang, A.; Jia, H. Copper foam effectively improves the thermal performance of graphene-aerogel composite phase-change materials for thermal storage. *Journal of Energy Storage* 2022, 51, 104485, doi:https://doi.org/10.1016/j.est.2022.104485.
 59. Qiu, L.; Liu, J.Z.; Chang, S.L.; Wu, Y.; Li, D. Biomimetic superelastic graphene-based cellular monoliths. *Nature communications* 2012, 3, 1-7.
 60. An, F.; Li, X.; Min, P.; Liu, P.; Jiang, Z.G.; Yu, Z.Z. Vertically Aligned High-Quality Graphene Foams for Anisotropically Conductive Polymer Composites with Ultrahigh Through-Plane Thermal Conductivities. *ACS applied materials & interfaces* 2018, 10, 17383-17392, doi:10.1021/acsami.8b04230.
 61. Yue, J.; Pan, J.; Deng, Y.; Li, J.; Bao, J. Enhanced properties of poly (styrene-b-ethylene-co-butylene-b-styrene) nanocomposites with in situ construction of interconnected graphene network. *Journal of Applied Polymer Science* 2019, 136, 47118.
 62. Wang, P.; Chong, H.; Zhang, J.; Lu, H. Constructing 3D graphene networks in polymer composites for significantly improved electrical and mechanical properties. *ACS applied materials & interfaces* 2017, 9, 22006-22017.

63. Li, A.; Zhang, C.; Zhang, Y.-F. RGO/TPU composite with a segregated structure as thermal interface material. *Composites Part A: Applied Science and Manufacturing* 2017, 101, 108-114, doi:<https://doi.org/10.1016/j.compositesa.2017.06.009>.
64. Alam, F.E.; Dai, W.; Yang, M.; Du, S.; Li, X.; Yu, J.; Jiang, N.; Lin, C.-T. In situ formation of a cellular graphene framework in thermoplastic composites leading to superior thermal conductivity. *Journal of Materials Chemistry A* 2017, 5, 6164-6169, doi:10.1039/C7TA00750G.
65. Yang, L.; Zheng, Y.; Hou, M.; Chen, W.; Wang, Z. Constructing of Highly Ordered 3D Network of Carbon Nanotube inside Polymer Matrix and the Improvements in Properties of the Composites. *Am. J. Polym. Sci. Technol* 2019, 5.
66. Liu, B.; Li, Y.; Fei, T.; Han, S.; Xia, C.; Shan, Z.; Jiang, J. Highly thermally conductive polystyrene/polypropylene/boron nitride composites with 3D segregated structure prepared by solution-mixing and hot-pressing method. *Chemical Engineering Journal* 2020, 385, 123829, doi:10.1016/j.cej.2019.123829.
67. Li, J.; Li, F.; Zhao, X.; Zhang, W.; Li, S.; Lu, Y.; Zhang, L. Jelly-Inspired Construction of the Three-Dimensional Interconnected BN Network for Lightweight, Thermally Conductive, and Electrically Insulating Rubber Composites. *ACS Applied Electronic Materials* 2020, 2, 1661-1669, doi:10.1021/acsaelm.0c00227.
68. Han, J.; Du, G.; Gao, W.; Bai, H. An Anisotropically High Thermal Conductive Boron Nitride/Epoxy Composite Based on Nacre-Mimetic 3D Network. *Advanced Functional Materials* 2019, 29, 1900412, doi:10.1002/adfm.201900412.
69. Wang, X.; Yu, Z.; Bian, H.; Wu, W.; Xiao, H.; Dai, H. Thermally conductive and electrical insulation BNNS/CNF aerogel nano-paper. *Polymers* 2019, 11, 660.
70. Fang, H.; Zhao, Y.; Zhang, Y.; Ren, Y.; Bai, S.-L. Three-Dimensional Graphene Foam-Filled Elastomer Composites with High Thermal and Mechanical Properties. *ACS applied materials & interfaces* 2017, 9, 26447-26459, doi:10.1021/acsami.7b07650.
71. Min, P.; Liu, J.; Li, X.; An, F.; Liu, P.; Shen, Y.; Koratkar, N.; Yu, Z.-Z. Thermally Conductive Phase Change Composites Featuring Anisotropic Graphene 3D framework for Real-Time and Fast-Charging Solar-Thermal Energy Conversion. *Advanced Functional Materials* 2018, 28, 1805365, doi:10.1002/adfm.201805365.
72. Yang, J.; Li, X.; Han, S.; Yang, R.; Min, P.; Yu, Z.-Z. High-quality graphene 3D framework for thermally conductive phase change composites with excellent shape stability. *Journal of Materials Chemistry A* 2018, 6, 5880-5886, doi:10.1039/c8ta00078f.
73. Ding, J.-H.; Zhao, H.-R.; Yu, H.-B. High-yield synthesis of extremely high concentrated and few-layered boron nitride nanosheet dispersions. *2D Materials* 2018, 5, 045015, doi:10.1088/2053-1583/aad51a.
74. Jiang, F.; Cui, S.; Rungnim, C.; Song, N.; Shi, L.; Ding, P. Control of a Dual-Cross-Linked Boron Nitride Framework and the Optimized Design of the Thermal Conductive Network for Its Thermoresponsive Polymeric Composites. *Chemistry of Materials* 2019, 31, 7686-7695, doi:10.1021/acs.chemmater.9b02551.
75. Jing, L.; Li, H.; Tay, R.Y.; Sun, B.; Tsang, S.H.; Cometto, O.; Lin, J.; Teo, E.H.T.; Tok, A.I.Y. Biocompatible Hydroxylated Boron Nitride Nanosheets/Poly(vinyl alcohol) Interpenetrating Hydrogels with Enhanced Mechanical and Thermal Responses. *ACS nano* 2017, 11, 3742-3751, doi:10.1021/acsnano.6b08408.
76. Wu, W.; Liu, H.; Wang, Z.; Lv, P.; Hu, E.; Zheng, J.; Yu, K.; Wei, W. Formation of thermal conductive network in boron nitride/polyvinyl alcohol by ice-templated self-assembly. *Ceramics International* 2021, 47, 33926-33929, doi:10.1016/j.ceramint.2021.08.266.
77. Wang, X.; Yu, Z.; Bian, H.; Wu, W.; Xiao, H.; Dai, H. Thermally Conductive and Electrical Insulation BNNS/CNF Aerogel Nano-Paper. *Polymers* 2019, 11, doi:10.3390/polym11040660.
78. Song, P.; Liu, B.; Liang, C.; Ruan, K.; Qiu, H.; Ma, Z.; Guo, Y.; Gu, J. Lightweight, Flexible Cellulose-Derived Carbon Aerogel@Reduced Graphene Oxide/PDMS Composites with

- Outstanding EMI Shielding Performances and Excellent Thermal Conductivities. *Nano-micro letters* 2021, 13, 91, doi:10.1007/s40820-021-00624-4.
79. Liu, Y.; Zhang, Y.; Liao, T.; Gao, L.; Wang, M.; Xu, X.; Yang, X.; Liu, H. Boron nitride-nanosheet enhanced cellulose nanofiber aerogel with excellent thermal management properties. *Carbohydrate polymers* 2020, 241, 116425, doi:10.1016/j.carbpol.2020.116425.
 80. Ji, H.; Sellan, D.P.; Pettes, M.T.; Kong, X.; Ji, J.; Shi, L.; Ruoff, R.S. Enhanced thermal conductivity of phase change materials with ultrathin-graphite foams for thermal energy storage. *Energy & Environmental Science* 2014, 7, 1185-1192.
 81. Zhao, Y.-H.; Wu, Z.-K.; Bai, S.-L. Study on thermal properties of graphene foam/graphene sheets filled polymer composites. *Composites Part A: Applied Science and Manufacturing* 2015, 72, 200-206, doi:https://doi.org/10.1016/j.compositesa.2015.02.011.
 82. Conrado, F.; Pavese, M. A Continuous 3D-Graphene Network to Overcome Threshold Issues and Contact Resistance in Thermally Conductive Graphene Nanocomposites. *Journal of Nanomaterials* 2017, 2017, 8974174, doi:10.1155/2017/8974174.
 83. Weng, C.; Li, W.; Wu, J.; Shen, L.; Yang, W.; Deng, C.; Bao, N. Thermal shock exfoliated and siloxane cross-linked graphene framework for high performance epoxy-based thermally conductive composites. *Journal of Materials Science* 2021, 56, 17601-17614, doi:10.1007/s10853-021-06147-y.
 84. Wu, Y.; Xue, Y.; Qin, S.; Liu, D.; Wang, X.; Hu, X.; Li, J.; Wang, X.; Bando, Y.; Golberg, D. BN nanosheet/polymer films with highly anisotropic thermal conductivity for thermal management applications. *ACS Appl Mater Interfaces* 2017, 9, 43163-43170.
 85. Zhu, H.; Li, Y.; Fang, Z.; Xu, J.; Cao, F.; Wan, J.; Preston, C.; Yang, B.; Hu, L. Highly thermally conductive papers with percolative layered boron nitride nanosheets. *ACS Nano* 2014, 8, 3606-3613.
 86. Sun, J.; Yao, Y.; Zeng, X.; Pan, G.; Hu, J.; Huang, Y.; Sun, R.; Xu, J.B.; Wong, C.P. Preparation of boron nitride nanosheet/nanofibrillated cellulose nanocomposites with ultrahigh thermal conductivity via engineering interfacial thermal resistance. *Adv Mater Interfaces* 2017, 4, 1700563.
 87. Hu, Z.; Wang, S.; Chen, G.; Wu, K.; Shi, J.; Liang, L.; Lu, M. An aqueous-only, green route to exfoliate boron nitride for preparation of high thermal conductive boron nitride nanosheet/cellulose nanofiber flexible film. *Compos Sci Technol.* 2018, 168, 287-295.
 88. Zhu, Z.; Li, C.; Songfeng, E.; Xie, L.; Geng, R.; Lin, C.-T.; Li, L.; Yao, Y. Enhanced thermal conductivity of polyurethane composites via engineering small/large sizes interconnected boron nitride nanosheets. *Compos Sci Technol* 2019, 170, 93-100.
 89. Li, G.; Tian, X.; Xu, X.; Zhou, C.; Wu, J.; Li, Q.; Zhang, L.; Yang, F.; Li, Y. Fabrication of robust and highly thermally conductive nanofibrillated cellulose/graphite nanoplatelets composite papers. *Compos Sci Technol.* 2017, 138, 179-185.
 90. Liang, Q.; Yao, X.; Wang, W.; Liu, Y.; Wong, C.P. A three-dimensional vertically aligned functionalized multilayer graphene architecture: an approach for graphene-based thermal interfacial materials. *ACS nano.* 2011, 5, 2392-2401.
 91. Wang, J.; Wu, Y.; Xue, Y.; Liu, D.; Wang, X.; Hu, X.; Bando, Y.; Lei, W. Super-compatible functional boron nitride nanosheets/polymer films with excellent mechanical properties and ultrahigh thermal conductivity for thermal management. *J. Mater. Chem. C* 2018, 6, 1363-1369.
 92. Kymäläinen, H.-R.; Sjöberg, A.-M. Flax and hemp fibres as raw materials for thermal insulations. *Building environment.* 2008, 43, 1261-1269.
 93. Weidenfeller, B.; Höfer, M.; Schilling, F.R. Thermal conductivity, thermal diffusivity, and specific heat capacity of particle filled polypropylene. *Compos. Part A Appl. Sci. Manuf* 2004, 35, 423-429.
 94. Wei, F.; Feng, C.-P.; Yang, J.; Yang, L.-Y.; Bai, L.; Bao, R.-Y.; Liu, Z.-Y.; Yang, M.-B.; Yang, W. Scalable Flexible Phase Change Materials with a Swollen Polymer Network Structure for Thermal Energy Storage. *ACS applied materials & interfaces* 2021, 13, 59364-59372, doi:10.1021/acami.1c20147.

95. Xie, B.-H.; Huang, X.; Zhang, G.-J. High thermal conductive polyvinyl alcohol composites with hexagonal boron nitride microplatelets as fillers. *Compos Sci Technol* 2013, 85, 98-103.
96. Yang, X.; Guo, Y.; Han, Y.; Li, Y.; Ma, T.; Chen, M.; Kong, J.; Zhu, J.; Gu, J. Significant improvement of thermal conductivities for BNNS/PVA composite films via electrospinning followed by hot-pressing technology. *Compos. B. Eng.* 2019, 175, 107070.
97. Yao, Y.; Zeng, X.; Sun, R.; Xu, J.-B.; Wong, C.-P.J.A.a.m.; interfaces. Highly thermally conductive composite papers prepared based on the thought of bioinspired engineering. *ACS Appl Mater Interfaces* 2016, 8, 15645-15653.
98. Zhang, J.; Li, C.; Yu, C.; Wang, X.; Li, Q.; Lu, H.; Zhang, Q.; Zhao, J.; Songfeng, E.; Hu, M. Large improvement of thermal transport and mechanical performance of polyvinyl alcohol composites based on interface enhanced by SiO₂ nanoparticle-modified-hexagonal boron nitride. *Compos Sci Technol* 2019, 169, 167-175.
99. Chowdhury, R.A.; Rai, A.; Glynn, E.; Morgan, P.; Moore, A.L.; Youngblood, J.P. Superior, processing-dependent thermal conductivity of cellulose Nanocrystal-Poly (vinyl alcohol) composite films. *Polymer* 2019, 164, 17-25.
100. Zeng, X.; Ye, L.; Yu, S.; Li, H.; Sun, R.; Xu, J.; Wong, C.-P. Artificial nacre-like papers based on noncovalent functionalized boron nitride nanosheets with excellent mechanical and thermally conductive properties. *Nanoscale* 2015, 7, 6774-6781.
101. Wu, K.; Fang, J.; Ma, J.; Huang, R.; Chai, S.; Chen, F.; Fu, Q. Achieving a Collapsible, Strong, and Highly Thermally Conductive Film Based on Oriented Functionalized Boron Nitride Nanosheets and Cellulose Nanofiber. *ACS applied materials & interfaces* 2017, 9, 30035-30045, doi:10.1021/acsami.7b08214.
102. Yao, Y.; Zeng, X.; Wang, F.; Sun, R.; Xu, J.-b.; Wong, C.-P. Significant Enhancement of Thermal Conductivity in Bioinspired Freestanding Boron Nitride Papers Filled with Graphene Oxide. *Chemistry of Materials* 2016, 28, 1049-1057, doi:10.1021/acs.chemmater.5b04187.
103. Fu, L.; Wang, T.; Yu, J.; Dai, W.; Sun, H.; Liu, Z.; Sun, R.; Jiang, N.; Yu, A.; Lin, C.-T. An ultrathin high-performance heat spreader fabricated with hydroxylated boron nitride nanosheets. *2D Materials* 2017, 4, 025047, doi:10.1088/2053-1583/aa636e.
104. Yao, Y.; Zeng, X.; Pan, G.; Sun, J.; Hu, J.; Huang, Y.; Sun, R.; Xu, J.B.; Wong, C.P. Interfacial Engineering of Silicon Carbide Nanowire/Cellulose Microcrystal Paper toward High Thermal Conductivity. *ACS applied materials & interfaces* 2016, 8, 31248-31255, doi:10.1021/acsami.6b10935.
105. Yao, Y.; Zeng, X.; Sun, R.; Xu, J.B.; Wong, C.P. Highly Thermally Conductive Composite Papers Prepared Based on the Thought of Bioinspired Engineering. *ACS applied materials & interfaces* 2016, 8, 15645-15653, doi:10.1021/acsami.6b04636.
106. Yu, C.; Zhang, Q.; Zhang, J.; Geng, R.; Tian, W.; Fan, X.; Yao, Y. One-step in situ ball milling synthesis of polymer-functionalized few-layered boron nitride and its application in high thermally conductive cellulose composites. *ACS Applied Nano Materials* 2018, 1, 4875-4883.
107. Yu, C.; Gong, W.; Tian, W.; Zhang, Q.; Xu, Y.; Lin, Z.; Hu, M.; Fan, X.; Yao, Y. Hot-pressing induced alignment of boron nitride in polyurethane for composite films with thermal conductivity over 50 Wm⁻¹ K⁻¹. *Composites Science and Technology* 2018, 160, 199-207.
108. Wang, X.; Wu, P. Highly Thermally Conductive Fluorinated Graphene Films with Superior Electrical Insulation and Mechanical Flexibility. *ACS applied materials & interfaces* 2019, 11, 21946-21954, doi:10.1021/acsami.9b07377.
109. Ha, T.; Kim, D.-G.; Ka, J.-W.; Kim, Y.S.; Koh, W.-G.; Lim, H.S.; Yoo, Y. Simultaneous effects of silver-decorated graphite nanoplatelets and anisotropic alignments on improving thermal conductivity of stretchable poly(vinyl alcohol) composite films. *Composites Part A: Applied Science and Manufacturing* 2020, 138, 106045, doi:https://doi.org/10.1016/j.compositesa.2020.106045.

110. Luo, F.; Zhang, M.; Chen, S.; Xu, J.; Ma, C.; Chen, G. Sandwich-structured PVA/rGO films from self-construction with high thermal conductivity and electrical insulation. *Composites Science and Technology* 2021, 207, 108707, doi:<https://doi.org/10.1016/j.compscitech.2021.108707>.
111. Wang, Y.; Zhang, X.; Ding, X.; Li, Y.; Zhang, P.; Shu, M.; Zhang, Q.; Gong, Y.; Zheng, K.; Wu, B.; et al. Enhanced thermal conductivity of carbon nitride-doped graphene/polyimide composite film via a “deciduous-like” strategy. *Composites Science and Technology* 2021, 205, 108693, doi:<https://doi.org/10.1016/j.compscitech.2021.108693>.
112. Song, J.; Chen, C.; Zhang, Y. High thermal conductivity and stretchability of layer-by-layer assembled silicone rubber/graphene nanosheets multilayered films. *Composites Part A: Applied Science and Manufacturing* 2018, 105, 1-8, doi:<https://doi.org/10.1016/j.compositesa.2017.11.001>.
113. Wu, K.; Lei, C.; Huang, R.; Yang, W.; Chai, S.; Geng, C.; Chen, F.; Fu, Q. Design and Preparation of a Unique Segregated Double Network with Excellent Thermal Conductive Property. *ACS applied materials & interfaces* 2017, 9, 7637-7647, doi:10.1021/acsami.6b16586.
114. Dai, W.; Yu, J.; Liu, Z.; Wang, Y.; Song, Y.; Lyu, J.; Bai, H.; Nishimura, K.; Jiang, N. Enhanced thermal conductivity and retained electrical insulation for polyimide composites with SiC nanowires grown on graphene hybrid fillers. *Composites Part A: Applied Science and Manufacturing* 2015, 76, 73-81, doi:<https://doi.org/10.1016/j.compositesa.2015.05.017>.
115. Shao, L.; Shi, L.; Li, X.; Song, N.; Ding, P. Synergistic effect of BN and graphene nanosheets in 3D framework on the enhancement of thermal conductive properties of polymeric composites. *Composites Science and Technology* 2016, 135, 83-91.
116. Renteria, J.D.; Ramirez, S.; Malekpour, H.; Alonso, B.; Centeno, A.; Zurutuza, A.; Cocemasov, A.I.; Nika, D.L.; Balandin, A.A. Strongly Anisotropic Thermal Conductivity of Free-Standing Reduced Graphene Oxide Films Annealed at High Temperature. *Advanced Functional Materials* 2015, 25, 4664-4672, doi:10.1002/adfm.201501429.
117. Hongli Zhu, Y.L., † Zhiqiang Fang, † Jiajun Xu, ‡ Fangyu Cao, ‡ Jiayu Wan, † Colin Preston, †; Bao Yang, * and Liangbing Hu ‡, *. Highly Thermally Conductive Papers with Percolative Layered Boron Nitride Nanosheets. *ACS nano* 2014, 8, 3606–3613.
118. Xie, B.-H.; Huang, X.; Zhang, G.-J. High thermal conductive polyvinyl alcohol composites with hexagonal boron nitride microplatelets as fillers. *Composites Science and Technology* 2013, 85, 98-103, doi:<https://doi.org/10.1016/j.compscitech.2013.06.010>.
119. Popov, E.; Goncharov, A.; Popov, Y.; Spasennykh, M.; Chekhonin, E.; Shakirov, A.; Gabova, A. Advanced techniques for determining thermal properties on rock samples and cuttings and indirect estimating for atmospheric and formation conditions. *IOP Conference Series: Earth and Environmental Science* 2019, 367, 012017, doi:10.1088/1755-1315/367/1/012017.
120. Popov, Y.; Beardsmore, G.; Clauser, C.; Roy, S. ISRM Suggested Methods for Determining Thermal Properties of Rocks from Laboratory Tests at Atmospheric Pressure. *Rock Mechanics and Rock Engineering* 2016, 49, 4179-4207, doi:10.1007/s00603-016-1070-5.
121. Ferrari, A.C.; Robertson, J. Interpretation of Raman spectra of disordered and amorphous carbon. *Physical review B* 2000, 61, 14095.
122. Klechikov, A.; Yu, J.; Thomas, D.; Sharifi, T.; Talyzin, A.V. Structure of graphene oxide membranes in solvents and solutions. *Nanoscale* 2015, 7, 15374-15384, doi:10.1039/c5nr04096e.
123. Kim, S.; Shimazu, J.; Fukaminato, T.; Ogata, T.; Kurihara, S. Thermal conductivity of graphene oxide-enhanced polyvinyl alcohol composites depending on molecular interaction. *Polymer* 2017, 129, 201-206, doi:10.1016/j.polymer.2017.09.055.
124. Yu, Y.; Sun, Y.; Cao, C.; Yang, S.; Liu, H.; Li, P.; Huang, P.; Song, W. Graphene-based composite supercapacitor electrodes with diethylene glycol as inter-layer spacer. *J. Mater. Chem. A* 2014, 2, 7706-7710, doi:10.1039/c4ta00905c.
125. Iijima, S. Helical microtubules of graphitic carbon. *nature* 1991, 354, 56-58.
126. Bandaru, P.R. Electrical properties and applications of carbon nanotube structures. *Journal of nanoscience and nanotechnology* 2007, 7, 1239-1267.

127. Ibrahim, K.S. Carbon nanotubes-properties and applications: a review. *Carbon letters* 2013, 14, 131-144.
128. Caradonna, A.; Badini, C.; Padovano, E.; Pietroluongo, M. Electrical and thermal conductivity of epoxy-carbon filler composites processed by calendaring. *Materials* 2019, 12, 1522.
129. Butt, H.A.; Lomov, S.V.; Akhatov, I.S.; Abaimov, S.G. Self-diagnostic carbon nanocomposites manufactured from industrial epoxy masterbatches. *Composite Structures* 2021, 259, 113244.
130. Aravand, M.; Lomov, S.V.; Verpoest, I.; Gorbatikh, L. Evolution of carbon nanotube dispersion in preparation of epoxy-based composites: From a masterbatch to a nanocomposite. *Express Polymer Letters* 2014, 8, 596-608.
131. Mičušík, M.; Omastová, M.; Krupa, I.; Prokeš, J.; Pissis, P.; Logakis, E.; Pandis, C.; Pötschke, P.; Pionteck, J. A comparative study on the electrical and mechanical behaviour of multi-walled carbon nanotube composites prepared by diluting a masterbatch with various types of polypropylenes. *Journal of Applied Polymer Science* 2009, 113, 2536-2551.
132. Pothmann, D.; Simar, S.; Schuler, D.; Dony, E.; Gaering, S.; Le Net, J.-L.; Okazaki, Y.; Chabagno, J.M.; Bessibes, C.; Beausoleil, J. Lung inflammation and lack of genotoxicity in the comet and micronucleus assays of industrial multiwalled carbon nanotubes Graphistrength© C100 after a 90-day nose-only inhalation exposure of rats. *Particle and fibre toxicology* 2015, 12, 1-28.
133. Butt, H.A.; Owais, M.; Sulimov, A.; Ostrizhiniy, D.; Lomov, S.V.; Akhatov, I.S.; Abaimov, S.G.; Popov, Y.A. CNT/Epoxy-Masterbatch Based Nanocomposites: Thermal and Electrical Properties. 2021, 417-420, doi:10.1109/nano51122.2021.9514322.
134. Yang, S.-Y.; Ma, C.-C.M.; Teng, C.-C.; Huang, Y.-W.; Liao, S.-H.; Huang, Y.-L.; Tien, H.-W.; Lee, T.-M.; Chiou, K.-C. Effect of functionalized carbon nanotubes on the thermal conductivity of epoxy composites. *Carbon* 2010, 48, 592-603, doi:10.1016/j.carbon.2009.08.047.
135. Wang, S.; Liang, R.; Wang, B.; Zhang, C. Dispersion and thermal conductivity of carbon nanotube composites. *Carbon* 2009, 47, 53-57, doi:10.1016/j.carbon.2008.08.024.
136. Ervina, J.; Mariatti, M.; Hamdan, S. Mechanical, electrical and thermal properties of multi-walled carbon nanotubes/epoxy composites: effect of post-processing techniques and filler loading. *Polymer Bulletin* 2016, 74, 2513-2533, doi:10.1007/s00289-016-1853-6.
137. Russ, M.; Rahatekar, S.S.; Koziol, K.; Farmer, B.; Peng, H.-X. Length-dependent electrical and thermal properties of carbon nanotube-loaded epoxy nanocomposites. *Composites Science and Technology* 2013, 81, 42-47.
138. Namasivayam, M.; Shapter, J. Factors affecting carbon nanotube fillers towards enhancement of thermal conductivity in polymer nanocomposites: A review. *Journal of Composite Materials* 2017, 51, 3657-3668, doi:10.1177/0021998317692398.
139. Gojny, F.H.; Wichmann, M.H.; Fiedler, B.; Kinloch, I.A.; Bauhofer, W.; Windle, A.H.; Schulte, K. Evaluation and identification of electrical and thermal conduction mechanisms in carbon nanotube/epoxy composites. *Polymer* 2006, 47, 2036-2045.
140. Safdari, M.; Al-Haik, M.S. Synergistic electrical and thermal transport properties of hybrid polymeric nanocomposites based on carbon nanotubes and graphite nanoplatelets. *Carbon* 2013, 64, 111-121.
141. Tagami, N.; Hyuga, M.; Ohki, Y.; Tanaka, T.; Imai, T.; Harada, M.; Ochi, M. Comparison of dielectric properties between epoxy composites with nanosized clay fillers modified by primary amine and tertiary amine. *IEEE Transactions on Dielectrics and Electrical Insulation* 2010, 17, 214-220.
142. Zhang, Y.; Heo, Y.-J.; Son, Y.-R.; In, I.; An, K.-H.; Kim, B.-J.; Park, S.-J. Recent advanced thermal interfacial materials: A review of conducting mechanisms and parameters of carbon materials. *Carbon* 2019, 142, 445-460, doi:10.1016/j.carbon.2018.10.077.

Appendix

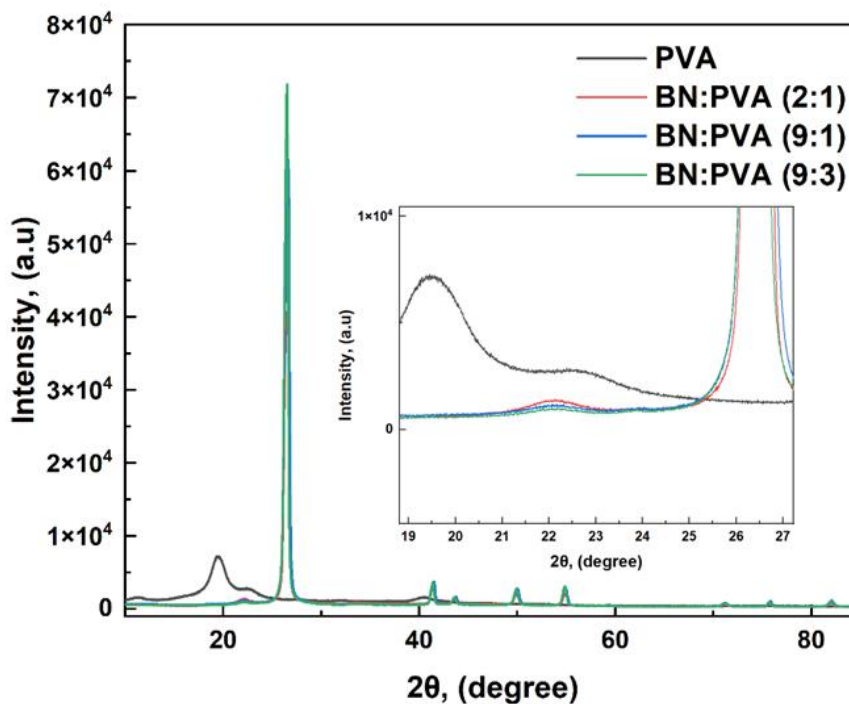


Figure 1. XRD pattern of PVA and BN/PVA composites (Chapter 3).

The X-ray diffraction (XRD) pattern of the BN-based PVA composites, with BN as a segregated filler network, reveals several distinctive peaks at 22.3°, 41.5°, 43.6°, 50.1°, 54.6°, 71.1°, and 82.6°. Notably, the characteristic diffraction peaks of neat PVA are also present, indicating the preservation of the PVA structure. However, no significant deviation or difference in diffraction peaks is observed for any of the BN/PVA composite 3D framework when compared to neat PVA. Interestingly, some peaks at 22.3° and 41.5° suggest the possibility of linkage between PVA and BN, although to a limited extent. These observations support the notion that BN is dispersed as a

segregated filler network within the PVA matrix, maintaining the structural integrity of both components.

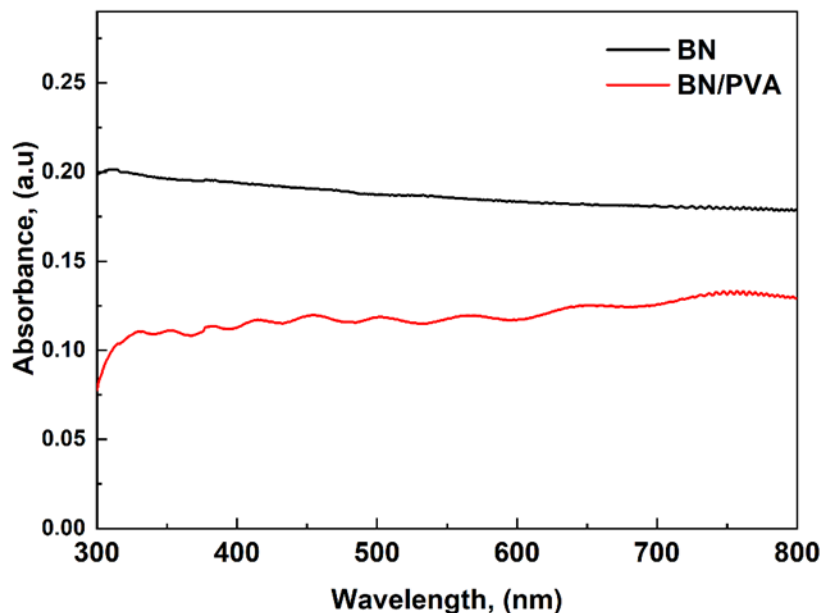


Figure 2. UV-Vis absorption spectra of PVA and BN/PVA (9:1) composite 3D framework (Chapter 3).

The UV-Vis absorption spectra of PVA and BN/PVA composite samples are shown in the figure 2. The BN/PVA cake exhibits transparency due to its low absorption intensity across a broad range of wavelengths. Due to limited light absorption in the UV region, pure PVA had low UV blocking properties then pure BN. The ability to absorb UV radiation was far better in pure BN compared to BN/PVA hybrid composite. As the BN concentration to PVA in the aerogel changed from (1:0) to (9:1), the intensity of UV absorption of aerogel decreased noticeably. The outcomes show that PVA gave BNNSs 3D framework significant UV blocking properties.



Figure 3. Typical BN/PVA aerogel prototype with the stoichiometric ratio of (2:1) (chapter 3).

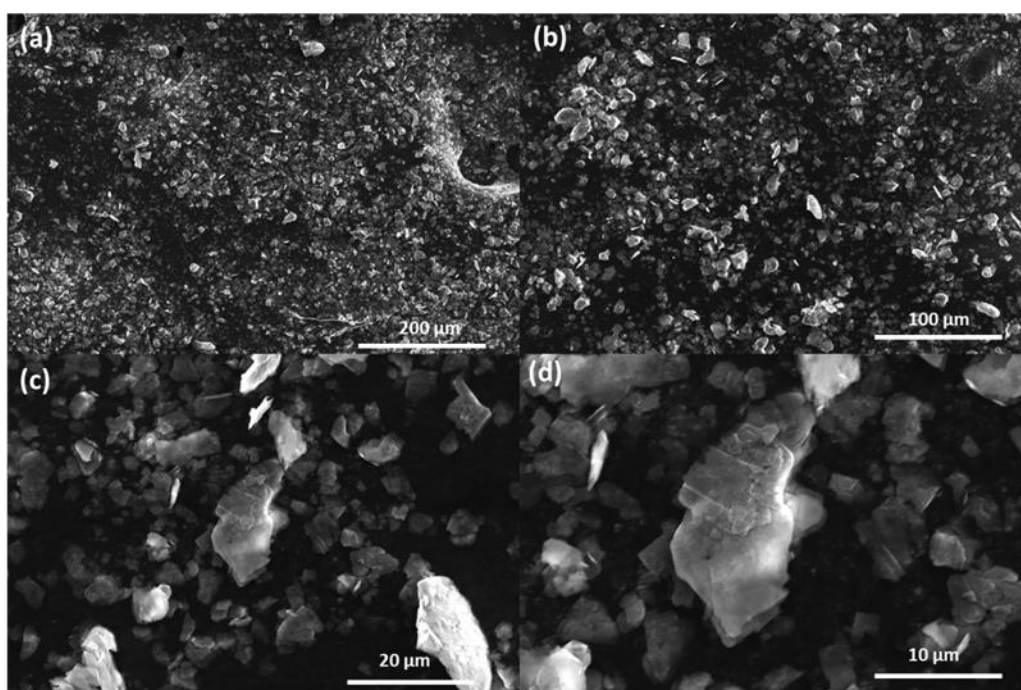


Figure 4. SEM images of pristine BN with an average particle size of $\sim 10\mu\text{m}$ at different magnifications (chapter 3).

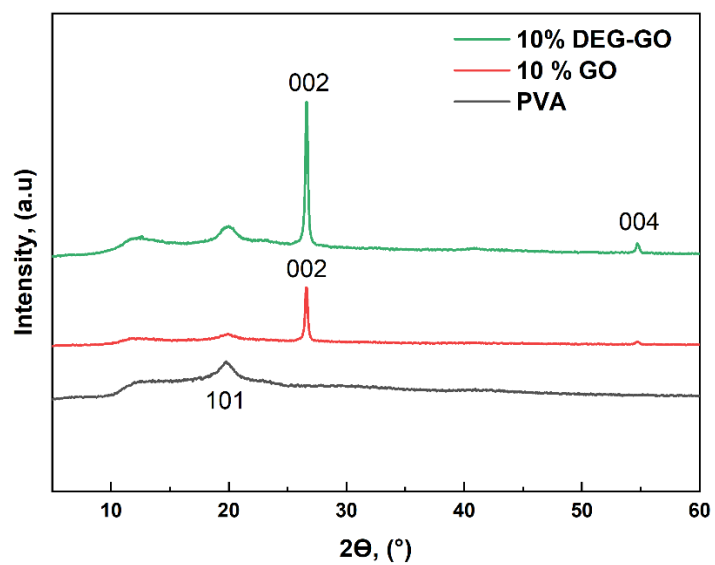


Figure 5. XRD pattern of PVA and it's composites (Chapter 4).